Master Thesis

Impact of Model Initialization on Predictability of Weather Regimes over the Euro-Atlantic Region on Inter-annual to Decadal Timescales

Carlos Delgado Torres

Supervisors:
Markus Donat (BSC)
Deborah Verfaillie (BSC)
Elsa Mohino Harris (UCM)

Climate Prediction Group
Earth Sciences Department
Barcelona Supercomputing Center

Máster en Meteorología y Geofísica
Departamento de Física de la Tierra y Astrofísica
Facultad de Ciencias Físicas
Universidad Complutense de Madrid

September 2019

Abstract

Weather regimes are large-scale circulation states that occur frequently in the climate system with persistence and recurrence. Their importance is due to the fact that they are related to the occurrence of extreme events, conditions on a synoptic scale and linked with the local weather and climate. Research in climate prediction has been fostered by the need of improved information about regional climate for many societal applications at long time scales. Knowledge of the future conditions of the climate system is essential for decision making in several areas, such as infrastructure planning, water resource management and climate change adaptation strategies. The objective of this study is to analyse the impact that the initialization of the models has on the predictability of the four weather regimes that occur in the Euro-Atlantic region, i.e., NAO+, NAO-, Blocking and Atlantic Ridge. Because of the complexity of the climate system it is difficult to predict its evolution, but sources of predictability are sought that may increase the skill of the model. With the initialization of the models, the aim is to phase the simulations and, therefore, to predict the actual evolution of the system. Among the results, significant improvements have been found in the skill of the model predicting the frequency of Blocking primarily during the summer season for the second forecast year. To try to understand the reason for this improvement, the possible teleconnections with the sea surface temperature are assessed and a relationship of the frequency of these two regimes with the ocean surface temperatures in the North Atlantic has been found, which may have increased the skill of the model.

Contents

1 Introduction

1.1 Decadal climate prediction

The objective of decadal climate prediction is to predict the evolution of the climate system due to external forcings (natural and anthropogenic) and internal climate variability on time scales from 1 to 10-30 years. Those external forcings and the slow oscillations of the climate system provide predictability at the inter-annual and decadal timescales, filling the gap between the seasonal forecasting and the climate projections. The aim of these predictions is not to simulate the actual day-to-day evolution, but instead the evolution of annual or decadal averages or frequency of extreme events on a synoptic scale.

The external forcings refer to forcing from outside the natural climate system, such as anthropogenic forcings (including aerosols, greenhouse gases and land use changes), changes in solar irradiance and large volcanic eruptions. These factors give rise to externally forced variations and can be both of natural and anthropogenic origin. In addition, these forcings are associated with other phenomena. For example, changes in solar irradiance have been associated with the North Atlantic Oscillation (NAO) by Ineson et al. (2011) and the modulation of Atlantic landfalling hurricanes by Hodges et al. (2014). Furthermore, although skill increases when volcanic eruptions are included in models, it is not possible to predict them, so the response of the system can only be calculated once the eruption has happened (González-Reviriego et al., 2018).

The slow oscillations of the climate system, known as internal variability, also provide sources of predictability, since there are some oscillations operating at inter-annual to decadal timescales. The dominant mode in the Euro-Atlantic region is the Atlantic Multi-decadal Variability (AMV), also known as the Atlantic Multi-decadal Oscillation (AMO), which is a climate cycle (quasi-periodicity of about 70 years) of the Sea Surface Temperature (SST) throughout the North Atlantic Ocean and is related to variability in the thermohaline circulation (Christensen et al., 2013). Some studies have related the AMV to the Atlantic Meridional Overturning Circulation (AMOC): the zonally-integrated component of surface and deep currents in the Atlantic Ocean (Knight et al., 2005; Pohlmann et al., 2013). Other studies such as Booth et al. (2012) explain that AMV is almost all externally forced.

Different components of the climate system can provide skill for decadal prediction. Typically, these components are the ocean, land surface and sea ice. Additionally, the skill can be improved by taking into account other components like the vegetation and the carbon cycle. It is important to note that the ocean is the component that gives more skill in inter-annual to decadal scales due to its higher thermal inertia, as can be seen in Figure 1a. By contrast, other components like the atmosphere and the land surface lose their memory long before and, therefore, their potential use as a source of predictability.

Figure 1b shows the time scales of weather, seasonal, inter-annual to decadal predictions and climate projections. It is also shown how initial and boundary conditions influence their skill. Weather and seasonal predictions are considered as initial value problems, while the climate projections are a boundary value problem. In between, inter-annual to decadal predictions combine both the initial value and the boundary condition problems. Thus, both the initial state and the forcings contribute to the forecast, although not always with the same importance: initial conditions are more important during the first few years and they become less relevant than the boundary conditions during the next years when the forcing becomes the dominant source of predictability (Kirtman et al., 2013).

1.2 Hindcasting and model initialization

Hindcasting consists in running models for a historical period in order to assess the quality of the model predicting the past climate evolution. For this, results of the model are compared with observed or reanalysis data. If results are coherent and resemble reality, the model would be considered skillful and it can be used for forecasting.

Hindcasting can be done by initializing the model towards an observed state or not. Initialized runs (Init), known as decadal predictions, compute the evolution of the climate system by integrating a model forward in time from a set of observation-based initial conditions. As time increases, they converge towards the evolution of Non-initialized runs (No-Init), known as historical simulations, which are only forced by changes in the external forcing described above.

The chaotic nature of the climate system limits the skill of models in predicting its evolution. Predictability can be analysed by computing the system evolution with small differences in both initial conditions and forcings, that is known as ensemble modelling. While the ensemble mean provides a more reliable value than a single member, the ensemble spread provides information about the internal variability in both the Init and the No-Init runs (Kirtman et al., 2013). In addition, the Init runs show the degree of similarity of the different members of the ensemble.

Ensemble generation for decadal prediction is in-

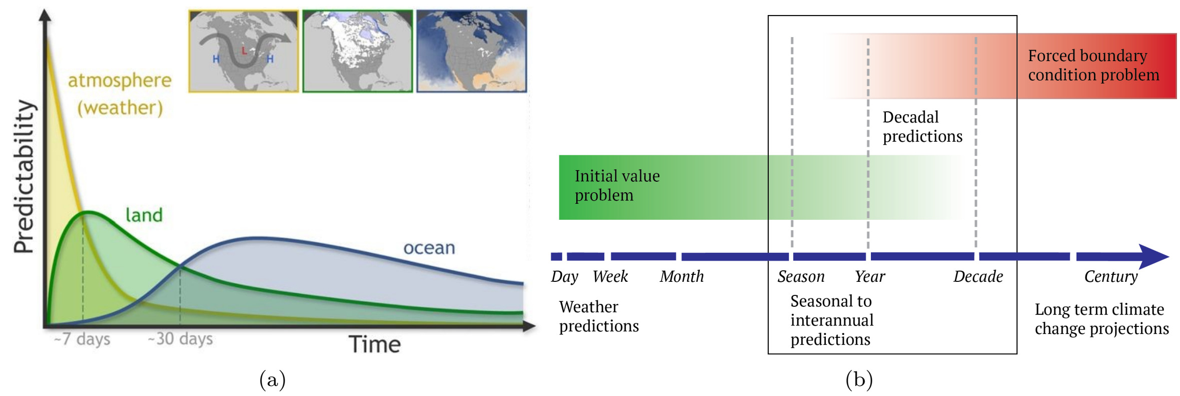

Figure 1. (*a*) Predictability according to time scale of different components of the climate system (Mariotti et al., 2018). (*b*) Time scales of weather, seasonal, inter-annual and decadal predictions and climate projections and the impact of the initial values and boundary conditions on them (Kirtman et al., 2013).

vestigated for several methods, for example, adding random perturbations to initial conditions, displacing atmospheric states in time and perturbing ocean initial conditions. In addition, there are other techniques used in weather and seasonal forecasting (Kirtman et al., 2013). Likewise, Meehl et al. (2013) have studied different initialization techniques, like including partial or fully coupled assimilation of ocean and/or atmospheric observations, forcing the ocean with atmospheric observations, and full-field versus anomaly initialization.

These two last techniques are the most used for seasonal-to-decadal climate predictions. In the full-field initialization, the best estimate of the real state is used to initialize the model. Although the initial error is small, the model quickly drifts towards its own climate state. To partially solve this problem, anomaly initialization is used. In this case, observed anomalies are added to an estimate of the model climate (Carrassi et al., 2014).

There are many studies that analyse the impact of the initialization of models. For example, the study carried out by García-Serrano et al. (2015) showed that uncertainty in the estimation of the level of AMV skill can be reduced by initializing climate models. Another study carried out by Doblas-Reyes et al. (2013) found that the initialization of forecast systems improves the quality of global-mean near-surface air temperature and temperature predictions over the North Atlantic region.

1.3 European weather regimes

The Fifth Assessment Report (AR5) of the United Nations Intergovernmental Panel on Climate Change (IPCC) defines weather regimes, also known as weather types, as a set of similar states of the climate system that occur more frequently than nearby states due to either more persistence or more recurrence (Christensen et al., 2013). They are quasi-stationary states that provide a simplified description of the variability in the climate system. The analysis of weather regimes can be carried out by analysing different meteorological variables such as sea level pressure (used in this study) or geopotential height at higher tropospheric levels, e.g., at 500 hPa.

The reason for using weather regimes is that they reduce the dimensionality of the weather situation and describe large-scale conditions typically associated with locally distinct weather status. As weather regimes describe large-scale conditions aggregated over a continental-scale region, they may be easier to predict than local weather conditions and, therefore, be a source of predictability in inter-annual to decadal prediction.

In the Euro-Atlantic region, the optimal season weather classification identifies four weather regimes, with a typical persistence of 3-7 days (Cortesi et al., 2019). Each one is associated with climate impacts in different regions of the Earth, i.e., teleconnections. Also, they can imply severe weather events such as flooding, heavy snow or heatwaves.

Figure 2 shows the spatial sea level pressure anomalies of the observed weather regimes in winter (defined as December, January and February), summer (defined as June, July and August), extended winter (defined as November, December, January, February, March and April) and extended summer (defined as May, June, July, August, September and October) seasons. It can be seen that the regimes patterns are better defined during the winter season. Furthermore, they are more persistent in time and have more influence on local climate during these months (Cortesi et al., 2019). The figure also shows the frequency of each cluster throughout the period analysed. The most frequent regimes in both seasons are the NAO+ and Blocking, with NAO+ being more frequent during the winter and Blocking during the summer. The data are taken from the JRA-55 reanalysis (described in Section 2.4) for the 1960-2010 period and the methodology used for its calculation is described in Section 3.2. The main characteristics of these four weather types are as follows:

- NAO+: This regime is characterised by an anomalously high pressure differential between the Azores islands and Iceland. It influences the jet stream, the storm track and blocking and, therefore, it affects the climate over the North Atlantic, Western Europe and the Mediterranean basin (Christensen et al., 2013). Due to its spatial distribution, there is an increase in the number and intensity of winter storms that cross the Atlantic Ocean in a north-easterly direction. This regime also causes mild and wet winters in northern Europe and decreasing winter precipitation in the Iberian Peninsula.
- NAO-: Opposite phase to NAO+, characterised by an anomalously low pressure differential between the Azores islands and Iceland. Westerlies are suppressed and the storm track moves southwards, carrying moist air towards the Mediterranean region, causing increased storm activity and precipitation in southern Europe and North Africa and cooling in northern Europe.
- Blocking (BL): Strong anticyclonic anomaly centred over Scandinavia and weaker cyclonic anomaly over Greenland. It is associated with persistent and slow high-pressure systems that can be associated with cold air outbreaks, heat-waves, floods and droughts (Christensen et al., 2013). This regime also produces atmospheric stagnation which leads to episodes of high pollution.
- Atlantic Ridge (AR): positive sea level pressure anomaly over the Atlantic Ocean and a negative one over Scandinavia. This weather regime is similar to the negative phase of the East Atlantic (EA) regime (Cortesi et al., 2019). This regime may also appear in its opposite form, i.e., negative sea level pressure anomaly over the Atlantic Ocean and positive anomaly over Scandinavia.

1.4 Objectives

The aim of this master thesis is to analyse the impact of model initialization on the predictability of European weather regimes on inter-annual to decadal scales. For this, observed weather regimes composites and time series are compared to predicted ones from both the historical runs (No-Init) and the decadal hindcast (Init).

The master thesis is organized as follows. Section 2 introduces both observed and experimental data used in this study. Section 3 contains the methodology used for the calculation of anomalies and weather regimes from the clustering algorithm. Results and discussion about the impact of model initialization on the predictability of weather regimes are shown in Section 4. Finally, conclusions are drawn in Section 5.

2 Data

2.1 Region and period

The region assessed in this study is the Euro-Atlantic region, delimited between 27°N-81°N and 85.5°W-45°E. This region can be seen in Figure 2.

With respect to the period analysed, data for the years 1960 to 2010 have been used. The reason for choosing this period is that the predictions can be compared with good quality observations. Additionally, averages of up to 5 years have been made for the analysis, so in some cases data up to 2014 have been used to make left-aligned moving means. The analysis has been made for short and extended seasons defined as follows:

- Summer: June, July and August (JJA).
- Winter: December, January and February (DJF).
- Extended summer: May, June, July, August, September and October (MJJASO).
- Extended winter: November, December, January, February, March and April (NDJFMA).

2.2 EC-Earth model

Climate models are tools to represent the behaviour of the Earth's climate based on mathematical representation using the laws of physics and thermodynamics. The EC-Earth model is an Earth System Model (ESM) developed by a consortium of European research institutions, in which Barcelona Supercomputing Center (BSC) is involved. It integrates a number of component models in order to simulate the whole earth system for uses such as seasonal to decadal climate prediction and climate projections. Earth System Models incorporate explicitly the interactions between the physical climate system and the biogeochemical and human processes. The experiments used in this study have been produced with the EC-Earth model v3.2, whose description can be seen in Doblas-Reyes et al. (2018).

The atmospheric component of the EC-Earth model is based on the Integrated Forecasting System (IFS) corresponding to the seasonal forecast

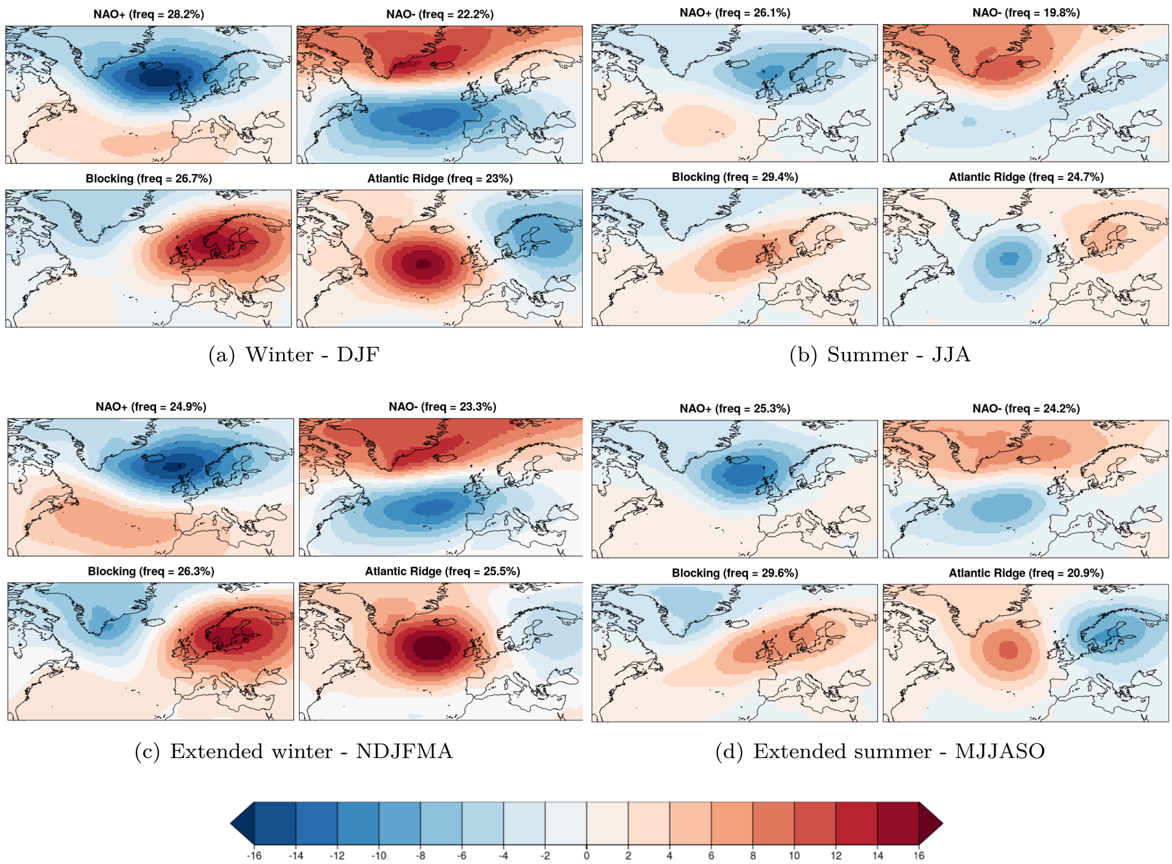

Figure 2. Composites of the averaged sea level pressure anomalies (hPa) of the observed weather regimes in normal and extended winter and summer seasons for the JRA-55 reanalysis during the 1960-2010 period. The region analysed is delimited between 27°N-81°N and 85.5°W-45°E

system of the European Centre for Medium-Range Weather Forecasts (ECMWF). Its horizontal spectral resolution is T255, i.e., triangular truncation of 255 of the infinite spherical-harmonic series that represent each prognostic variable. This resolution provides 256 latitude and 512 longitude grid points, with 0.54° ($\sim$ 78 km) of distance between two of them at the equator. In the vertical, it uses hybrid sigma-pressure coordinates, solving the equations in 91 levels up to 0.02 hPa (Hazeleger et al., 2010).

The EC-Earth model also uses the land and vegetation module of the IFS: the Hydrology Tiled ECMWF Scheme of Surface Exchanges over Land (HTESSEL). It has a simple snow scheme with an explicit snow layer (Orth et al., 2017).

The ocean component is based on the Nucleus for European Modelling of the Ocean (NEMO) model, ORCA1 configuration. It uses a tripolar grid with an horizontal resolution of 1° (362 latitude and 292 longitude grid points) and 75 vertical levels, with the top one located 10 meters below the ocean surface (Breivik et al., 2015). It gets the atmospheric forcing from the IFS.

The sea ice component is the Louvain-la-Neuve Sea Ice Model, version 2 (LIM2), with three layers: one for snow and two for ice. It has different components: thermodynamics, dynamics, advection, ridging and rafting (Uotila et al., 2016).

The Atmospheric chemistry component is the Tracer Model, version 5 (TM5). It is a three-dimensional global atmospheric chemistry transport model with the ability to simulate the composition of the atmosphere at both global and regional scales (Huijnen et al., 2010). However, this component was not activated in the historical runs and decadal predictions used in this study.

The coupling of all its components is carried out by the Ocean Atmosphere Sea Ice Soil (OASIS) coupler model (Hazeleger et al., 2010).

2.3 Hindcast experiments

In this study, the first ten historical simulations (No-Init) available from the twenty-six simulations currently being prepared with the EC-Earth model for the sixth phase of the Coupled Model Intercomparison Project (CMIP6) were used. All the historical runs are started from the Pre-Industrial (PI) control run, taking their initial states every 20 years. The PI control run starts from the spin-up, which has reached a reasonable equilibrium state. The only difference between those historical simulations is the initial state, so they are ideally independent and are able to give a better representation of all possible climate states. These simulations are forced by external forcings observed from 1850 onwards (Taylor et al., 2012).

In reference to the decadal predictions (Init), the first five members available were used. They are also run with the EC-Earth model, with the full-field initialization technique. For these runs, atmospheric initial conditions have been taken from ERA-40 reanalysis for the period 1960-1978 and ERA-Interim reanalysis for the period 1979-2018. The ocean and sea ice initial conditions have been taken form historical ocean-sea ice reconstruction using the NEMO model forced by the Drakkar Forcing Set v4.3 (DFS4.3) atmospheric reanalysis and strongly constrained by the Ocean ReAnalysis System 4 (ORAS4) ocean reanalysis using 3D-nudging data assimilation (Eyring et al., 2016). The predictions are initialized every year in November, predicting the next 11 years. Therefore, a greater improvement would be expected for the first winter season than for the summer season by starting the model in November. The forcings used for the period analysed are the same as those used in the historical experiments.

2.4 JRA-55 reanalysis

The Japanese 55-year Reanalysis (JRA-55) project is conducted by the Japan Meteorological Agency for the period from 1958 onward. This global reanalysis has a 4D-VAR assimilation algorithm. The horizontal grid system is a reduced Gaussian grid with an horizontal resolution TL319 (1.25° $\sim$ 55 km). 60 vertical hybrid levels are defined with half-levels as the boundary, up to 0.1 hPa (Kobayashi et al., 2015). Products are available for six-hourly, daily and monthly values. Additionally, land surface and two-dimensional fields are output at three-hourly intervals.

Sea level pressure data from this reanalysis are used during clustering analysis to evaluate both historical simulations and decadal predictions.

2.5 ERSST.v4 dataset

The monthly Extended Reconstructed Sea Surface Temperature version 4 (ERSST.v4) dataset is developed by the National Oceanic and Atmospheric Administration (NOAA) from 1854 onward. This global dataset provides monthly SST with 2° x 2° grid points as horizontal resolution. The anomalies are calculated relative to the 1971-2000 monthly climatology. The data are derived from the International Comprehensive Ocean–Atmosphere Dataset (ICOADS) and the missing data are filled using statistical methods (Huang et al., 2015; Liu et al., 2015).

SST data from this dataset are used to measure the relation of the weather regimes frequency with the SST time series.

3 Methodology

3.1 Climatologies and anomalies

Monthly climatologies are calculated for both experiment and reanalysis datasets and it is smoothed out by applying a Locally Estimated Scatterplot Smoothing (LOESS) filter (Cleveland and Devlin, 1988). This filter avoids discontinuities in the limits between different months, removing the short-term variability and retaining the annual cycle (Torralba, 2019).

Daily standardized anomalies are obtained based on the smoothed monthly climatology, which are previously weighted by the cosine of the latitude to take into account the different sizes of the grid boxes in the region studied. After that, they are introduced into the clustering algorithm to compute the weather regimes for both the reanalysis and the experiments (Section 3.2).

3.2 K-means clustering algorithm

Clustering analysis has been used in this study to obtain the seasonal weather regimes of daily sea level pressure standardized anomalies over the Euro-Atlantic region. It is an optimization method, which arranges a set of days within groups, called clusters, seeking the most steady states. It is necessary to apply the clustering analysis to the standardized anomalies, since this allows to compare different seasons and regions. After analysis, they are converted into non-standardized anomalies for map representation.

There are several clustering algorithms, but one of the most commonly used in climate research is the k-means algorithm. The k-means clustering algorithm minimizes the sum of the squared distances from each point to the centroid of the clusters to which they belong, providing the common spatial patterns in the analysed area. This algorithm starts with an initial cluster partition and, with an iterative process, it assigns the daily maps to the nearest cluster (assignment phase) and recalculates its centroid in each iteration (update phase). A drawback of the algorithm is that it tends to produce groups with similar sizes, leading to worse clustering results. More information about this algorithm and other clustering algorithms can be found in Philipp et al. (2010).

Clustering analysis can be applied to the actual sea level pressure field (where the dimensions are each point in the map grid, as in Torralba (2019)) or over principal components (where the dimensions are the first Empirical Orthogonal Functions (EOFs), as in González (2018)). In this study, the clustering analysis is applied to daily fields of sea level pressure in order to keep as much information as possible about the data, also taking into account the extreme values.

The number of clusters k to generate has to be specified in advance. Fereday et al. (2008) assessed the optimal number of clusters and concluded that there is no objective choice of the number of clusters. Also, they found that for small k values the full range of patterns is not correctly represented, while if a large k is chosen different clusters look very similar. The number of clusters generated in this study is $k = 4$, corresponding to the weather regimes defined in Section 1.3: NAO+, NAO-, Blocking and Atlantic Ridge.

Weather regimes are calculated using two different methods:

- Method 1: observed weather regimes are calculated by a cluster analysis with the k-means algorithm. After that, simulated weather regimes are calculated by projecting them on the observed ones. This projection is carried out with the *minimum Euclidean distance* method. With this method, the modelled weather situations are forced to fit into the observed ones, and so it is analysed how often the model simulates situations that fit into the observed patterns.
- Method 2: both observed and simulated weather regimes are calculated independently by a cluster analysis with the k-means algorithm. This method shows how the model defines its own weather regimes and allows to compare the spatial patterns of modelled and observed dominating weather patterns.

After obtaining the weather regimes for all seasons, all members and both methods, it is necessary to match the clusters, since the clustering algorithm does not provide them in a pre-defined order. For example, cluster 1 can be NAO+ in one case and Blocking in another case. To do so, weather regimes obtained for every case are sorted based on their spatial correlation with the observed ones in winter season, displayed in Figure 2a.

3.3 Metrics

The metric used to measure the spatial correlation between the ensemble mean of the weather regimes obtained after applying the k-means algorithm and the reference weather regimes is the Anomaly Correlation Coefficient (ACC). It is defined in terms of deviations from mean historical climatological values, as can be seen in Equation 1 (Murphy, 1995). Its value can be between -1 and +1. If the ACC is equal to +1, it means that the maps are positively correlated in a perfect way. On the contrary, if it is equal to -1, the maps are inversely correlated. If this coefficient is zero, there is no linear correlation between the two maps.

$$ACC = \frac{\sum_{i=1}^{n}(v_i - \bar{v})(o_i - \bar{o})}{\sqrt{\sum_{i=1}^{n}(v_i - \bar{v})^2 \sum_{i=1}^{n}(o_i - \bar{o})^2}} \tag{1}$$

Where n is the number of grid points, v_i represents the values of the map wanted to match, $\bar{v}$ its climatological value, o_i the values of the reference map and $\bar{o}$ the climatological value of that reference map.

To measure time correlation, the correlation coefficient of Pearson r is used. Like the ACC, its value is between -1 and +1 and is defined according to Equation 2 (Gorgas et al., 2015). This coefficient is used to measure the correlation between the reanalysis and the ensemble mean of both the historical simulations and the decadal predictions. In the case of decadal predictions, the correlation between the different members is also measured.

$$r = \frac{\sigma_{v,o}}{\sigma_v \sigma_o} \tag{2}$$

Where $\sigma_{v,o}$ is the covariance between v and o and σ_v and σ_o the variance of the time series.

To analyse whether the time series correlation between experiments and reanalysis is statistically significant, a t-test is carried out. In this test, the test statistic follows a Student's t-distribution with $n-2$ degrees of freedom and a significance level, denoted α, and the correlation is significant if Equation 3 is fulfilled (Gorgas et al., 2015). The number of years used in this study is 51, so there are 49 degrees of freedom.

$$\frac{|r|\sqrt{n-2}}{\sqrt{1-r^2}} \geq t_{\alpha/2,n-2} \tag{3}$$

This test is also used to assess the significance of the correlation between the SST and the frequency of the weather regimes.

It should be noted that the significance of correlations may be overestimated in cases that have been averaged over different years, as the series have been smoothed, which reduces the degrees of freedom. This would be possible to fix by using an effective size of the time series (Metz, 1991).

To compare the initialization improvement of the simulations, cases which the confidence intervals of the correlation coefficient of historical simulations and decadal predictions do not overlap are sought.

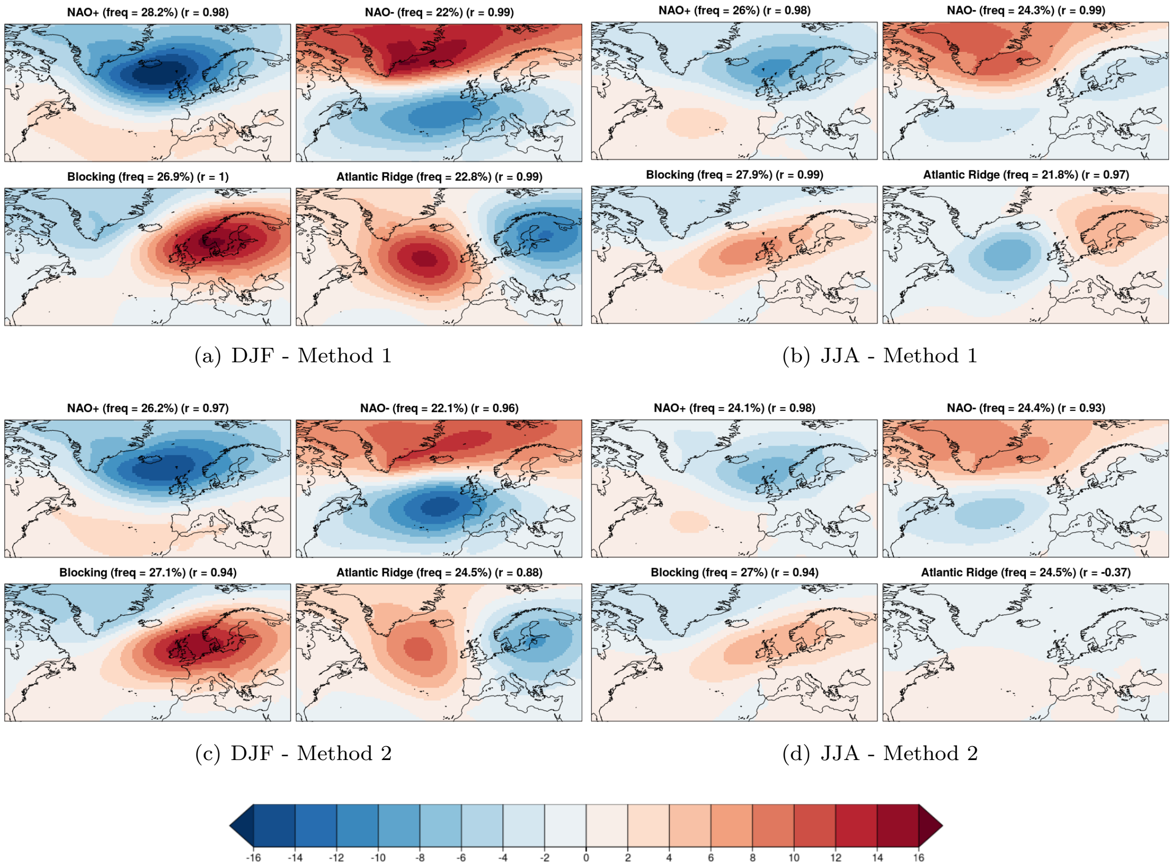

Figure 3. Composites of the averaged sea level pressure anomalies (hPa) of the simulated weather regimes in winter and summer seasons with both methods for the 1960-2010 period using historical runs. The frequency and the spatial correlation with the observed regimes are also displayed for each weather regime.

4 Results and discussion

Due to the amount of figures, only those referring to normal seasons (DJF and JJA) will be shown here. However, the figures corresponding to the extended seasons (NDJFMA and MJJASO) and to averaging different numbers of years (from 2 to 5) to carry out the comparison are shown in Annex A (for the historical simulations) and Annex B (for the decadal predictions). In the case of some figures, all results are shown together (including those of the extended seasons) for a better comparison.

4.1 Historical simulations (No-Init)

In this section, the results of historical simulations, i.e., uninitialized simulations, are analysed.

Figure 3 shows the composites of the averaged sea level pressure anomalies of the simulated weather regimes in the winter and summer seasons with both methods applied to the 1960-2010 period. Also, the frequency of each weather regime and the spatial correlation with their respective observed clusters are displayed.

As it can be seen, the four clusters are more intense and better defined in the winter season. Similarly, the intensity of clusters is higher in method 1 than in method 2. This may be because, at the beginning of the k-means algorithm, maps may be assigned to some centroid that does not correspond to it because the clusters are not fully defined yet. On the contrary, in method 1, the clusters are already defined, so each map is projected onto the centroid that actually corresponds.

With respect to the spatial correlation between simulated and observed weather regimes, NAO+, NAO- and Blocking show a correlation between 0.98 and 1 for method 1 and a correlation between 0.93 and 0.98 for method 2. These results indicate that the spatial patterns of the weather regimes in the model are very similar to the observed weather regimes that occur in the analysed region. In the case of the Atlantic Ridge weather regime, it shows a good correlation for method 1, but it shows the lowest spatial correlation for method 2, with a value of 0.88 in winter and -0.37 in summer. The negative value of the correlation indicates that the cluster has been obtained spatially opposed to the observed one. Many times, using method 2, one of the clusters is obtained in its opposite form, which

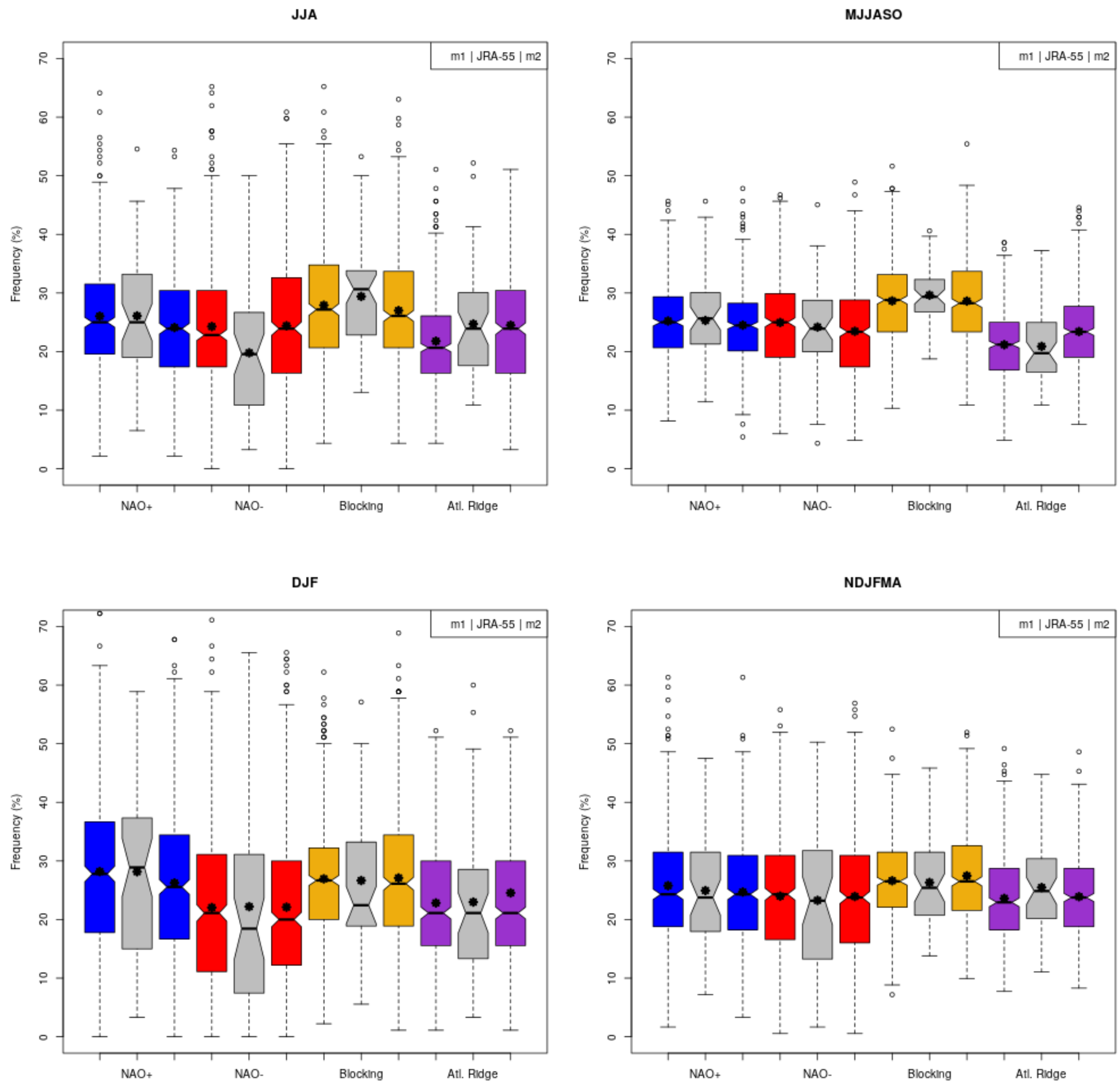

Figure 4. Box-and-whisker diagrams of the time series of each weather regime in short and extended seasons with both methods for the 1960-2010 period using historical runs. Grey boxes correspond to the reanalysis. On the left of each one, coloured boxes correspond to historical (No-Init) simulations and clusters identified with method 1 and, on the right, with method 2. The filled dots represents the mean of the time series and the unfilled dots the outliers. Historical simulation boxes have been obtained using the different members without averaging.

is normal when applying this algorithm. The spatial correlation is improved for every cluster in the extended season, due to more robust results when using a greater number of days. These composites relating to the extended season can be seen in Figure A.1 in Annex A. The high spatial correlation obtained with method 1 is largely a consequence of applying patterns identified based on reanalysis data to the model, while the good correlation with method 2 means the model defines the cluster distributions reasonably similar to the observed climate.

The different cluster frequencies are between 21.7% and 28.2%, similarly to the reanalysis. Blocking is the most frequent weather regime in summer for both methods (same as in the reanalysis), while NAO+ is the most frequent one in winter for method 1 and in the reanalysis (but is second behind Blocking in method 2). However, weather regimes do not occur every year with the same frequency, and there is a variability of occurrence from year to year. This variability can been seen in Figure 4, where a box-and-whisker diagram shows the mean, the quartiles, the extremes values and the outliers[1] of the annual time series of each weather regime. The grey boxes correspond to the reanalysis, while the coloured boxes correspond to the historical experiments (with method 1 at the left of

[1]An outlier is a value that lies more than one and a half times the length of the box from either end of the box, i.e., the interquartile range.

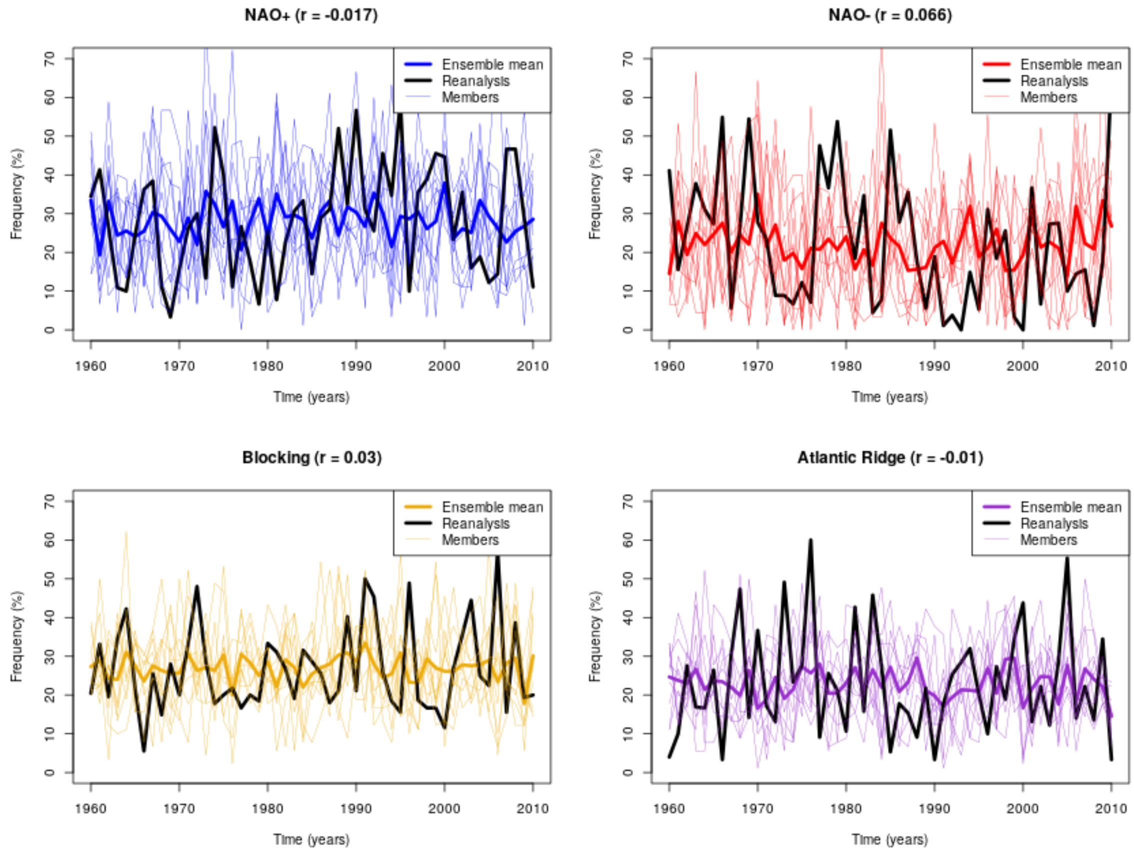

(a) DJF - Method 1

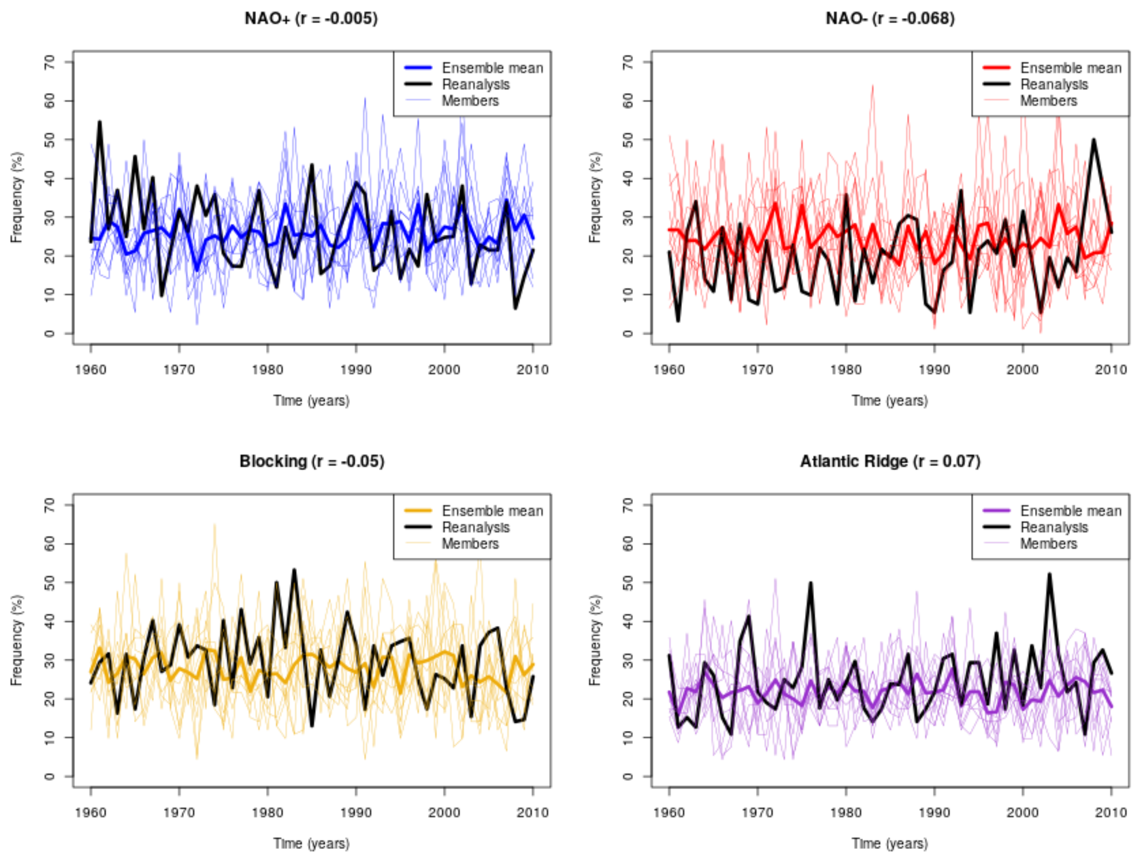

(b) JJA - Method 1

Figure 5. Time series of the frequencies of the simulated and observed weather regimes in winter and summer seasons with both methods for the 1960-2010 period using historical runs. The thin coloured lines correspond to each member, the thick coloured lines to the ensemble mean and the black lines to the reanalysis. The time series correlations between simulations and reanalysis are also displayed for each weather regime.

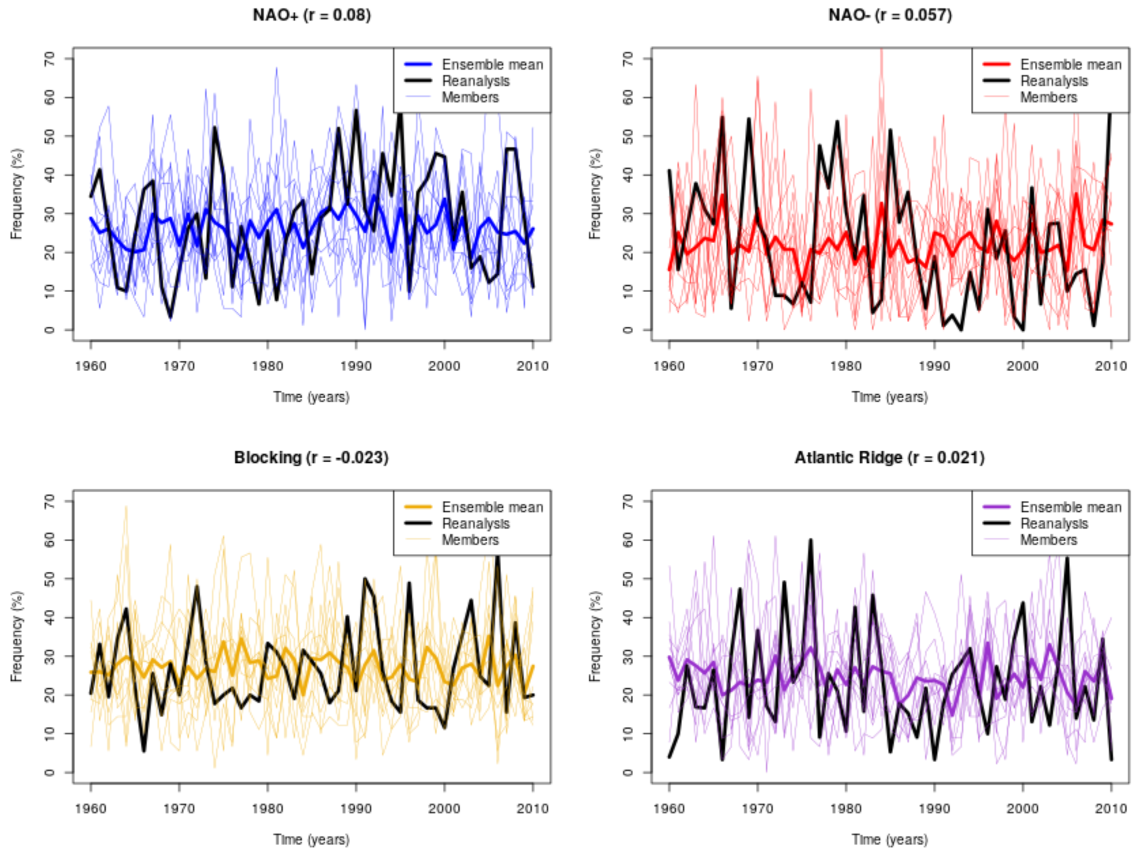

(c) DJF - Method 2

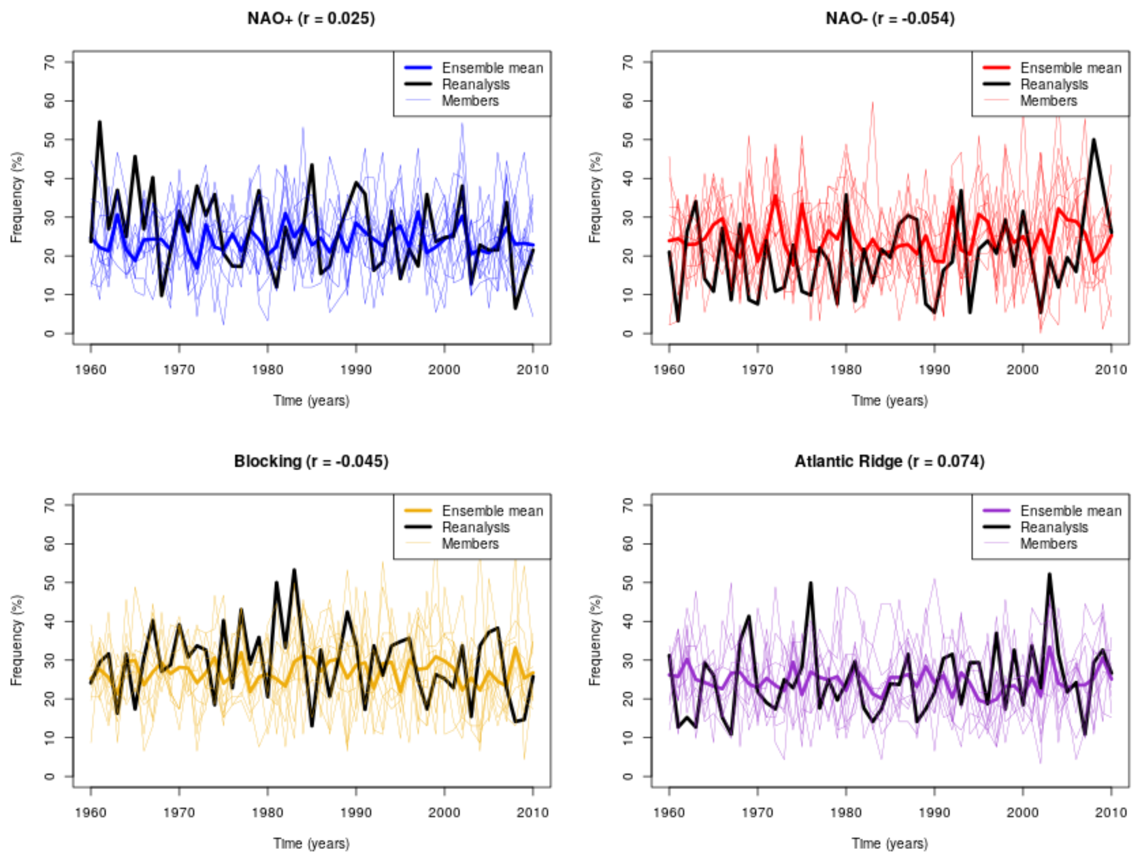

(d) JJA - Method 2

Figure 5. (Cont).

each observed box and with method 2 at the right). The mean frequency is also displayed with dots in every box.

The box-and-whisker diagrams indicate a generally good match between the observed and simulated variability of the weather regimes. For most of them, both the mean, the median and the quartiles of the simulated time series show a value similar to those of the observed time series. Nevertheless, there are some cases in which simulations do not match the reanalysis. For example, during the summer, the frequency of NAO- is overestimated with both methods and the frequency of Atlantic Ridge is underestimated using method 1. The opposite happens in the extended summer, when this last cluster is overestimated with method 2. During the winter, the model slightly underestimates the mean frequency of NAO+ and overestimates the one of NAO-. Also, the model underestimates the spread of both NAO phases, while only NAO- spread is underestimated in the extended winter. During the extended summer, there is an overestimation of the frequency spread of the Blocking weather regime. The frequencies of the rest of weather regimes in extended seasons match very well with the reanalysis.

As it can be seen, the most frequent regime during the summer is Blocking, both for the normal season and for the extended one. During the winter, NAO+ and Blocking regimes are the most frequent ones for both the reanalysis and the experiments, while in the extended winter the frequencies of all clusters are similar, with Blocking being a little higher.

With reference to the frequencies of the weather regimes, they show a wider spread in winter than in summer, specially both phases of the NAO, for which the spreads are the widest ones. In contrast, the narrowest spread occurs during the extended seasons, especially in extended summer, when the frequencies of all the weather regimes show the narrowest spread for both the reanalysis and the simulations.

The diagrams for averaging from 2 to 5 years to see the lower frequency oscillations in the atmosphere can be seen in Figure A.2 in Annex A. The averaging has been carried out with a left-aligned moving mean, so data up to 2014 had to be used for the average of the last years. They show less frequency spread as more years are averaged and, generally, simulations match with reanalysis using both methods. However, one thing to note is the underestimation by the model of the NAO- spread during the normal and extended winter season and the overestimation of the frequency value during the summer season.

Figure 5 shows the time series of the frequencies of the simulated and observed weather regimes in winter and summer season with both methods for the 1960-2010 period. The time series related to extended seasons can be seen in Figure A.3 in Annex A. The thin coloured lines correspond to each member of the ensemble, while the thick coloured lines correspond to the ensemble mean and the black lines to the reanalysis. The series correlation between simulations and reanalysis is also displayed above each graph.

As discussed below, in general, the model reproduces well the frequency variability of all weather regimes, since each member oscillates in the range of the reanalysis. However, since the simulations are not initialised, the different phasing between them causes that the correlations between the observed time series and the ensemble mean of the historical simulations are close to zero. This low correlation and absence of trend suggests that external forcings during the period under analysis do not project changes in the frequency of weather regimes.

4.2 Decadal predictions (Init)

In this section, a similar analysis to the previous one is carried out, but for the initialised decadal predictions. In the same way, figures of the spatial distribution, box-and-whisker diagrams and time series of the weather regimes are shown.

As explained in Section 1.2, initialization consists in introducing the observations as initial conditions of the model run. This is intended to phase in the oscillations of the climate system in order to try to predict its evolution. For this study, results of decadal predictions, which are initialized each year in November, are analysed from the first to the fifth forecast year, also assessing all the possible combinations of averages of these years.

Figure 6 shows the composites of the averaged sea level pressure anomalies of the predicted weather regimes in winter and summer with both methods for the forecast year 1. As for the figures of the historical simulations, the frequency of each cluster and the spatial correlation with the reanalysis are shown. The same figure for the extended seasons can be seen in Figure B.1 in Annex B.

The averaging of the different forecast years does not relevantly affect the composites, as the model simulates the same weather regimes for all predicted years (not shown). In addition, with method 1 it assigns to each cluster very similar frequencies to those obtained in the historical simulations and all clusters have a nearly perfect spatial correlation with the reanalysis. Also, they are still more defined in winter than in summer.

On the contrary, the spatial correlation of NAO+ and Blocking presents lower values than in historical simulations with method 2 and, similarly,

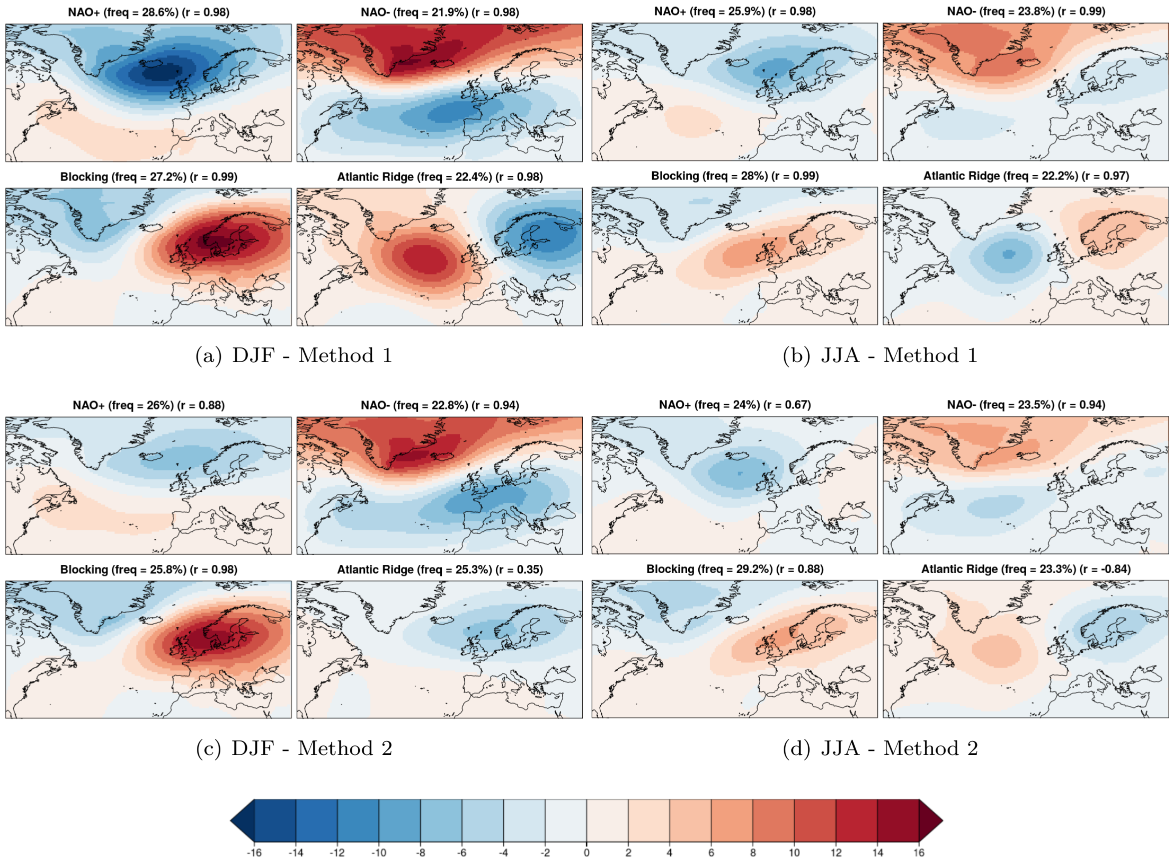

Figure 6. Composites of the averaged sea level pressure anomalies (hPa) of the predicted weather regimes in winter and summer seasons with both methods for the 1960-2010 period using decadal predictions for year 1. The frequency and the spatial correlation with the observed ones are also displayed for each weather regime.

the Atlantic Ridge has a negative spatial correlation with this method in some cases, most common in summer, but its absolute value has increased respect to that of the historical simulations.

When comparing normal seasons and extended, extended summer has a higher spatial correlation than normal summer. With regard to winter, the correlation is slightly higher in the extended season with method 1 and lower with method 2.

As explained above, the frequency of each weather regime is not the same every year, but varies from year to year. This variability of occurrence during the analysed period can be seen in the box-and-whiskers diagrams shown in Figure 7. They provide information on the mean, median, quartiles, extreme values and outliers of the time series of the weather regimes. These time series are related to reanalysis (grey boxes, same as in Figure 4) and predictions (to the left of each grey box with method 1 and to the right with method 2).

The diagrams are very similar to those of historical simulations, showing similar values of the mean frequency, median and interquartile ranges. This similarity makes sense since it is the same model, so it tends to reproduce the same variability. Nevertheless, the most notable difference is the lesser presence of outliers in the decadal predictions, so these predictions result in fewer unusual values, comparing better to the reanalysis, which have few or no outliers.

The initialised predictions still have the same biases as the non-initialized simulations. The frequency of NAO+ is well simulated in general, being a little underestimated in the short winter, where both the mean and the spread are underestimated with method 2. With respect to NAO-, the model still overestimates the value of its frequency with both methods in summer, while it slightly underestimates its spread in the extended winter, similarly to historical simulations. Another repeated biases are the overestimation of the Blocking frequency spread, the overestimation of its frequency in winter and the underestimation in summer. This does not happen in the extended winter, when its variability is very well reproduced. The frequency of the Atlantic Ridge regime is reasonably well simulated during the winter. However, during the summer there is an underestimation with method 1 in the short season and an overestimation with method 2 in the extended season.

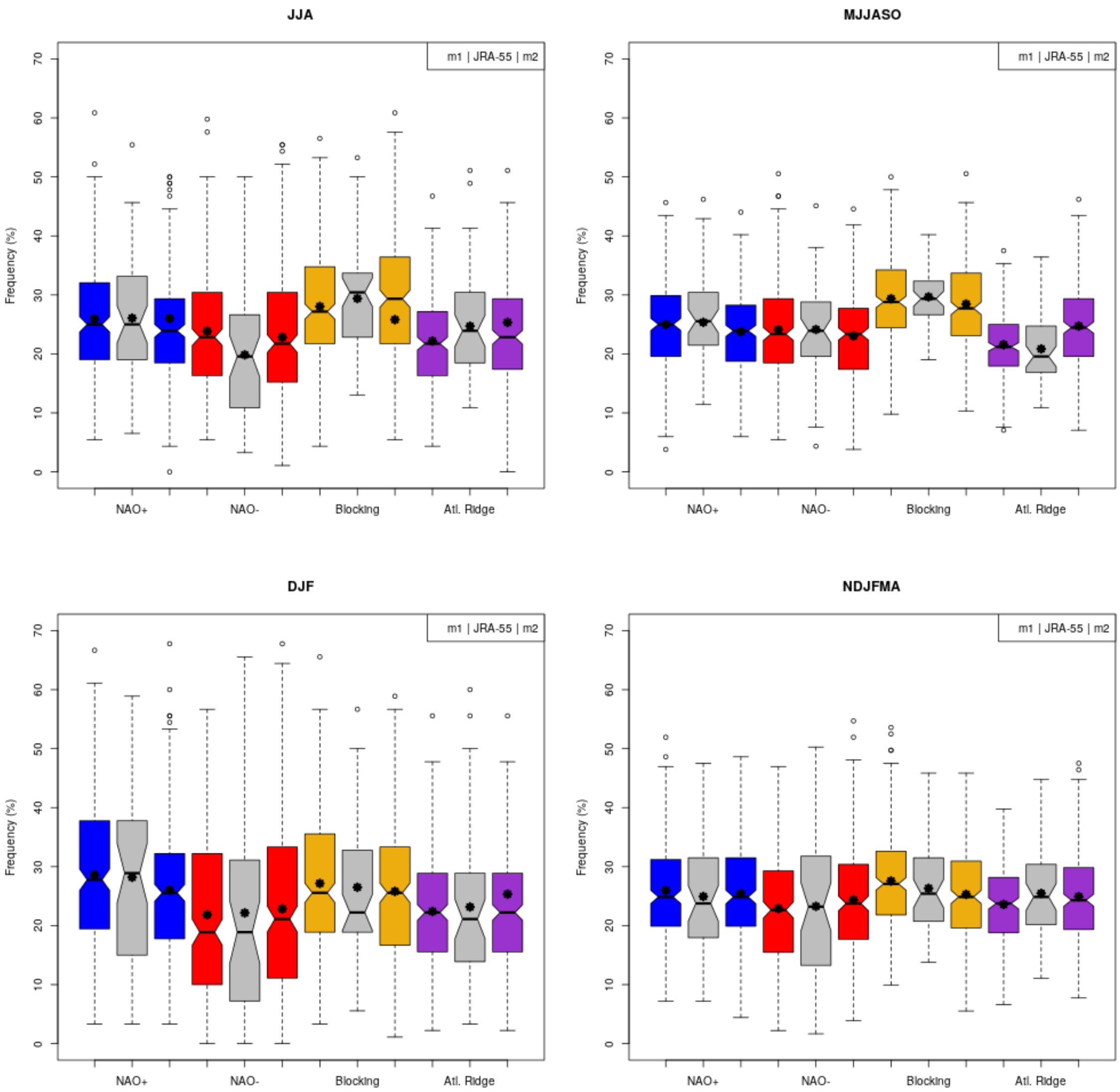

Figure 7. Box-and-whisker diagrams of the time series of each weather regime in short and extended seasons with both methods in 1960-2010 period using decadal predictions for year 1. Grey boxes correspond to reanalysis. On the left of each one, coloured boxes correspond to predictions with method 1 and, on the right, with method 2. The filled dots represents the mean of the time series and the unfilled dots the outliers. Decadal predictions boxes have been made with the different members without averaging.

The diagrams related to the prediction of the second to fifth year, shown in Figure B.2 in Annex B, have the same behaviour as that of year 1. In general, they overestimate and underestimate the frequency of the different regimes in the same seasons as the previous figure. Similarly, the number of outliers continues to be lower than that obtained in historical simulations.

Analogous to what was done in the historical simulations, the average of different forecast years was done to filter the signal and try to see the lower frequency oscillations of the climate system. The prediction for year 1 is considered to be that of the same year in which it is initialized (it is important to remember that predictions are initialized in November, so lead year 1 ends in October of the following year). The results for all combinations of forecast year averages are shown in Figure B.3. In order to make the average, data from decadal predictions were necessary until 2014, since the average has been calculated with a left-aligned moving mean. These diagrams show a narrower spread as they are averaged over a greater number of years. Similarly, they show, in general, fewer number of outliers with more averaged years. However, the same cases remain where the model overestimates or underestimates the mean frequency or spread of the time series.

The model generally reproduces well both the value and the spread of the frequency of the weather regimes, but for their prediction it is important to increase the temporal correlation to know periods in which a regime will be more or less frequent than normal. Figure 8 represents the time series

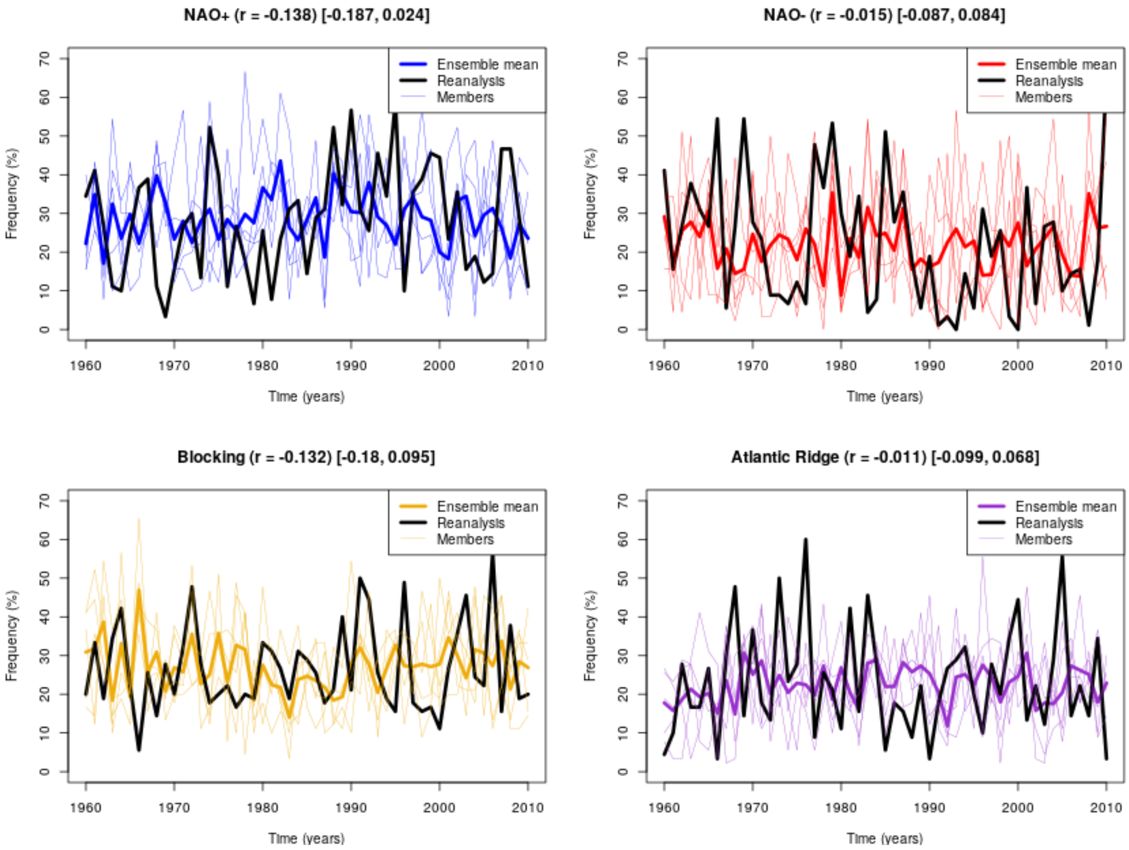

(a) DJF - Method 1

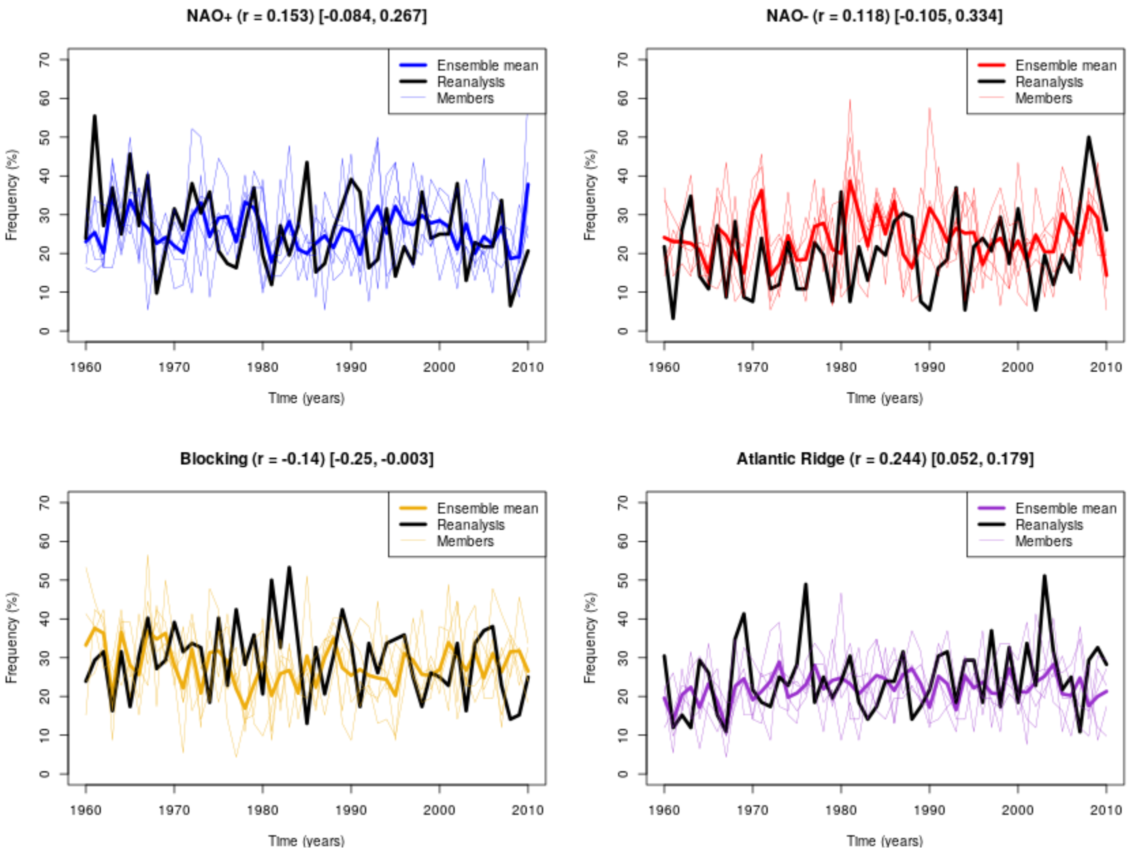

(b) JJA - Method 1

Figure 8. Time series of the frequencies of the predicted and observed weather regimes in winter and summer seasons with both methods for the 1960-2010 period using decadal predictions for year 1. The thin coloured lines correspond to each member, the thick coloured lines to the ensemble mean and the black lines to the reanalysis. The time series correlations between predictions and reanalysis are displayed for each weather regime, also showing the maximum and minimum value of the correlation calculated from each member separately.

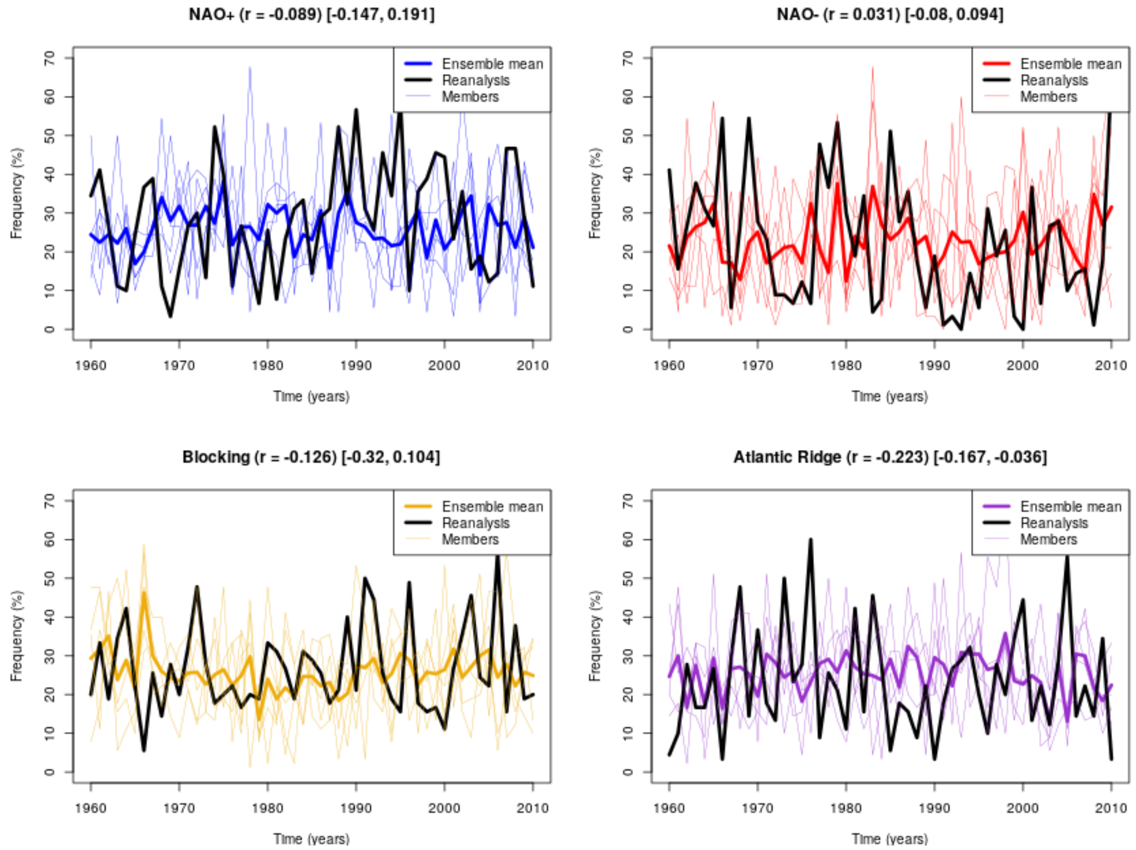

(c) DJF - Method 2

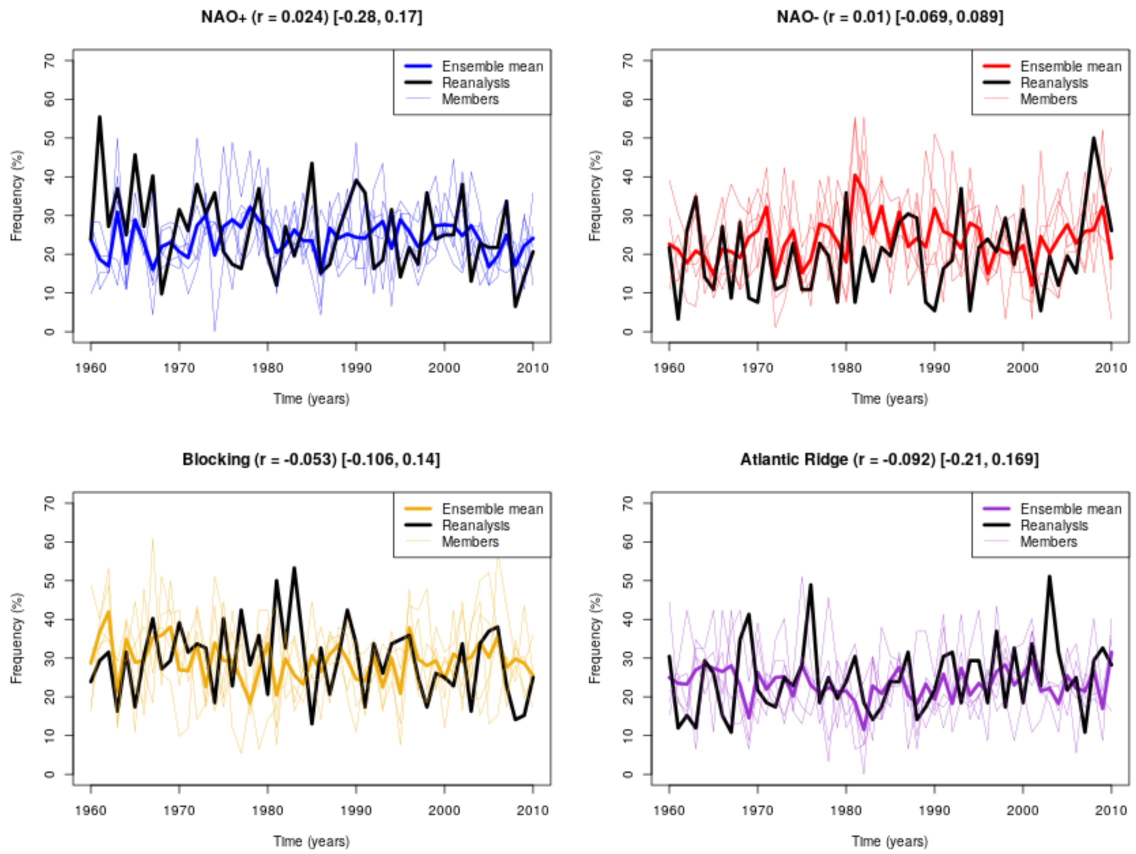

(d) JJA - Method 2

Figure 8. (Cont).

of the observed frequency of the weather regimes (black line), those predicted by each member (thin coloured lines) and the ensemble mean of the predictions (thick coloured line) using decadal predictions for year 1. Also, the time series correlations between predictions and reanalysis are displayed for the ensemble mean and for the maximum and minimum value obtained from each member taken separately. The figures corresponding to the predicted years 2, 3, 4 and 5 can be seen in Figures B.5 - B.8 in Annex B and the ones corresponding to averaging all possible combinations of forecast years in Figures B.9 - B.18.

One of the main differences with respect to the time series of historical simulations is that, when calculating the ensemble mean by averaging the different members used, the variability is cancelled slightly less during the whole period. This is due to the fact that, with the initialization, an attempt is made to put the members of the ensemble in phase. As in historical simulations, as a larger number of years is averaged, the spread of the time series decreases.

It should also be noted that the time series of the frequencies in the extended seasons have a lower spread than in the normal seasons. This may be due to the greater presence of transition days during the autumn and spring months, which are assigned to the nearest centroid in the k-means algorithm, but which would not really have to belong to any weather regime and have been assigned almost randomly. Another cause is the greater number of days used for each value in the time series (~90 for normal seasons and ~180 for extended seasons), which smooths the series.

4.3 Impact of model initialization

Figure 9 summarizes the correlation between simulated and observed time series of the weather regimes obtained with historical simulations and decadal predictions. The columns correspond to the historical simulations averaged over X years (No-Init_X) and to the decadal predictions averaged from year X to year Z (yX-Z). The rows correspond to the different seasons analysed and the method used to define the clusters is displayed in brackets. The correlations relative to the positive phase of the NAO are displayed in the left triangles, the negative phase in the lower ones, the Blocking in the right ones and the Atlantic Ridge in the upper ones. Red colours indicate that the correlation coefficient is positive, while blue colours indicate that it is negative. Those correlations that are positive and statistically significant at 95% confidence level are marked with a dot in the figure. It should be noted that the correlation can be overestimated as more years are averaged because the series become smoother.

As it can be seen, the time series relative to the historical simulations present a correlation coefficients very close to zero. In the averages of several years of these simulations the correlation increases a little, but it is a consequence of the smoothing, as explained above. The correlation coefficients corresponding to the decadal predictions increase in some cases, but also decrease in others.

Although every weather regime shows both positive and negative correlation depending on the season and the chosen forecast year, it seems that Blocking is the regime that presents the highest

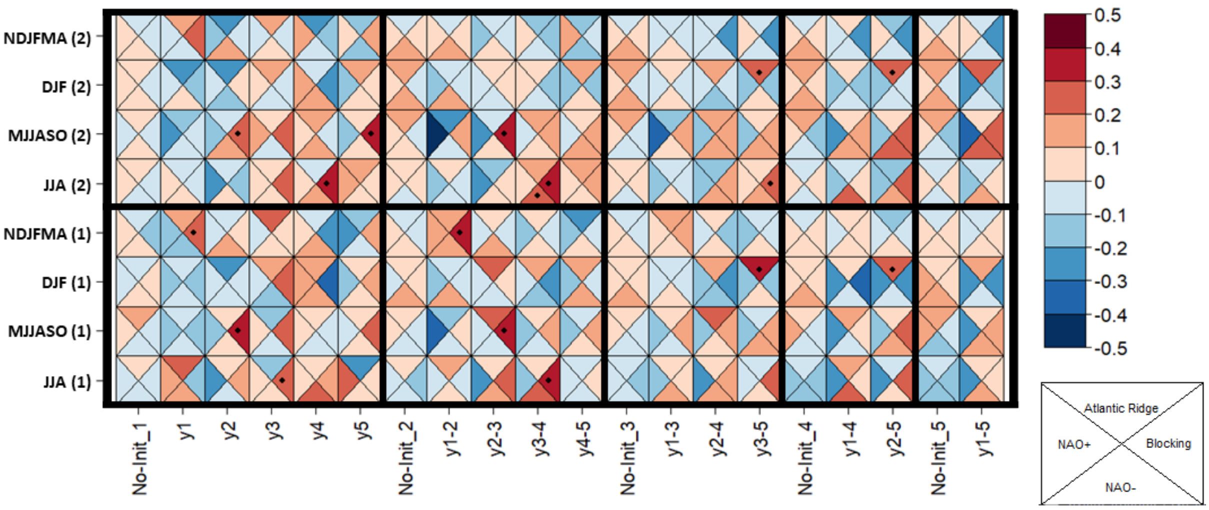

Figure 9. Time series correlation between simulations and reanalysis of each weather regime. In the horizontal axis, "No-Init_X" refers to historical simulations averaged X years, while "yX-Z" refers to decadal predictions averaged from year X to year Z. In the vertical axis, the number in brackets indicates the method used. Dots indicate the correlation is positive and statistically significant at 95% confidence level with a t-test.

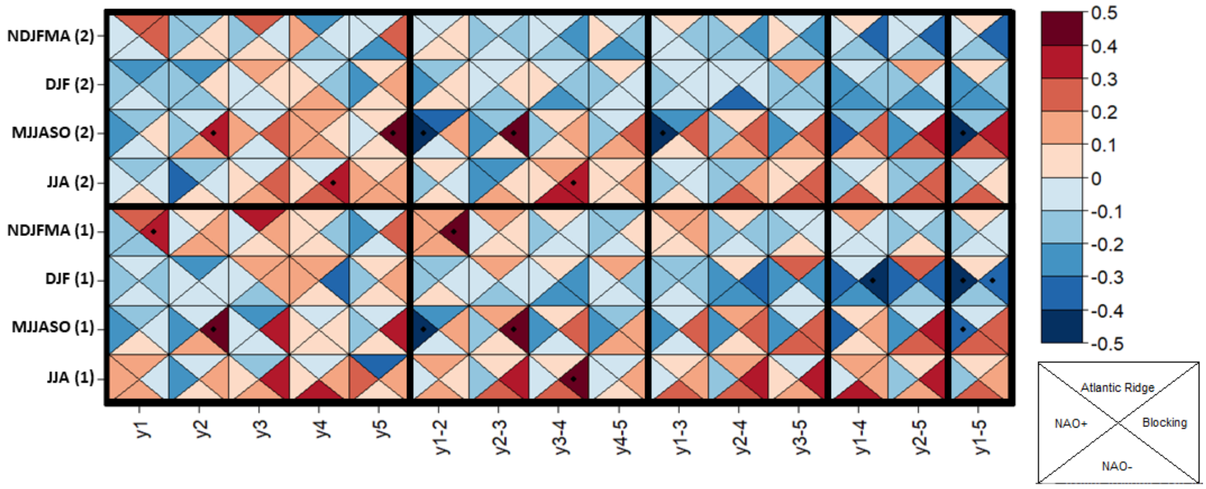

Figure 10. Time series correlation difference between historical simulations and decadal predictions. In the horizontal axis, "yX-Z" refers to predictions averaged from year X to year Z. In the vertical axis, the number in brackets indicates the method used. Dots indicate the correlation of the decadal prediction is statistically different to that of the historical simulation at 95% confidence level.

correlation with the reanalysis and has a few cases that show statistically significant correlations at the 95% confidence level with the t-test. This occurs, above all, during the summer season, both normal and extended, with both methods. The forecast years in which this correlation is greatest are year 2, 3 and 4, including some of the averages in which they are considered. For the winter months, the Blocking regime also shows cases where the correlation is significant, but only using method 1 for year 1 and the average of forecast years 1 and 2.

The next regime with the highest number of statistically significant cases is the Atlantic Ridge, which achieves the highest correlation with both methods averaging the last forecast years analysed during the winter season, i.e., 2-5 and 3-5 forecast years. Then follows the NAO- regime, which has only one time series that correlates significantly with the reanalysis: averaging the predicted years 3 and 4 for summer with method 2. Finally, the positive phase of the NAO shows no statistically significant correlation between its simulated and observed time series.

With the aim of highlighting where the initialization of the model has had a positive impact on the predictability of weather regimes, the difference between the correlation coefficient of the decadal predictions and that of the historical simulations is calculated, and is displayed in Figure 10. The red colours correspond to those cases in which the impact of initialisation has been positive, i.e., the correlation coefficient has been increased. On the contrary, the blue colours indicate that the initialization has had a negative impact on the predictions. In this case, dots indicate the correlation coefficient of the decadal prediction is statistically different to that of the historical simulation at 95% confidence level. Thus, red colour with dot means the correlation coefficient of the initialised simulation is significantly greater and blue colour with dot means it is significantly lesser.

As the previous one, this figure does not show a clear pattern of the impact of initialization on improving the correlation of weather regimes time series. Their predictability is improved in some cases and worsened in others. Nevertheless, it seems that Blocking and NAO- regimes are the ones that have most increased their predictability by the initialization of the model.

In the case of Blocking, the correlation coefficient has increased its value in summer, especially in the extended season, in which are all significant improvements obtained. This occurs with both methods, and the increase is higher for the second and third forecast years. This improvement in the simulation of the Blocking frequency also occurs in the first forecast year and in the average of the first and the second year during the extended winter. On the other hand, there is a worsening in its simulation during the winter when averaging years 1-4 and 1-5.

The second regime that has most increased the correlation of its time series of frequency with reanalysis, NAO-, shows an improved correlation with both methods in summer. However, there are not simulations that have increased the correlation coefficient significantly due to initialization.

The other two regimes do not show so many cases in which initialization can provide an extra predictability of their frequency. Neither Atlantic Ridge nor NAO+ show cases where improvement has been statistically significant. Regarding Atlantic Ridge, the first and third forecast years show the greatest improvements in the simulation of this

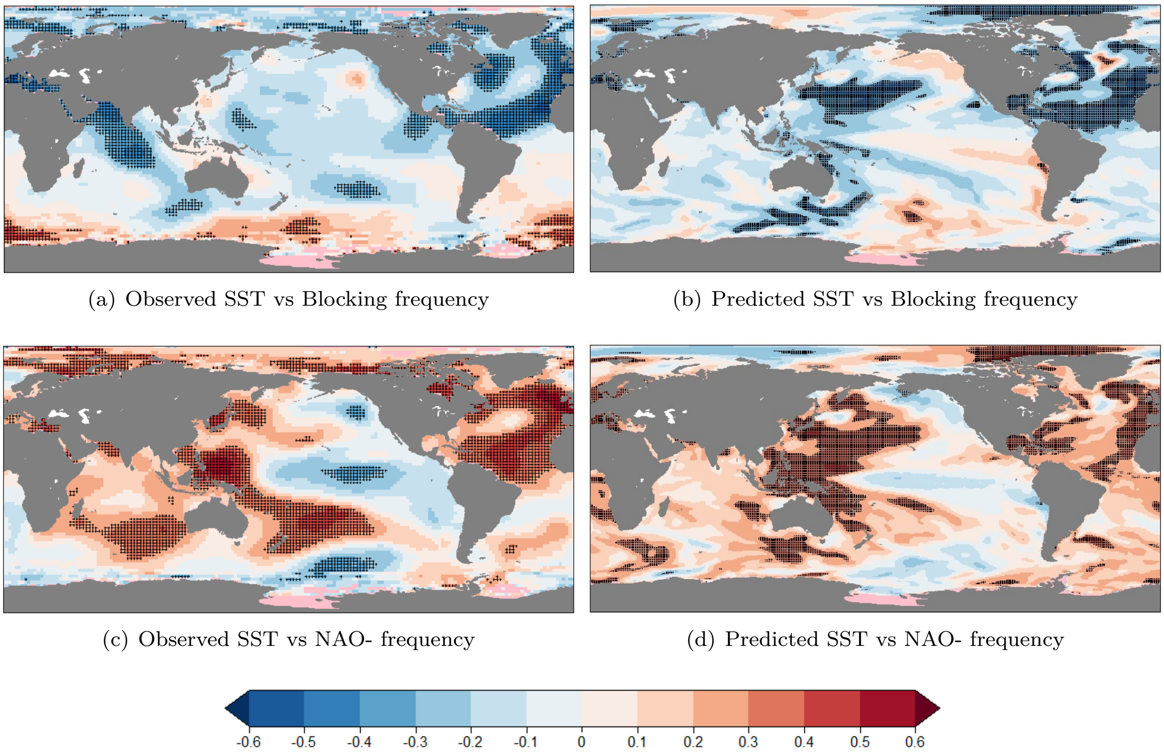

(a) Observed SST vs Blocking frequency

(b) Predicted SST vs Blocking frequency

(c) Observed SST vs NAO- frequency

(d) Predicted SST vs NAO- frequency

Figure 11. Time series correlation between the observed and predicted (for forecast year 2) SST and the observed frequency of Blocking and NAO- regimes in the extended summer. Data for the 1962-2012 period have been used for the observed frequency of the regimes and the observed SST, and data for the forecast year 2 of the simulations initialized in the years 1960-2010 for the predicted SST. Crosses indicate the correlation is significant in that grid point at 95% confidence level with a t-test.

weather regime. With respect to NAO+, its correlation after initialization worsens in almost all cases. In addition, it shows numerous cases in which initialization significantly decreases correlation, especially in winter and extended summer. Then, the initialization does not have a clear positive impact for this regime.

In general, the season that has the best impact due to the model initialization is the summer, both the normal and the extended season, although it also shows cases in which initialization has had a negative impact.

4.4 Teleconnections with the Sea Surface Temperature

As seen in the previous section, the greatest improvements after model initialization have been found during the second and third year predicted for the Blocking regime during the summer, mainly in the extended season. To try to understand the reason for this improvement, we look for teleconnections with the SST, variable that presents a slow variability and that could contribute to the model skill in the prediction of the Blocking frequency. Then, observed frequency of the weather regimes and both predicted (from initialized simulations) and observed SST are compared.

Figure 11 shows the time series correlation between the observed and predicted (for forecast year 2) SST and the observed frequency of Blocking and NAO- regimes in the extended summer for the 1962-2012 period. Therefore, data for the 1962-2012 period have been used for the observed frequency of the regimes and the observed SST, and data of the initialised simulations in the years 1960-2010 for the forecast year 2 for the predicted SST. Crosses indicate the grid points at which correlation is statistically significant at the 95% confidence level with a t-test. Regime frequencies are taken from the JRA-55 reanalysis and the observed SST is taken from the ERSST.v4 dataset.

The Blocking regime is associated with periods of drought, heat waves and flooding over Europe. Blocking events, which usually last 5 or more days, also affect wind patterns and, therefore, ocean circulation and downward and upward pumping of water. Häkkinen et al. (2011) show frequent atmospheric Blocking coincide over AMV time scales and suggest that Blocking frequency is more important than the NAO in climate variability in the Atlantic Ocean. In addition, Blocking is also related to warm water displacements to the north, both on the surface and in lower layers. In Häkkinen et al. (2011), they found that the warmest periods occur in the North Atlantic Ocean when the frequency of the Blocking regime is high during the winter. However, as can be seen in Figure 11, this does not happen during the extended summer season, but the SST in the North Atlantic is negatively correlated with the frequency of the Blocking regime, that is, when this ocean is colder, Blocking is more frequent. This is shown for both reanalysis and predictions. Therefore, the initialization of the model two years earlier has improved the prediction of the Blocking frequency and is probably due to the initialization of the SST in the North Atlantic region, as it is where the two figures show a great similarity.

Regarding the other regime, a high correlation has also been found in the North Atlantic region between the SST and the frequency of the NAO-. In this case the correlation is positive, so anomalous high temperatures of the North Atlantic Ocean are associated with higher frequencies of this regime, as can be seen in Figures 11c y 11d. In this case, other regions such as the Western Pacific Ocean also show this positive correlation in both reanalysis and predictions. Thus, in addition to AMV, other modes of variability could influence the increase of the skill of the model by predicting this weather regime during the extended summer. This opposite-signed relationship between the NAO and the AMV was also found by Peings and Magnusdottir (2014) during the winter season, when the positive phase of the AMO is related to more frequent NAO-.

5 Conclusions

In this study, European weather regimes have been analysed for the 1960-2010 period in order to assess the impact of model initialization on their predictability. For that, both historical simulations and decadal predictions have been used.

The model simulates very well the spatial distribution of the weather regimes, showing a high spatial correlation with the reanalysis for both phases of the NAO and Blocking regimes for both methods (with slightly higher values with method 1). Regarding the AR, this regime shows the lowest spatial correlation, even being negative in some cases with method 2.

The most frequent regime during the summer season is Blocking and the least frequent regime is the NAO-. For the winter season, NAO+ and Blocking are the most frequent ones, mainly in the short season, while the frequencies are more similar in the extended winter.

Variability in historical simulations is cancelled out by averaging the different members of the ensemble due to the different phasing between the simulations. Thus, the temporal correlation of the ensemble mean with the reanalysis is always close to zero. If external forcings played an important role in the frequency of weather regimes, it would be expected that the historical simulation reproduce it when averaging all members, but they do not.

In general, the mean values of the frequencies of the four weather types are well simulated by the model. However, during the summer, the model overestimates the frequency of NAO- and underestimates the AR with method 1, and overestimates AR with method 2. During the winter, the model underestimates the spread of NAO- and overestimates that of Blocking. Also, the frequencies of all clusters show a narrower spread during the summer season.

In most cases, initialization does not provide significant improvements in the prediction of weather regimes. This may be due to the fact that the system loses memory very quickly (in a few days) and, when carrying out the study on averages of 3 and 6 months, the impact of initialization is not noticed.

Nevertheless, some situations have been found in which initialization has a positive impact on predictions and the skill of the model in predicting weather regimes time series has been significantly increased. This may be due to the fact that other components, such as the ocean and ice, have a longer memory and are better sources of predictability in decadal predictions. This memory can be transferred from the ocean to the atmosphere by teleconnections, as seen in the case of the SST. The season in which this improvement is greatest is the summer season, when the skill in NAO- and Blocking regimes prediction always improves for both individual and averaged forecast years with method 1. For method 2, the improvement is slightly lower for these two regimes, especially for the first years predicted. Regarding the other two regimes, Atlantic Ridge shows few improvement, while the predictability of NAO+ decreases in the initialised runs.

In general, this impact due to initialization is much greater in summer than in winter. Although the initialization is carried out in November, only Blocking and Atlantic Ridge regimes show a high correlation during the first forecast year in the extended winter season, which starts in November. The reason why the rest of the cases in the first forecast year are not improved may be due to the shock suffered by the model when it is initialized. This shock is due to the fact that the initial conditions given to the model for initialization are very different from its climatology and the model is not able to reproduce well the evolution of that state of the system (Pohlmann et al., 2017).

The frequency of Blocking and NAO- regimes may be influenced by the AMV and the initialization of the model is able to influence the North Atlantic region and increase the skill of the model predicting these two regimes.

There may be possible improvements to this study, such as using a more complex classification algorithm instead of the k-means, using anomaly initialization for the decadal predictions or using geopotential height at 500 hPa instead of sea level pressure during the summer to reduce spatial noise (Cortesi et al., 2019). Similarly, a improvement in the analysis of the correlation of time series that have been generated from the average of different simulated years would be to use an effective size of those time series.

In addition, the rest of the cases, both other years and other seasons, in which the correlation has been improved by initialization can be further investigated to understand this improvement in the model skill and to seek the sources of predictability that make it possible.

Acknowledgements

I would like to express my gratitude to Markus Donat, Deborah Verfaillie and Elsa Mohino for all their help and all that I have been able to learn from them. I acknowledge use of the s2dverification (http://cran.r-project.org/web/packages/s2dverification) and startR (https://cran.r-project.org/web/packages/startR/index.html) R software packages. I also thank Verónica Torralba, Nicola Cortesi, Lluis Palma, Roberto Bilbao and Francisco Javier Doblas-Reyes for their technical and scientific support.

References

Booth, B. B., N. J. Dunstone, P. R. Halloran, T. Andrews and N. Bellouin, 2012. Aerosols implicated as a prime driver of twentieth-century North Atlantic climate variability. *Nature*, 484(7393), 228. doi: 10.1038/nature10946.

Breivik, Ø., K. Mogensen, J. R. Bidlot, M. A. Balmaseda, and P. A.E.M. Janssen, 2015. Surface wave effects in the NEMO ocean model: Forced and coupled experiments. *Journal of Geophysical Research: Oceans*. ISSN 21699291. doi: 10.1002/2014JC010565.

Carrassi, A., R. J. T. Weber, V. Guemas, F. J. Doblas-Reyes, M. Asif, and D. Volpi, 2014. Full-field and anomaly initialization using a low-order climate model: A comparison and proposals for advanced formulations. *Nonlinear Processes in Geophysics*. ISSN 16077946. doi: 10.5194/npg-21-521-2014.

Christensen, J. H., K. K. Kumar, E. Aldrian, S. I. An, I.F.A. Cavalcant, M. de Castro, W. Dong, P. Goswami, A. Hall, J.K. Kanyanga, A. Kitoh, J. Kossin, N.-C. Lau, J. Renwick, D.B. Stephenson, S.-P. Xie, and T. Zhou, 2013. Climate phenomena and their relevance for future regional climate change. *Climate Change 2013 the Physical Science Basis: Working Group I Contribution to the Fifth Assessment Report of the Intergovernmental Panel on Climate Change*. ISBN 9781107415324. doi: 10.1017/CBO9781107415324.028.

Cleveland, W. S., and S. J. Devlin, 1988. Locally weighted regression: An approach to regression analysis by local fitting. *Journal of the American Statistical Association*. ISSN 1537274X. doi: 10.1080/01621459.1988.10478639.

Cortesi, N., V. Torralba, N. González-Reviriego, A. Soret, and F. J. Doblas-Reyes, 2019. Characterization of European wind speed variability using weather regimes. *Climate Dynamics*. ISSN 0930-7575. doi: 10.1007/s00382-019-04839-5. URL http://link.springer.com/10.1007/s00382-019-04839-5.

Doblas-Reyes, F. J., I. Andreu-Burillo, Y. Chikamoto, J. García-Serrano, V. Guemas, M. Kimoto, T. Mochizuki, L. R.L. Rodrigues, and G. J. Van Oldenborgh, 2013. Initialized near-term regional climate change prediction. *Nature Communications*, 4. ISSN 20411723. doi: 10.1038/ncomms2704.

Doblas-Reyes, F. J., J. Acosta Navarro, M. Acosta, O. Bellprat, R. Bilbao, M. Castrillo, N. Fuckar, V. Guemas, L. Lledó, M. Ménégoz, C. Prodhomme, K. Serradell, O. Tintó, L. Batté, D. Volpi, A. Ceglar, R. Haarsma, and F. Massonnet, 2018. Using EC-Earth for climate prediction research. (154):1–49. doi: 10.21957/fd9kz3.

Eyring, V., S. Bony, G. A. Meehl, C. A. Senior, B. Stevens, R. J. Stouffer and K.E. Taylor, 2016. Overview of the Coupled Model Intercomparison Project Phase 6 (CMIP6) experimental design and organization. *Geoscientific Model Development*, 9(LLNL-JRNL-736881). doi: 10.5194/gmd-9-1937-2016

Fereday, D. R., J. R. Knight, A. A. Scaife, C. K. Folland, and A. Philipp, 2018. Cluster analysis of North Atlantic-European circulation types and links with tropical Pacific Sea surface temperatures. *Journal of Climate*, 21(15):3687–3703. ISSN 08948755. doi: 10.1175/2007JCLI1875.1.

García-Serrano, J., V. Guemas, and F. J. Doblas-Reyes, 2015. Added-value from initialization in predictions of Atlantic multi-decadal variability. *Climate Dynamics*. ISSN 14320894. doi: 10.1007/s00382-014-2370-7.

González, C, 2018. Synoptic analysis of local snow events in Sierra de Guadarrama. Master Thesis, Complutense University of Madrid.

González-Reviriego, N., L. P. Caron, B. S. Murali, and F. J. Doblas-Reyes, 2018. Overview of near-term decadal climate prediction and its applications technical note. Technical report, Barcelona Supercomputing Center.

Gorgas, J., N. Cardiel, and J. Zamorano, 2015. Estadística Básica para Estudiantes de Ciencias. Departamento de Astrofísica y Ciencias de la Atmósfera, Facultad de Ciencias Físicas, Universidad Complutense de Madrid.

Häkkinen, S., P. B. Rhines, and D. L. Worthen, 2011. Atmospheric blocking and Atlantic multidecadal ocean variability. *Science*. ISSN 10959203. doi: 10.1126/ science.1205683.

Hazeleger, W., C. Severijns, T. Semmler, S. Stefanescu, S. Yang, X. Wang, K. Wyser, E. Dutra, J. M. Baldasano, R. Bintanja, P. Bougeault, R. Caballero, A. M.L. Ekman, J. H. Christensen, B. Van Den Hurk, P. Jimenez, C. Jones, P. Kållberg, T. Koenigk, R. McGrath, P. Miranda, T. Van Noije, T. Palmer, J. A. Parodi, T. Schmith, F. Selten, T. Storelvmo, A. Sterl, H. Tapamo, M. Vancoppenolle, P. Viterbo, and U. Willén, 2010. EC-Earth: A seamless Earthsystem prediction approach in action. *Bulletin of the American Meteorological Society*. ISSN 00030007. doi: 10.1175/2010BAMS2877.1.

Hodges, R. E., T. H. Jagger, and J. B. Elsner, 2014. The sunhurricane connection: Diagnosing the solar impacts on hurricane frequency over the North Atlantic basin using a space-time model. *Natural Hazards*. ISSN 0921030X. doi: 10.1007/s11069-014-1120-9.

Huang, B., V. F. Banzon, E. Freeman, J. Lawrimore, W. Liu, T. C. Peterson, T. M. Smith, P. W. Thorne, S. D. Woodruff, and H. M. Zhang, 2015. Extended reconstructed sea surface temperature version 4 (ERSST.v4).

Part I: Upgrades and intercomparisons. *Journal of Climate*. ISSN 08948755. doi: 10.1175/JCLI-D-14-00006.1.

Huijnen, V., J. Williams, M. Van Weele, T. Van Noije, M. Krol, F. Dentener, A. Segers, S. Houweling, W. Peters, J. De Laat, F. Boersma, P. Bergamaschi, P. Van Velthoven, P. Le Sager, H. Eskes, F. Alkemade, R. Scheele, P. Nédélec, and H. W. Pätz, 2010. The global chemistry transport model TM5: Description and evaluation of the tropospheric chemistry version 3.0. *Geoscientific Model Development*. ISSN 1991959X. doi: 10.5194/gmd-3-445-2010.

Ineson, S., A. A. Scaife, J. R. Knight, J. C. Manners, N. J. Dunstone, L. J. Gray, and J. D. Haigh, 2011. Solar forcing of winter climate variability in the Northern Hemisphere. *Nature Geoscience*. ISSN 17520894. doi: 10.1038/ngeo1282.

Kirtman, B., S. Power, J. A. Adedoyin, G. J. Boer, R. Bojariu, I. Camilloni, F. J. Doblas-Reyes, Fiore A. M., M. Kimoto, G. A. Meehl, M. Prather, A. Sarr, C. Schär, R. Sutton, G. J. van Oldenbourgh, G. Vecchi, and H. J. Wang, 2013. Near-term climate change: Projections and predictability. ISBN 9781107415324. doi: 10.1017/CBO9781107415324.023.

Knight, J. R., R. J. Allan, C. K. Folland, M. Vellinga, and M. E. Mann, 2005. A signature of persistent natural thermohaline circulation cycles in observed climate. *Geophysical Research Letters*. ISSN 00948276. doi: 10.1029/2005GL024233.

Kobayashi, S., Y. Ota, Y. Harada, A. Ebita, M. Moriya, H. Onoda, K. Onogi, H. Kamahori, C. Kobayashi, H. Endo, K. Miyaoka, and K. Takahashi, 2015. The JRA-55 Reanalysis: General Specifications and Basic Characteristics. *Journal of the Meteorological Society of Japan. Ser. II*. ISSN 0026-1165. doi: 10.2151/jmsj.2015-001.

Liu, W., B. Huang, P. W. Thorne, V. F. Banzon, H. M. Zhang, E. Freeman, J. Lawrimore, T. C. Peterson, T. M. Smith, and S. D. Woodruff, 2015. Extended reconstructed sea surface temperature version 4 (ERSST.v4): Part II. Parametric and structural uncertainty estimations. *Journal of Climate*. ISSN 08948755. doi: 10.1175/JCLI-D-14-00007.1.

Mariotti, A., P. M. Ruti, and M. Rixen, 2018. Progress in subseasonal to seasonal prediction through a joint weather and climate community effort. *Climate and Atmospheric Science*. doi: 10.1038/s41612-018-0014-z.

Meehl, G. A., L. Goddard, J. Murphy, R. J. Stouffer, G. Boer, G. Danabasoglu, K. Dixon, M. A. Giorgetta, A. M. Greene, E. D. Hawkins, G. Hegerl, D. Karoly, N. Keenlyside, M. Kimoto, B. Kirtman, A. Navarra, R. Pulwarty, D. Smith, D. Stammer, and T. Stockdale, 2009. Decadal prediction: Can it be skillful? *Bulletin of the American Meteorological Society*. ISSN 00030007. doi: 10.1175/2009BAMS2778.1.

Meehl, G. A., A. Hu, J. M. Arblaster, J. Fasullo, and K. E. Trenberth, 2013. Externally forced and internally generated decadal climate variability associated with the interdecadal pacific oscillation. *Journal of Climate*. ISSN 08948755. doi: 10.1175/JCLI-D-12-00548.1.

Metz, W., 1991: Optimal relationship of large-scale flow patterns and the barotropic feedback due to high-frequency eddies. *Journal of the Atmospheric Sciences*, 48, 1141–1159. doi: 10.1175/1520-0469(1991)048,1141:OROLSF.2.0.CO;2.

Murphy, A. H, 1995. The coefficients of correlation and determination as measures of performance in forecast verification. *Weather and Forecasting*. ISSN 08828156. doi: 10. 1175/1520-0434(1995)010<0681:TCOCAD>2.0.CO;2.

Orth, R., E. Dutra, I. F. Trigo, and G. Balsamo, 2017. Advancing land surface model development with satellite based Earth observations. *Hydrology and Earth System Sciences*. ISSN 16077938. doi: 10.5194/ hess-21-2483-2017.

Peings, Y. and G. Magnusdottir, 2014. Forcing of the wintertime atmospheric circulation by the multidecadal fluctuations of the North Atlantic ocean. *Environmental Research Letters*. ISSN 17489326. doi: 10.1088/ 1748-9326/9/3/034018.

Philipp, A., J. Bartholy, C. Beck, M. Erpicum, P. Esteban, X. Fettweis, R. Huth, P. James, S. Jourdain, F. Kreienkamp, T. Krennert, S. Lykoudis, S. C. Michalides, K. Pianko-Kluczynska, P. Post, D. R. Álvarez, R. Schiemann, A. Spekat, and F. S. Tymvios, 2010. Cost733cat - A database of weather and circulation type classifications. *Physics and Chemistry of the Earth*, 35 (9-12):360–373. ISSN 14747065. doi: 10.1016/j.pce. 2009.12.010.

Pohlmann, H., D. M. Smith, M. A. Balmaseda, N. S. Keenlyside, S. Masina, D. Matei, W. A. Müller, and P. Rogel, 2013. Predictability of the mid-latitude Atlantic meridional overturning circulation in a multi-model system. *Climate Dynamics*. ISSN 09307575. doi: 10.1007/s00382-013-1663-6.

Pohlmann, H., J. Kröger, R. J. Greatbatch and W. A. Müller, 2017. Initialization shock in decadal hindcasts due to errors in wind stress over the tropical Pacific. *Climate Dynamics*. 49: 2685. doi: 10.1007/s00382-016-3486-8.

Taylor, K. E., R. J. Stouffer, and G.A. Meehl, 2012. An overview of CMIP5 and the experiment design. ISSN 00030007.

Torralba, V., 2019. Seasonal climate prediction for the wind energy sector: methods and tools for the development of a climate service. PhD thesis, Complutense University of Madrid.

Uotila, P., D. Iovino, M. Vancoppenolle, M. Lensu, and C. Rousset, 2016. On the influence of sea-ice physics in multidecadal ocean-ice hindcasts. *Geoscientific Model Development Discussions*. doi: 10.5194/gmd-2016-187.

Annex A: Additional figures for the historical simulations

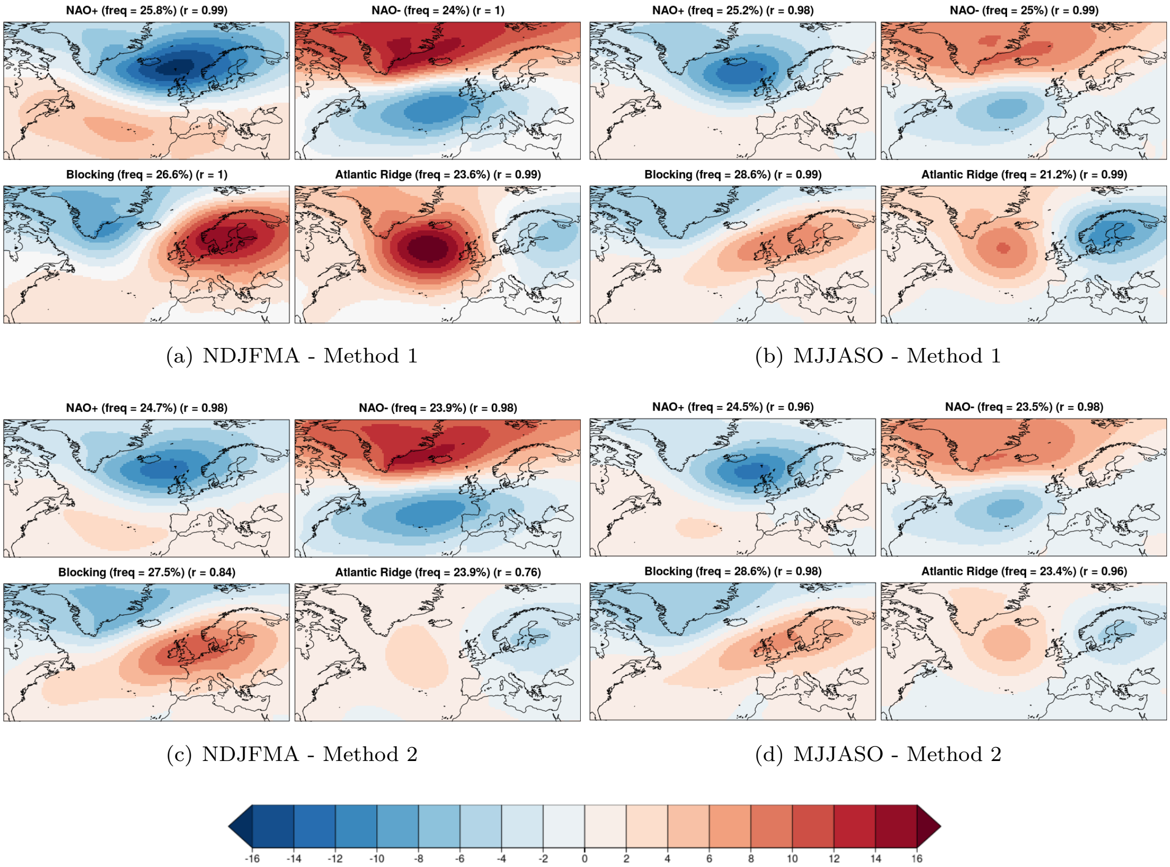

(a) NDJFMA - Method 1

(b) MJJASO - Method 1

(c) NDJFMA - Method 2

(d) MJJASO - Method 2

Figure A.1. Same as Figure 3, but for the extended seasons.

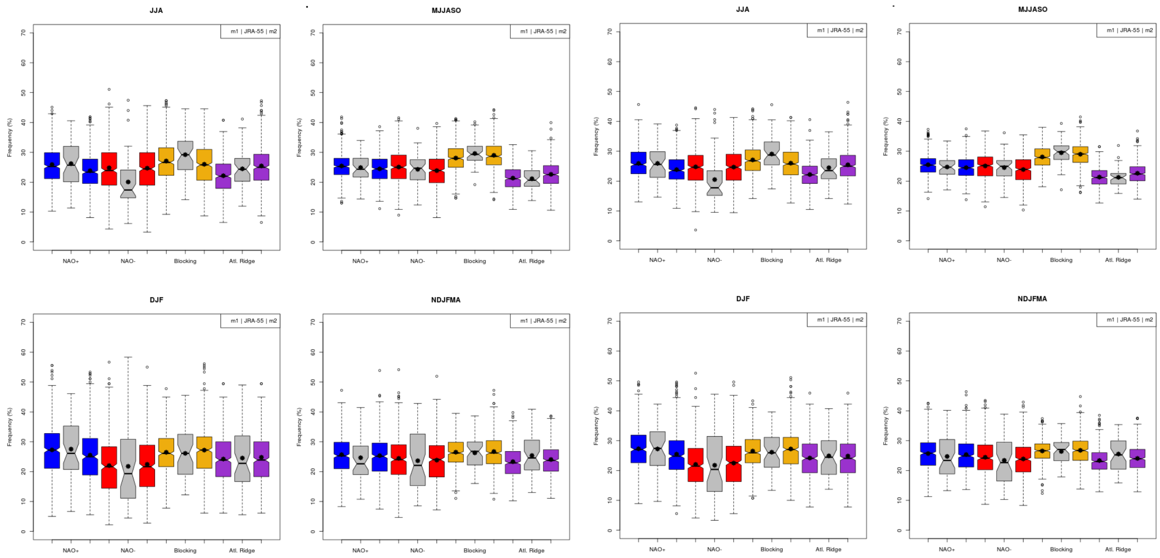

(a) 2 years averaged

(b) 3 years averaged

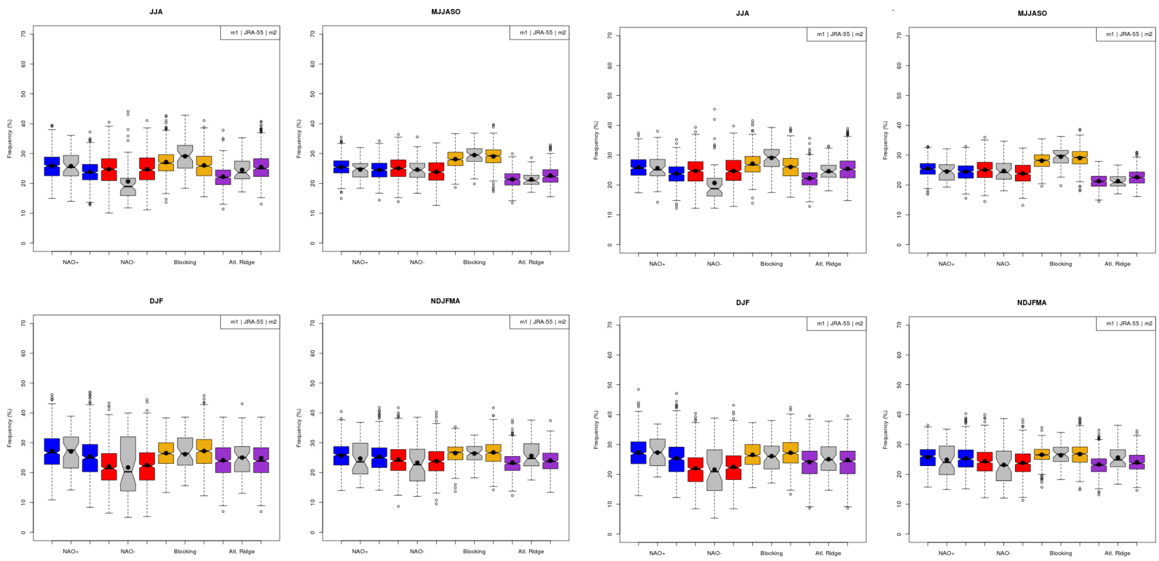

(c) 4 years averaged

(d) 5 years averaged

Figure A.2. Same as Figure 4, but for 2, 3 4, and 5 years averaged.

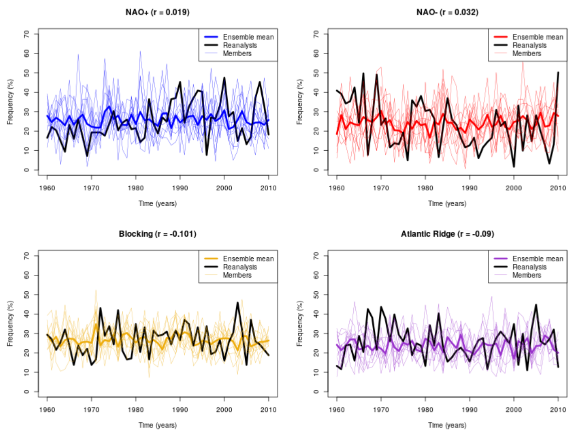

(a) NDJFMA - Method 1

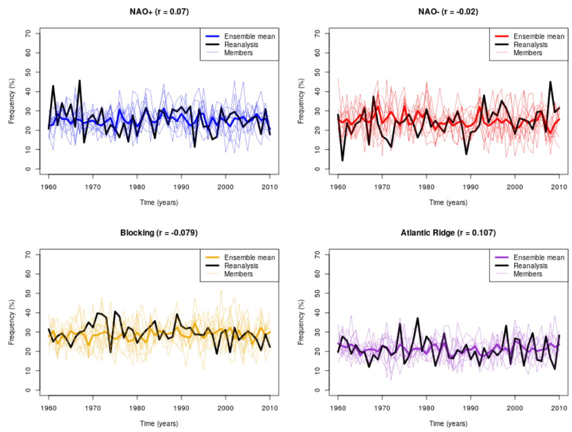

(b) MJJASO - Method 1

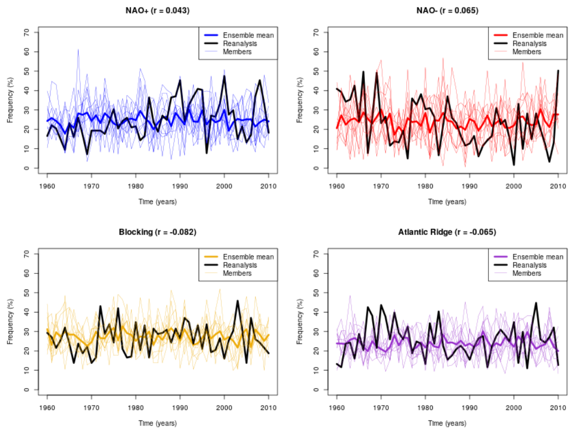

(c) NDJFMA - Method 2

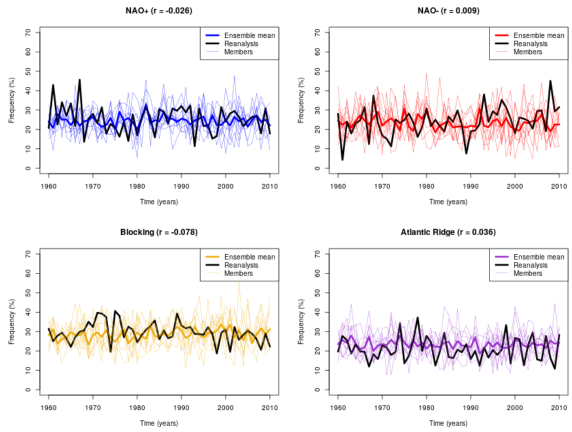

(d) MJJASO - Method 2

Figure A.3. Same as Figure 5, but for the extended seasons.

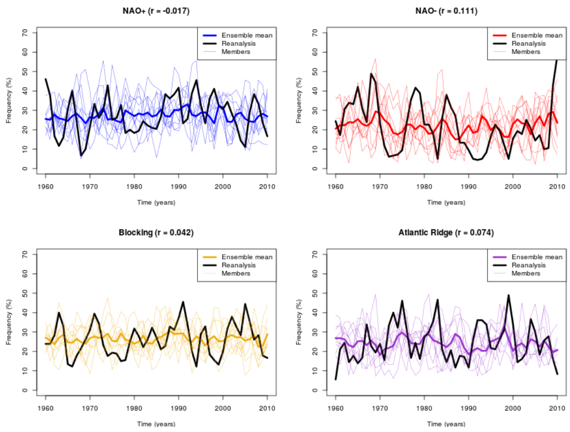

(a) DJF - Method 1

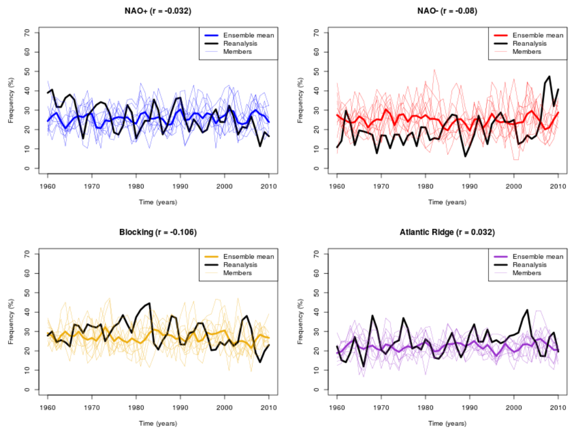

(b) JJA - Method 1

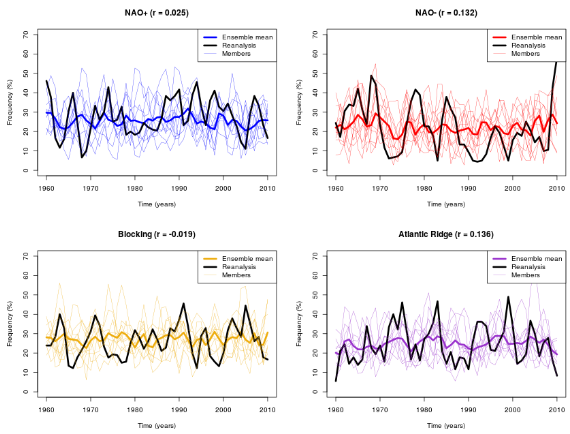

(c) DJF - Method 2

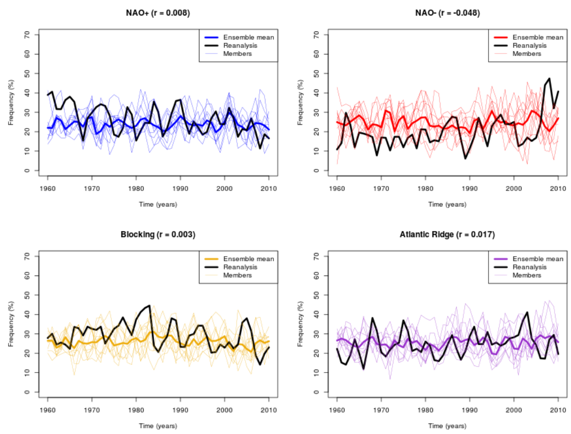

(d) JJA - Method 2

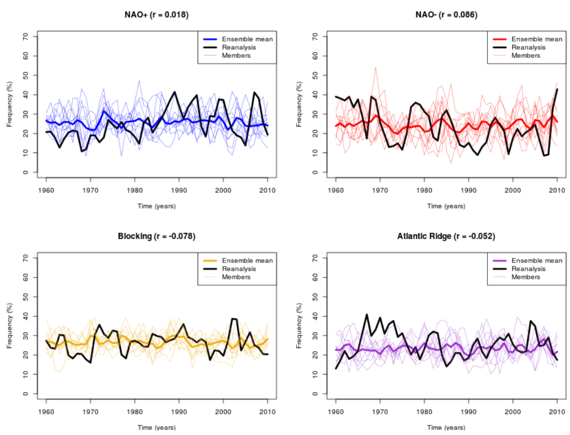

(e) NDJFMA - Method 1

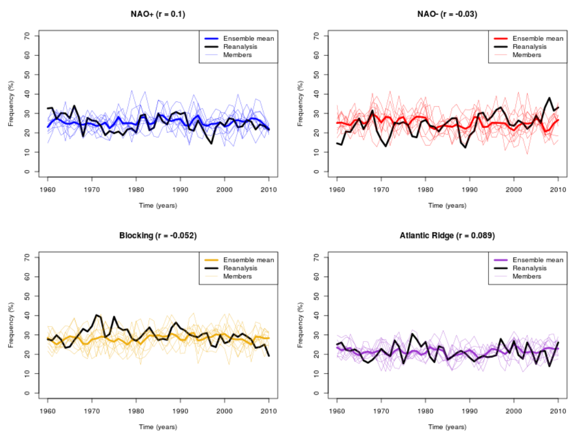

(f) MJJASO - Method 1

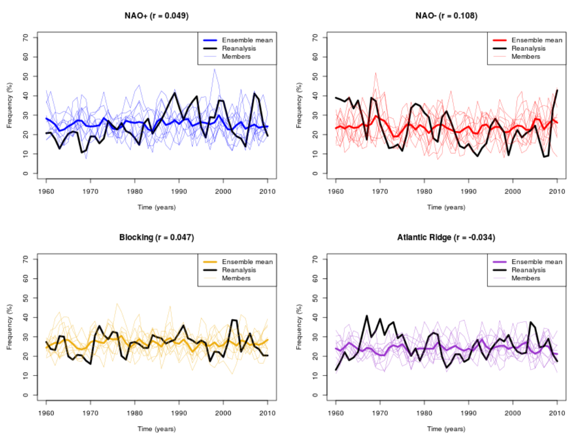

(g) NDJFMA - Method 2

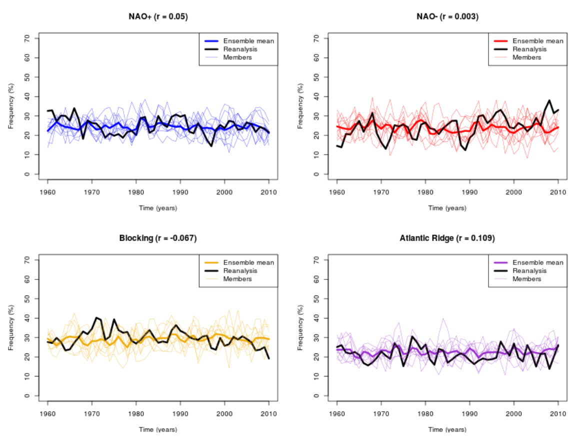

(h) MJJASO - Method 2

Figure A.4. Same as Figure 5, but averaging 2 years. Extended seasons are also included.

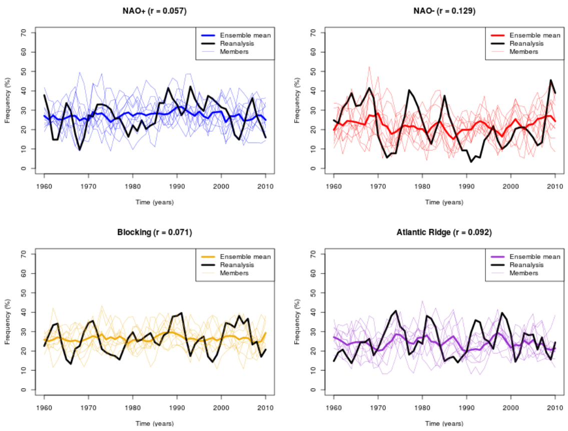

(a) DJF - Method 1

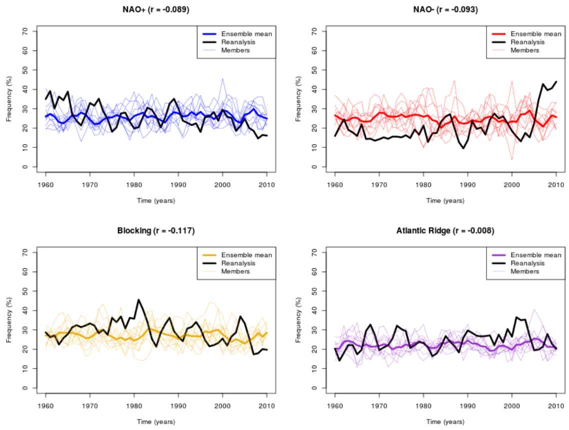

(b) JJA - Method 1

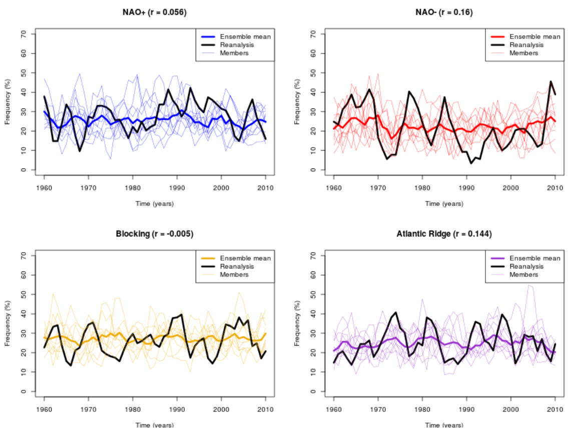

(c) DJF - Method 2

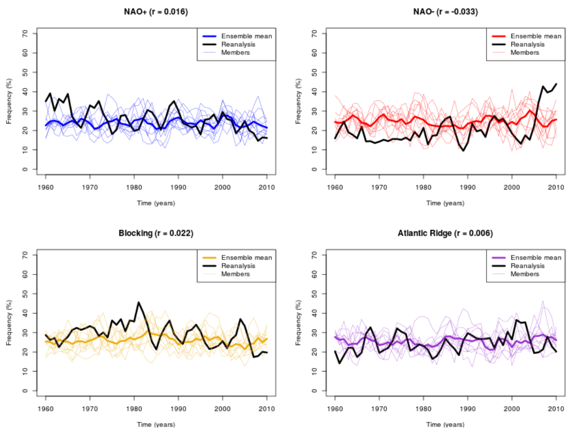

(d) JJA - Method 2

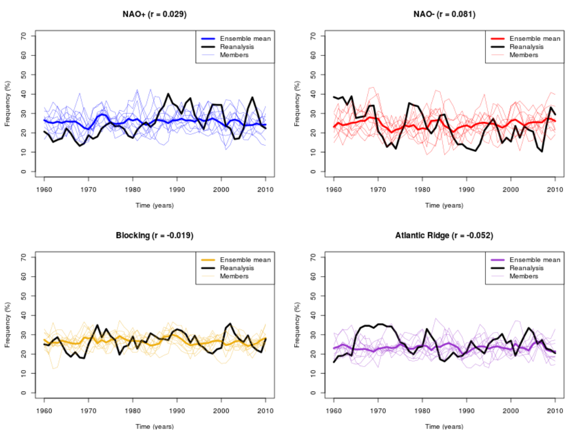

(e) NDJFMA - Method 1

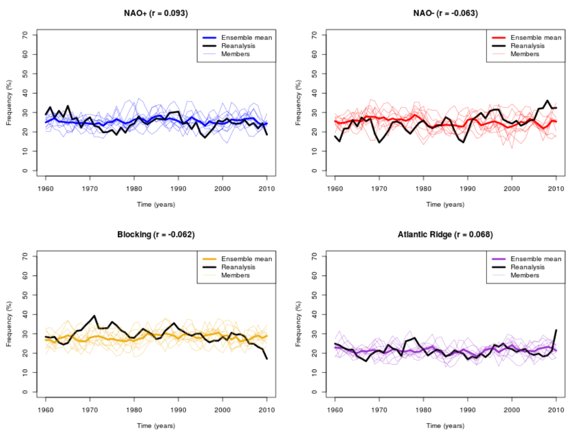

(f) MJJASO - Method 1

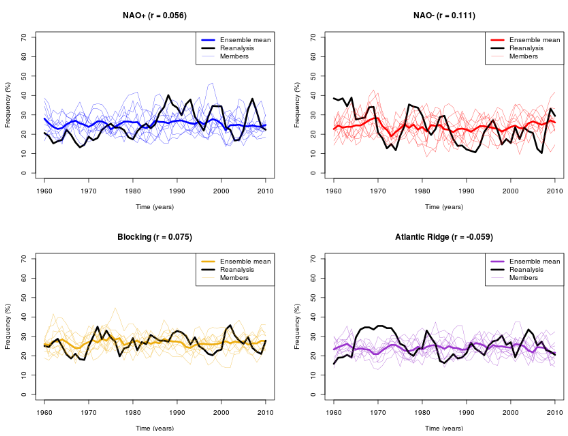

(g) NDJFMA - Method 2

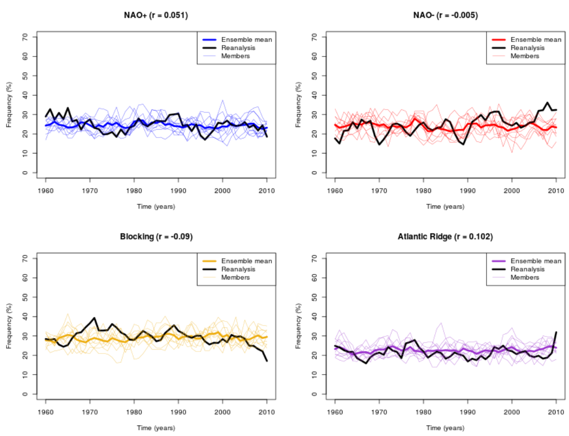

(h) MJJASO - Method 2

Figure A.5. Same as Figure 5, but averaging 3 years. Extended seasons are also included.

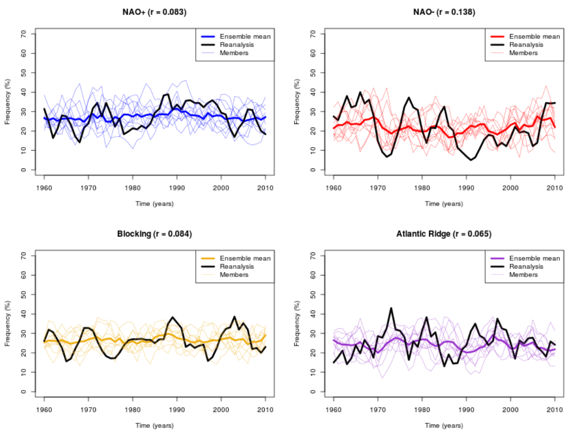

(a) DJF - Method 1

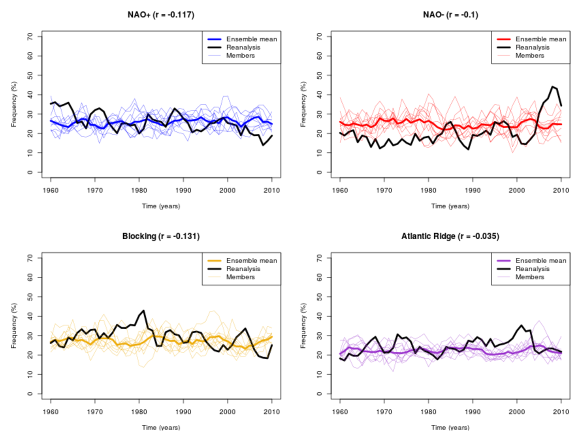

(b) JJA - Method 1

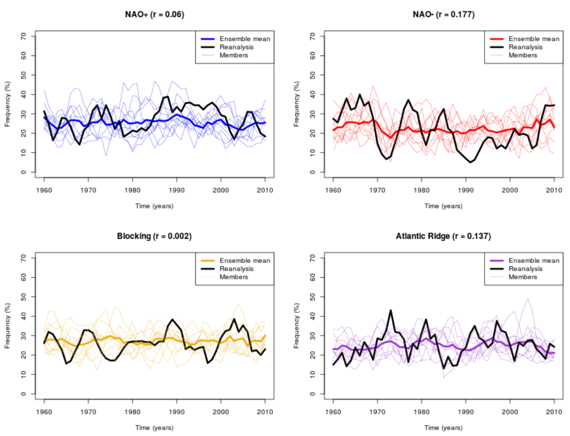

(c) DJF - Method 2

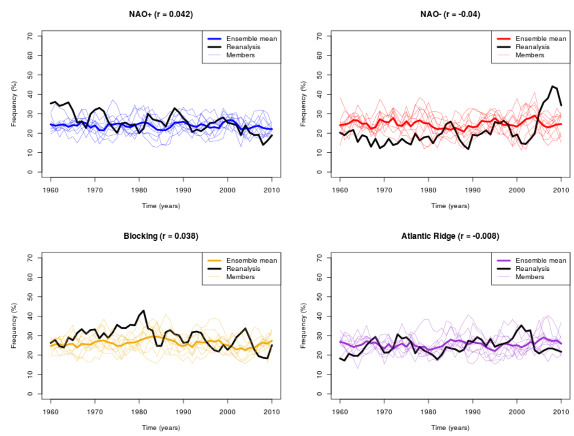

(d) JJA - Method 2

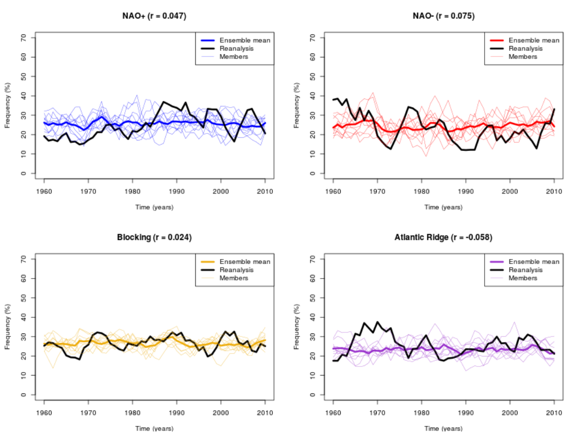

(e) NDJFMA - Method 1

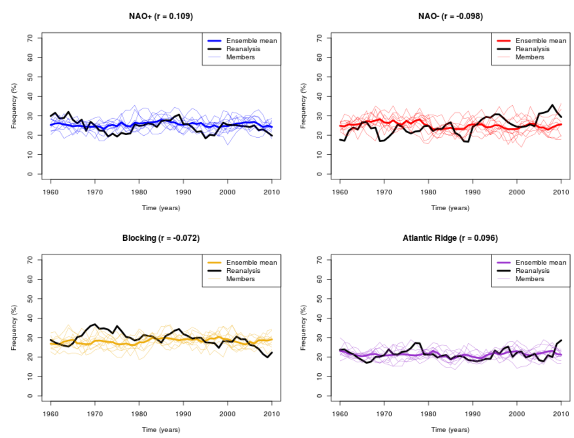

(f) MJJASO - Method 1

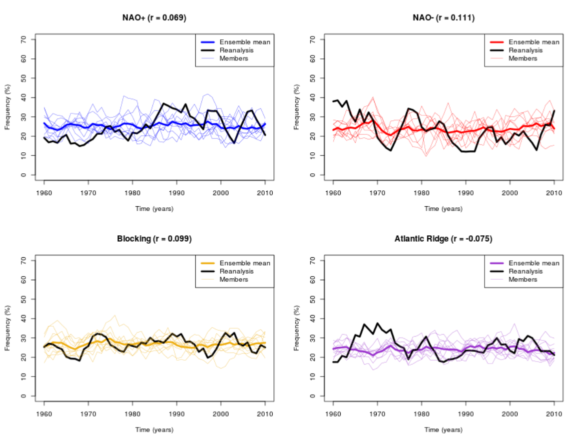

(g) NDJFMA - Method 2

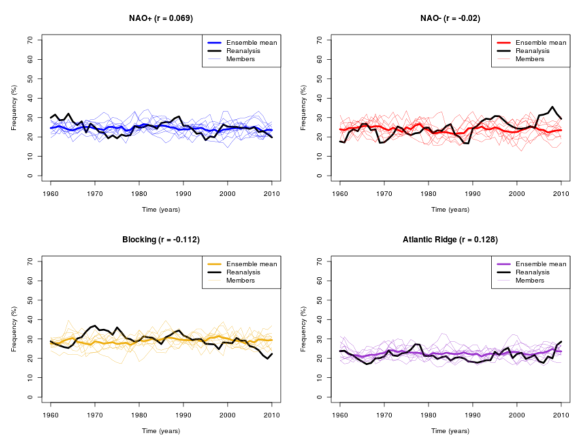

(h) MJJASO - Method 2

Figure A.6. Same as Figure 5, but averaging 4 years. Extended seasons are also included.

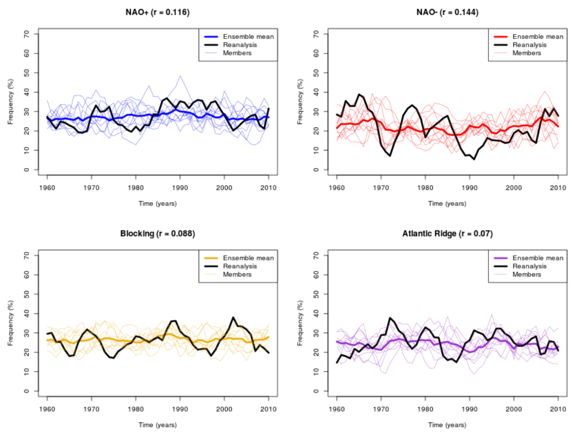

(a) DJF - Method 1

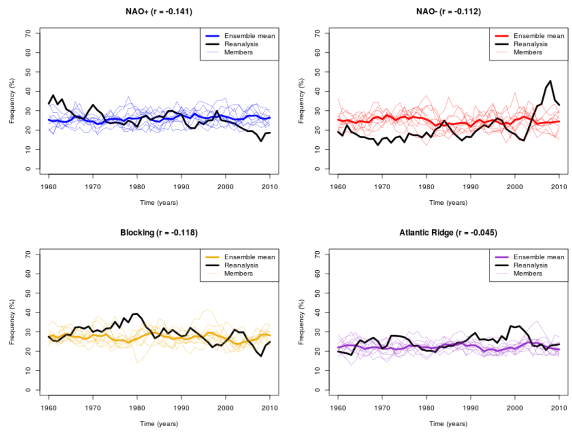

(b) JJA - Method 1

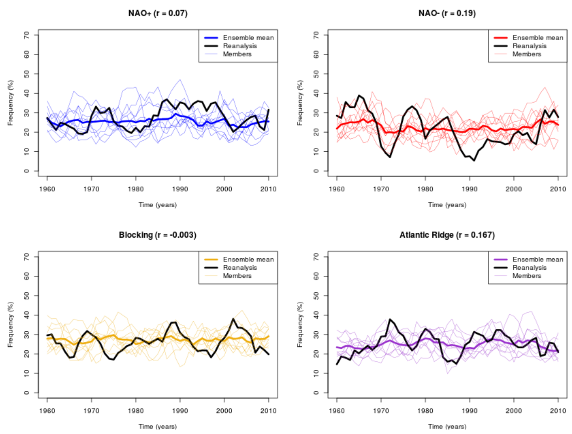

(c) DJF - Method 2

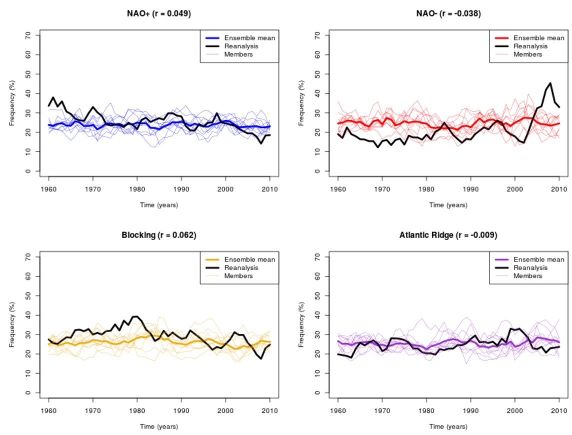

(d) JJA - Method 2

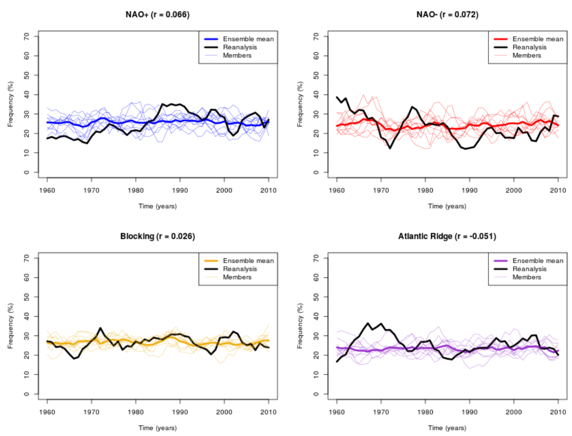

(e) NDJFMA - Method 1

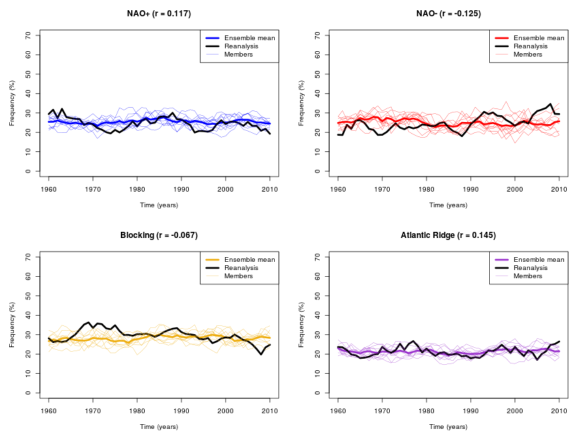

(f) MJJASO - Method 1

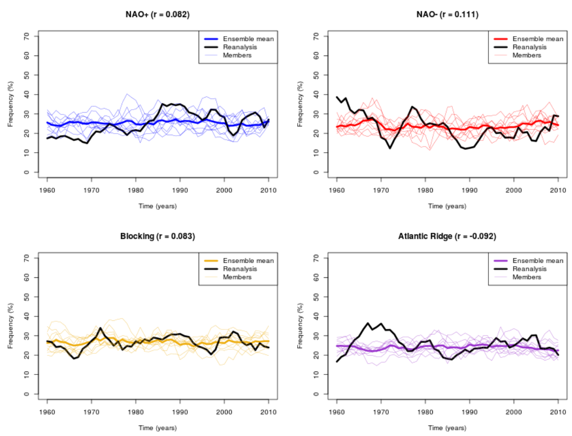

(g) NDJFMA - Method 2

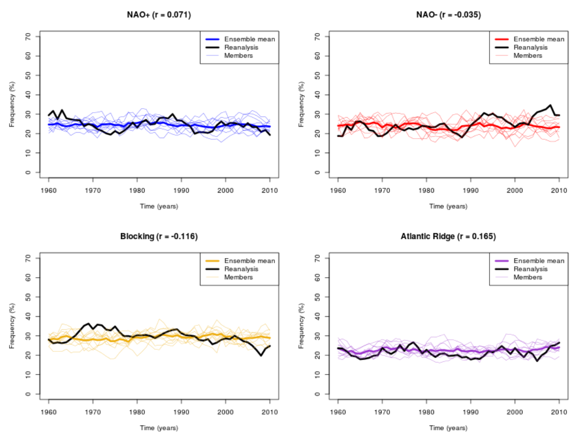

(h) MJJASO - Method 2

Figure A.7. Same as Figure 5, but averaging 5 years. Extended seasons are also included.

Annex B: Additional figures for the decadal predictions

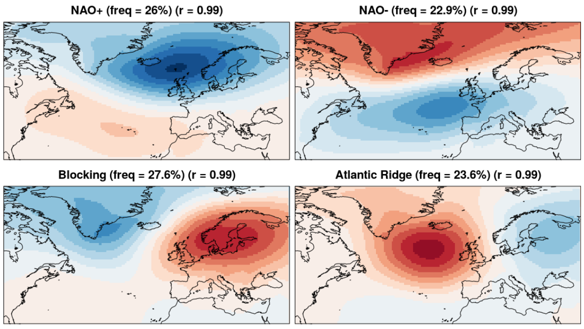

(a) NDJFMA - Method 1

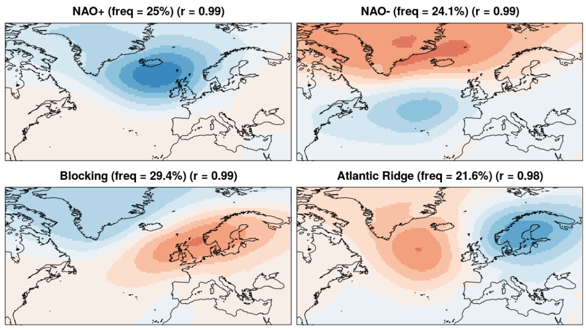

(b) MJJASO - Method 1

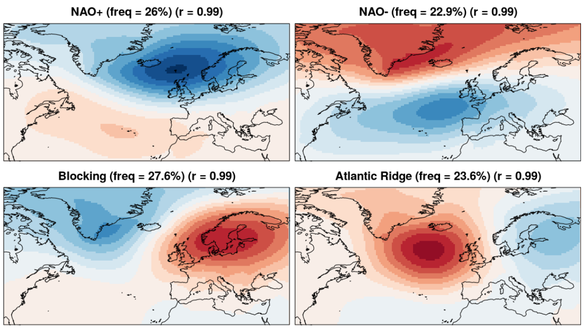

(c) NDJFMA - Method 2

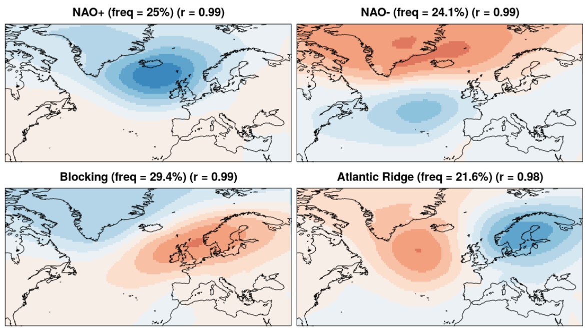

(d) MJJASO - Method 2

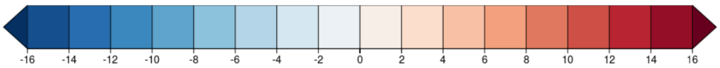

Figure B.1. Same as Figure 6, but for the extended seasons.

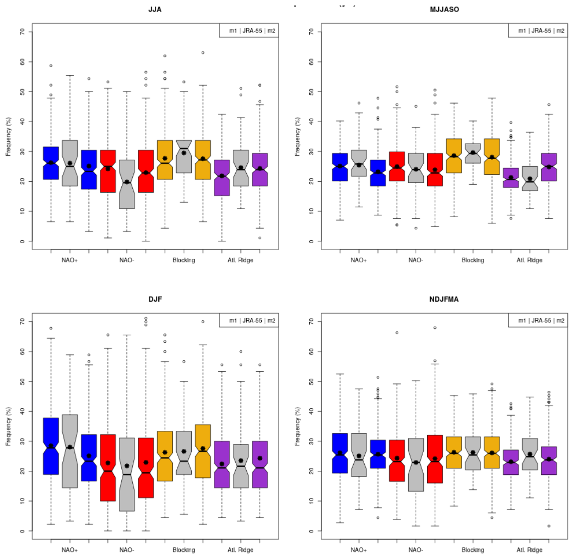

(a) Year 2

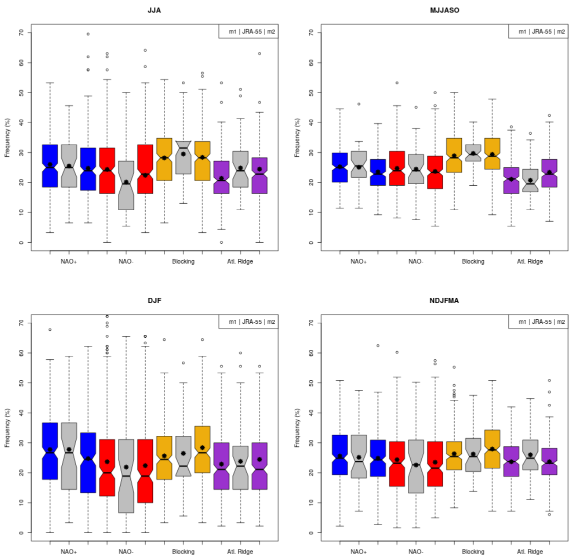

(b) Year 3

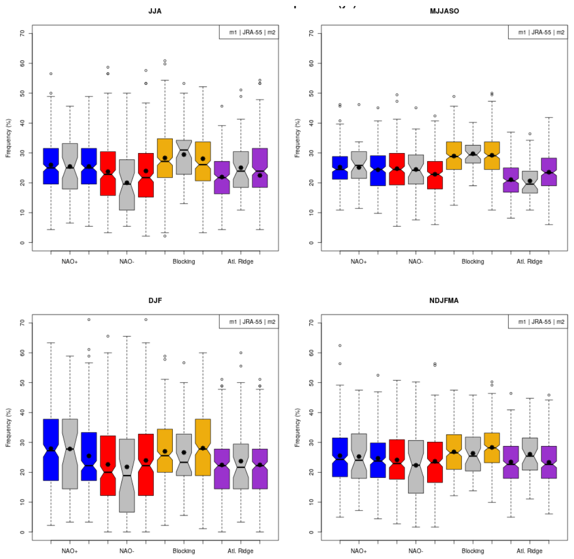

(c) Year 4

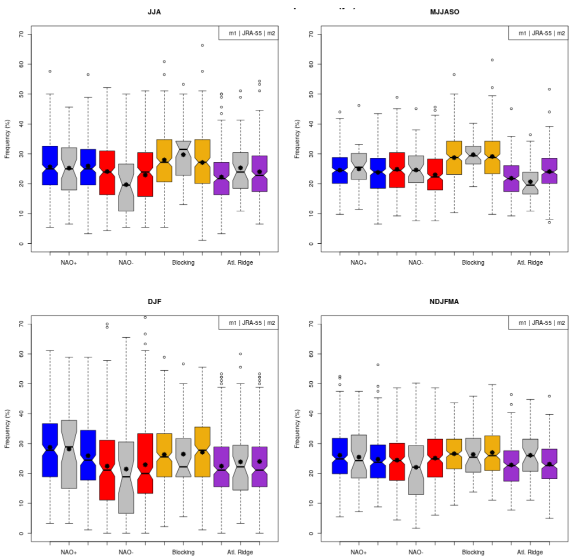

(d) Year 5

Figure B.2. Same as Figure 7, but for years 2 to 5.

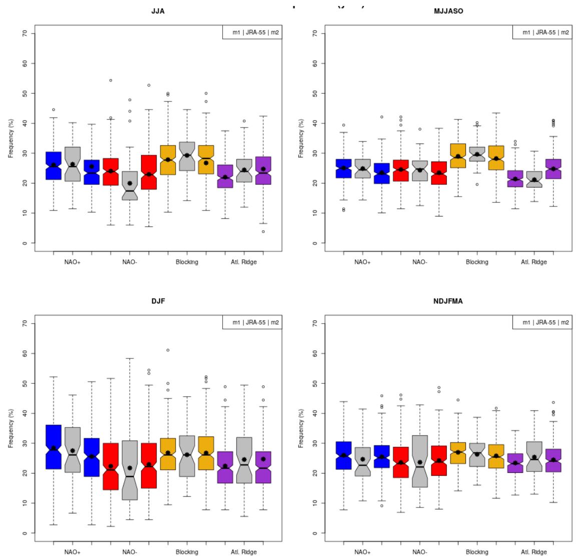

(a) Years 1 to 2

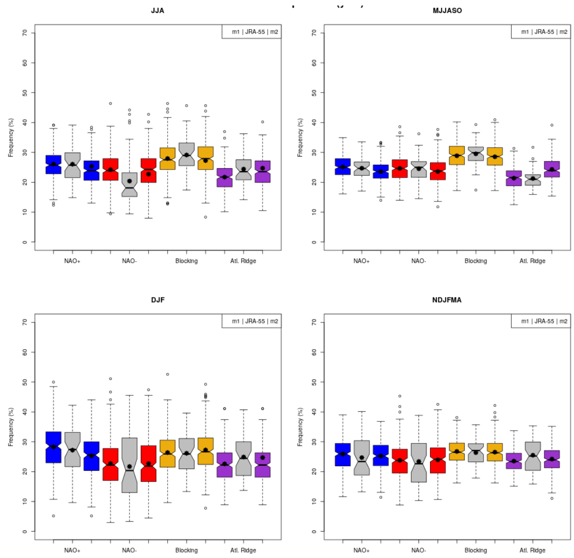

(b) Years 1 to 3

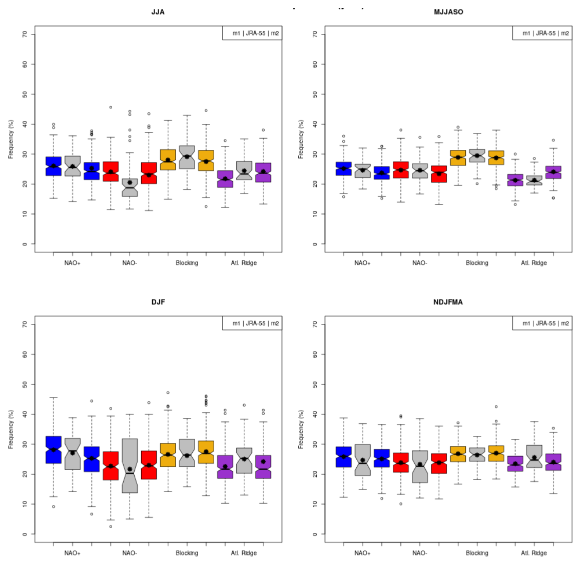

(c) Years 1 to 4

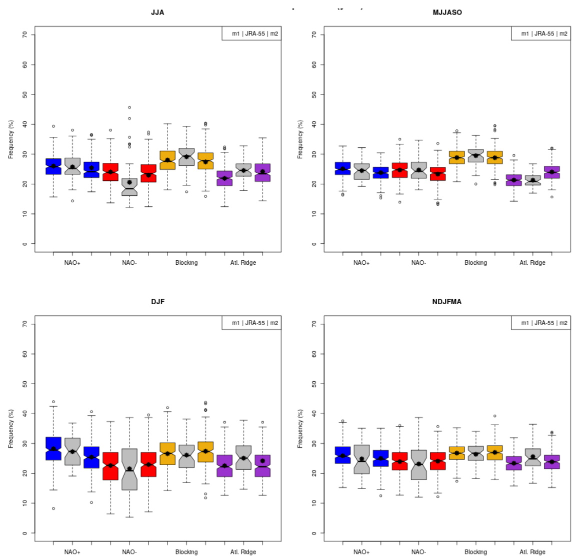

(d) Years 1 to 5

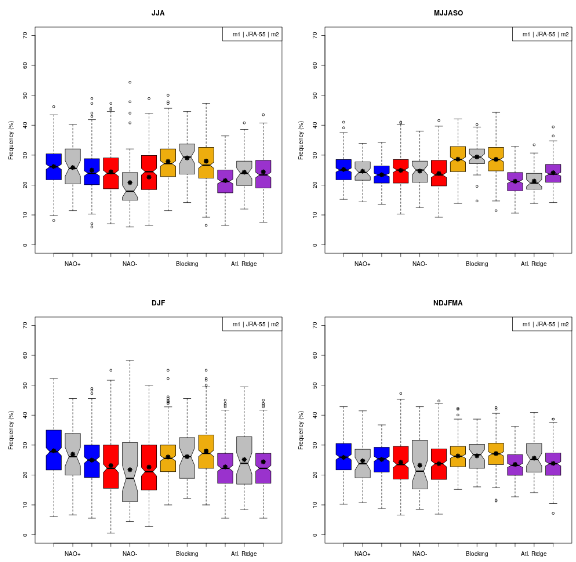

(e) Years 2 to 3

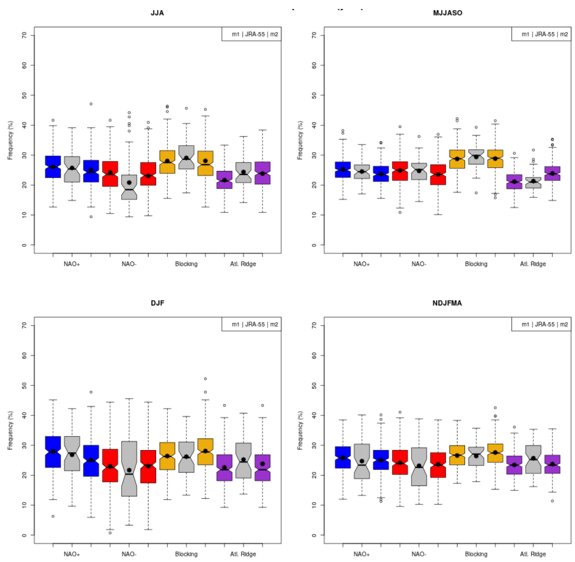

(f) Years 2 to 4

Figure B.3. Same as Figure 7, but for 2 to 5 years averaged.

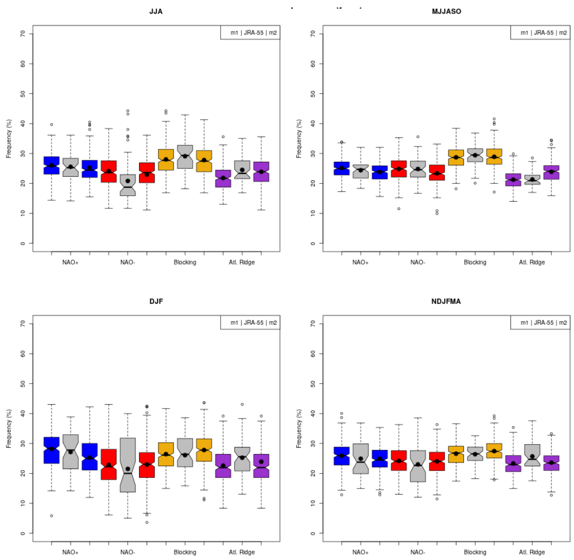

(g) Years 2 to 5

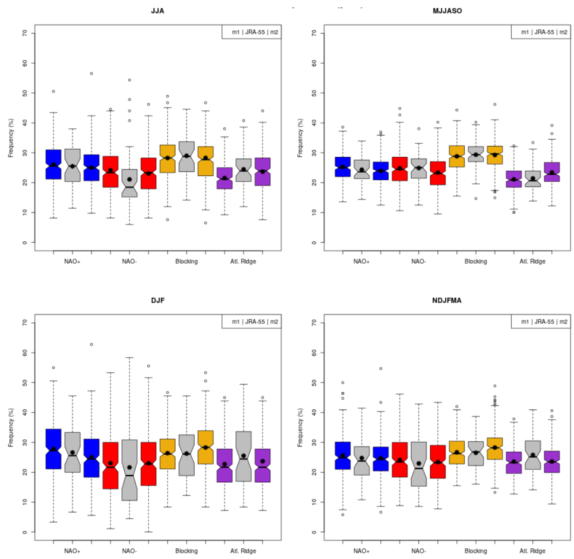

(h) Years 3 to 4

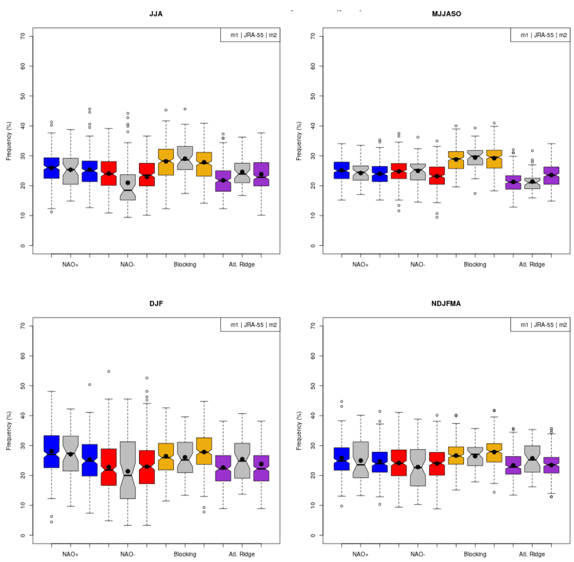

(i) Years 3 to 5

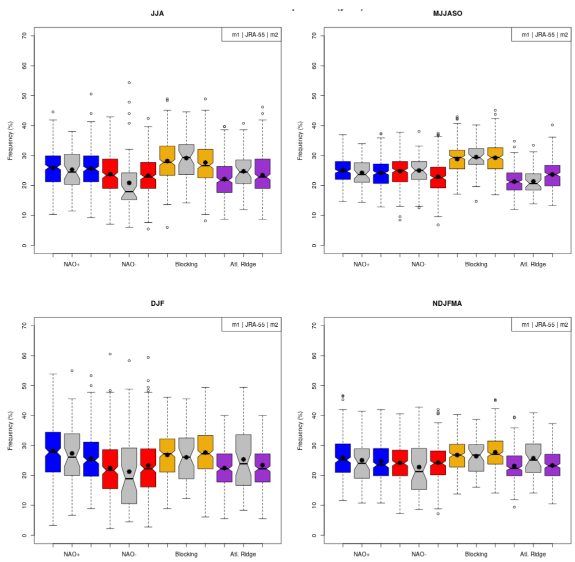

(j) Years 4 to 5

Figure B.3. (Cont).

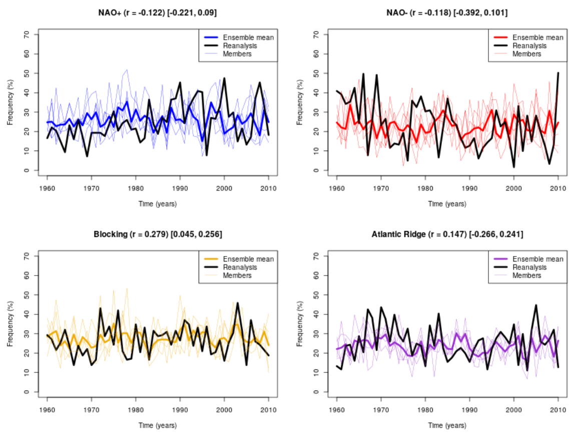

(a) NDJFMA - Method 1

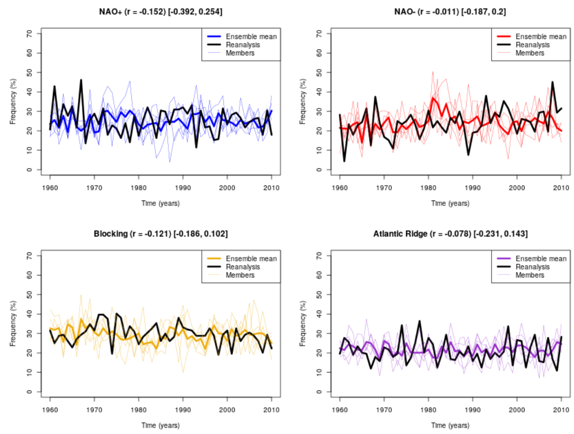

(b) MJJASO - Method 1

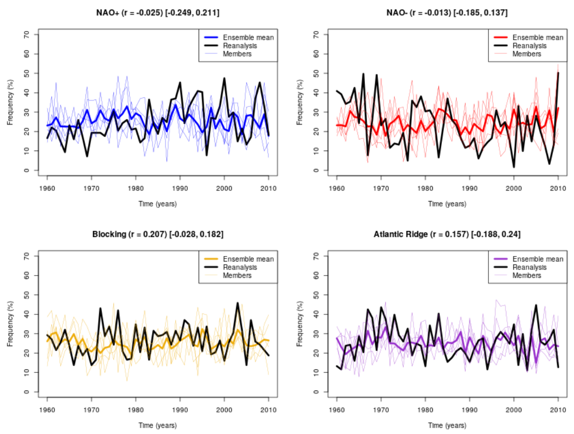

(c) NDJFMA - Method 2

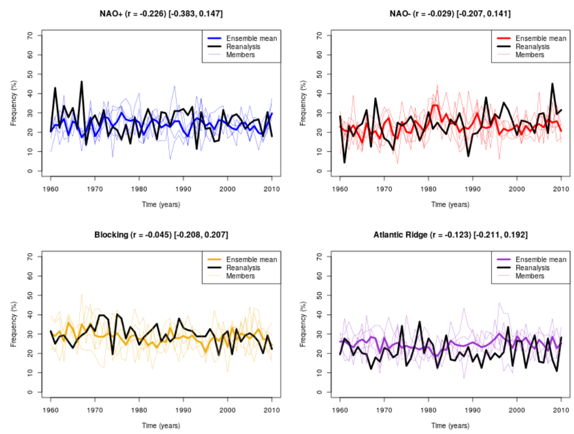

(d) MJJASO - Method 2

Figure B.4. Same as Figure 8, but for the extended seasons.

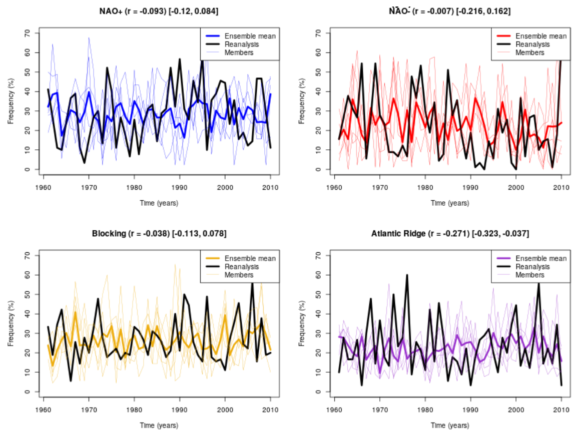

(a) DJF - Method 1

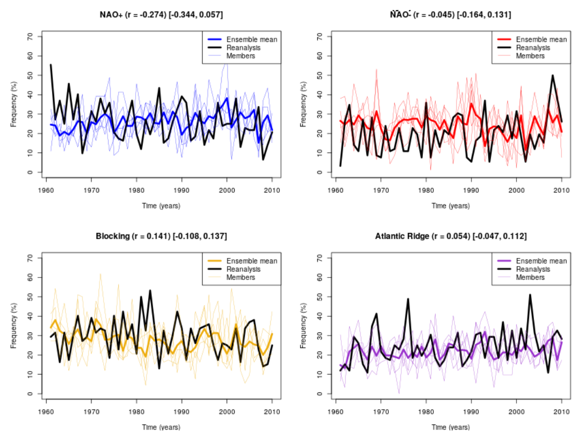

(b) JJA - Method 1

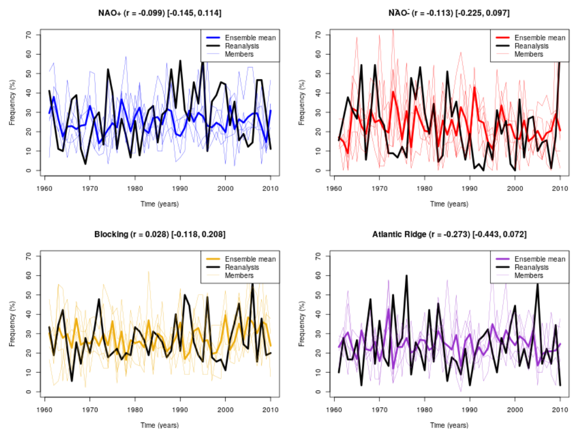

(c) DJF - Method 2

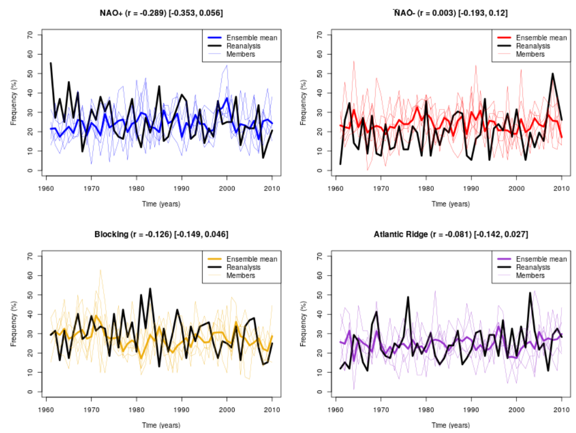

(d) JJA - Method 2

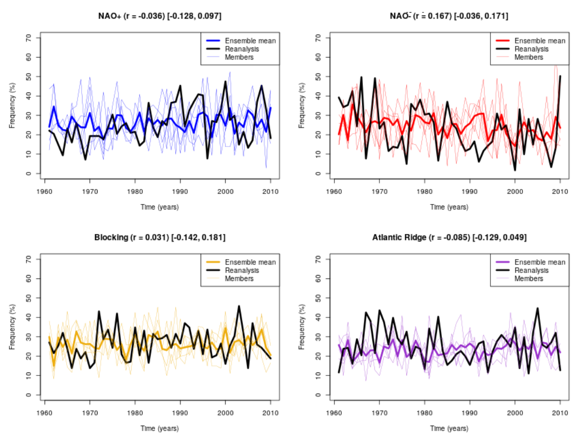

(e) NDJFMA - Method 1

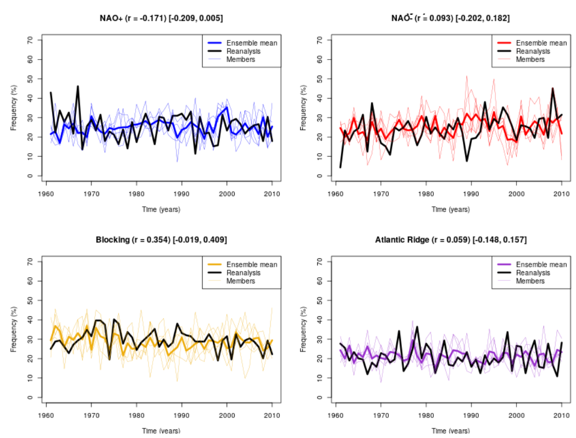

(f) MJJASO - Method 1

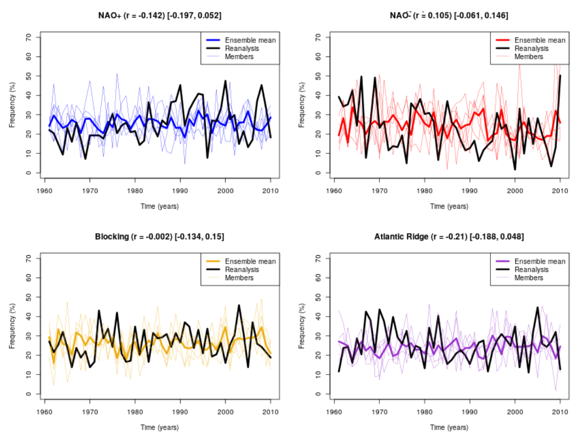

(g) NDJFMA - Method 2

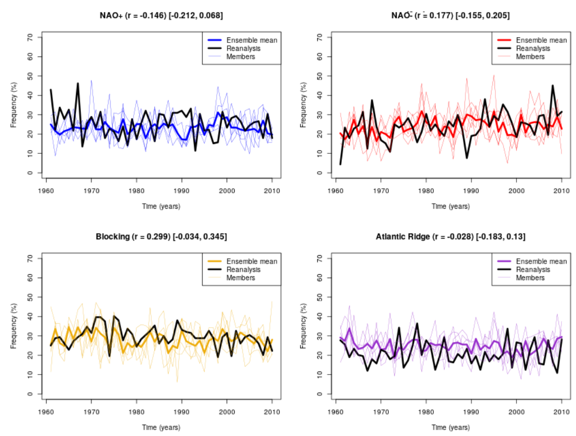

(h) MJJASO - Method 2

Figure B.5. Same as Figure 8, but for year 2. Extended seasons are also included.

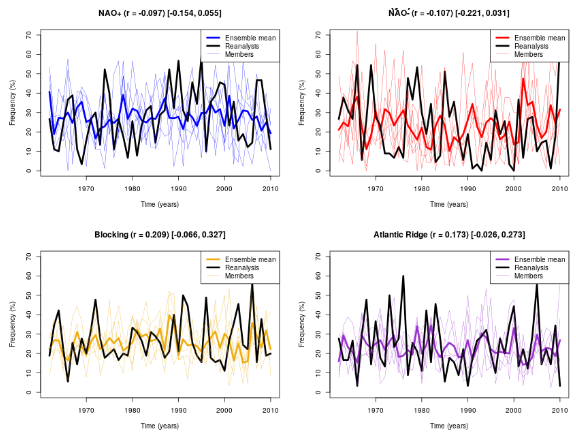

(a) DJF - Method 1

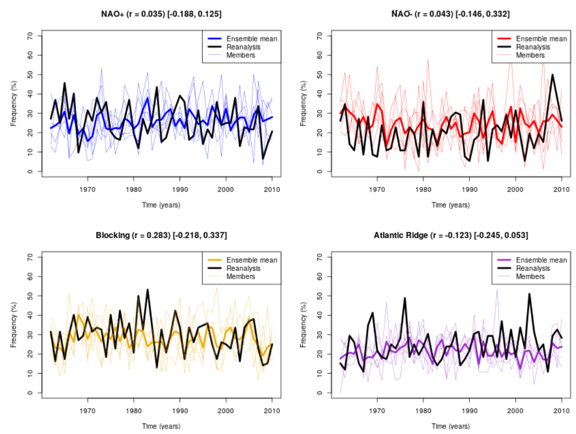

(b) JJA - Method 1

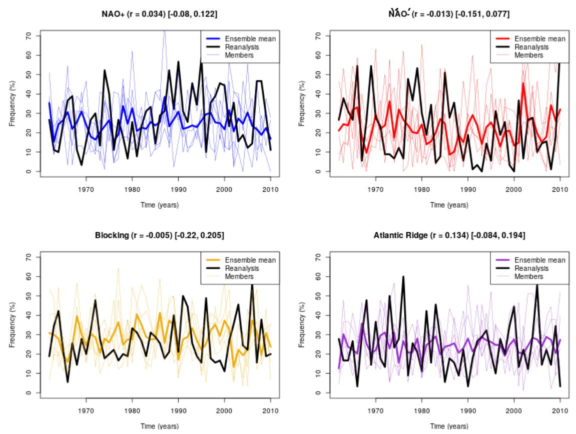

(c) DJF - Method 2

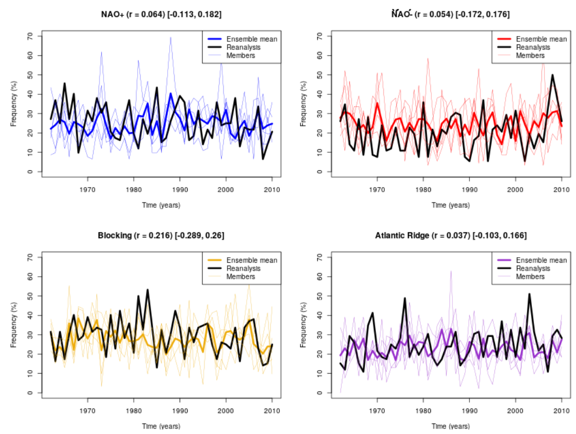

(d) JJA - Method 2

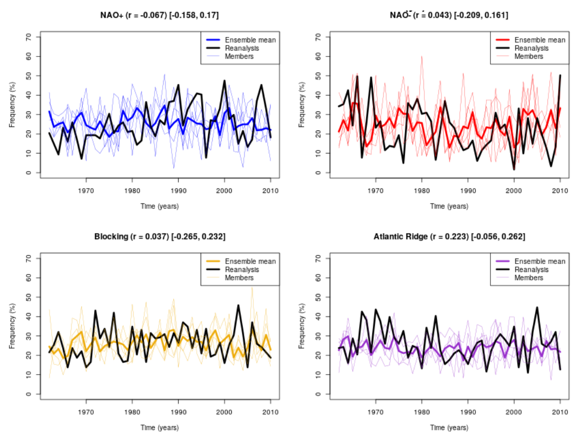

(e) NDJFMA - Method 1

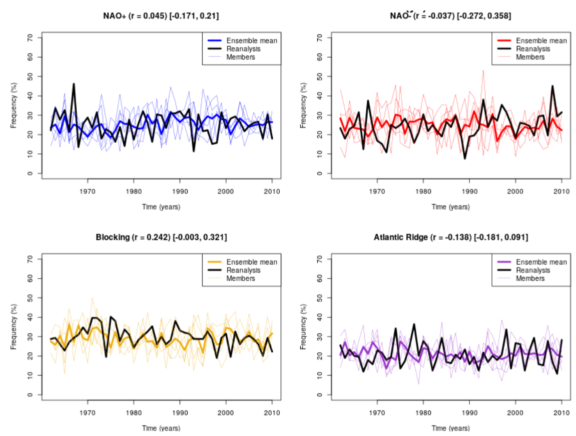

(f) MJJASO - Method 1

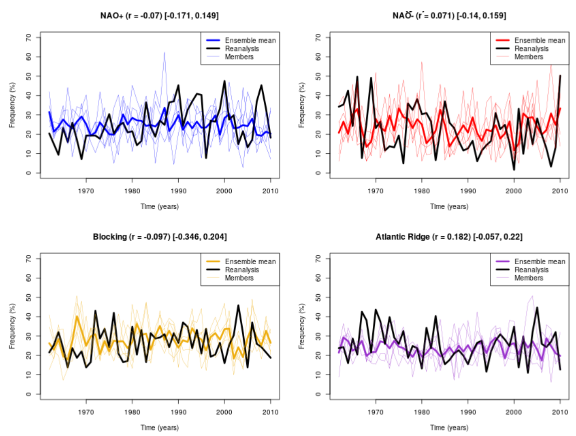

(g) NDJFMA - Method 2

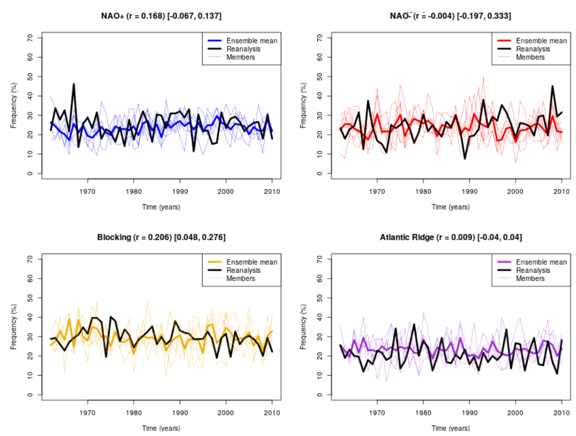

(h) MJJASO - Method 2

Figure B.6. Same as Figure 8, but for year 3. Extended seasons are also included.

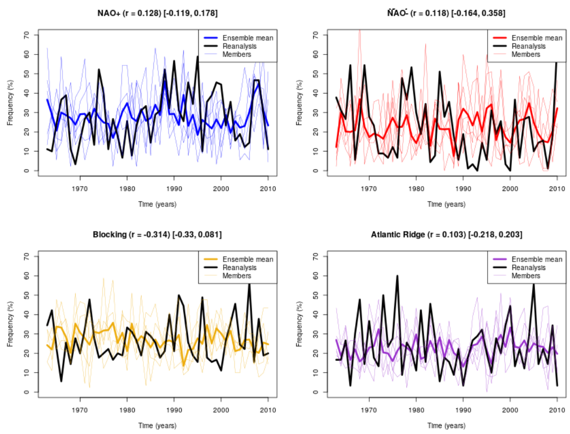

(a) DJF - Method 1

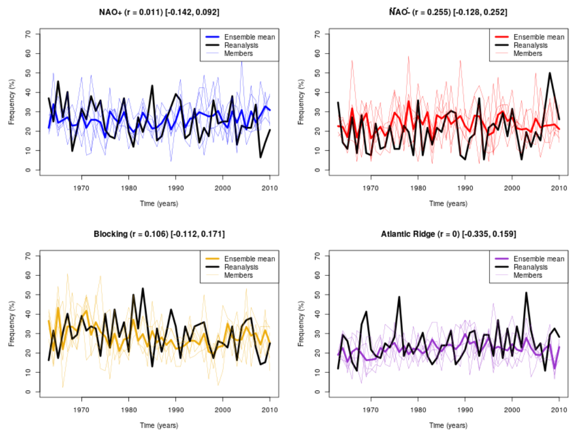

(b) JJA - Method 1

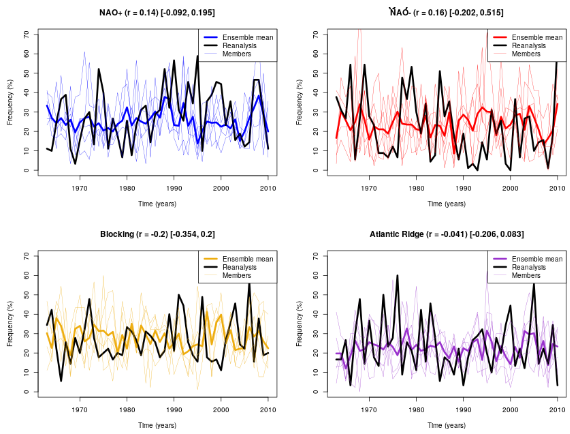

(c) DJF - Method 2

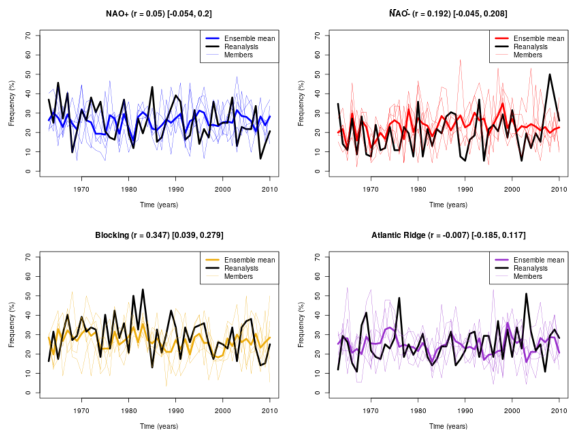

(d) JJA - Method 2

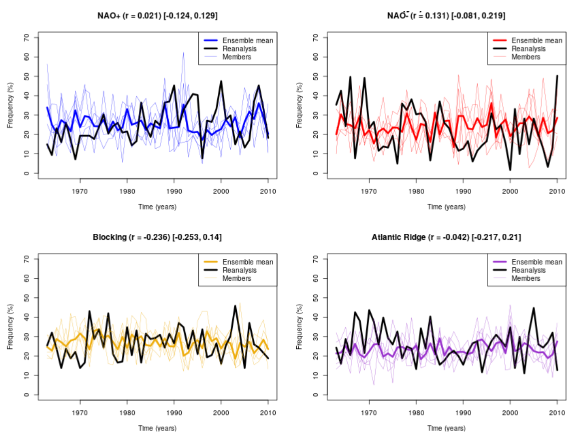

(e) NDJFMA - Method 1

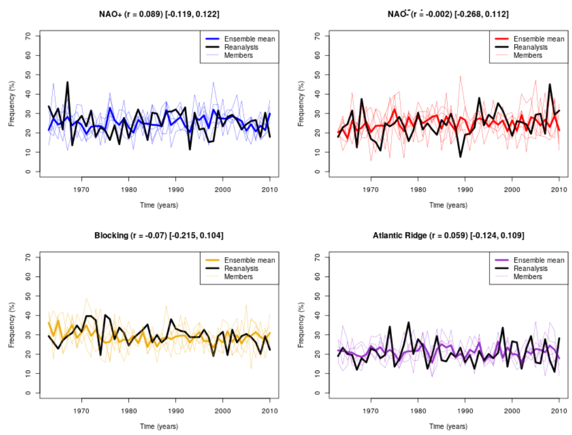

(f) MJJASO - Method 1

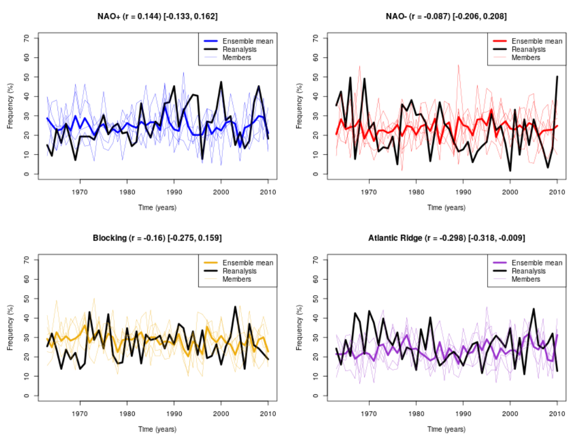

(g) NDJFMA - Method 2

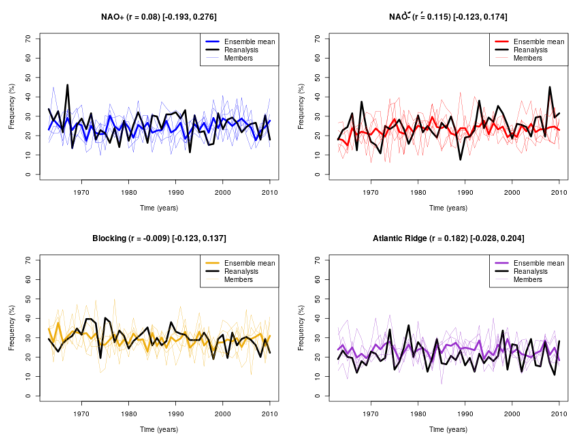

(h) MJJASO - Method 2

Figure B.7. Same as Figure 8, but for year 4. Extended seasons are also included.

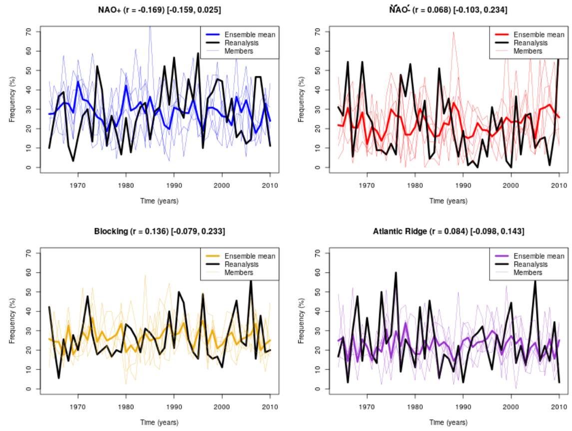

(a) DJF - Method 1

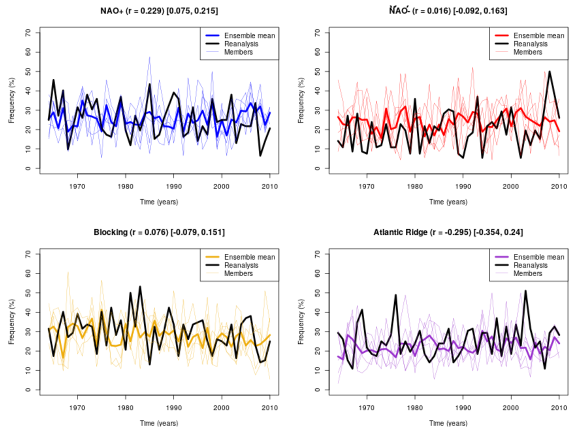

(b) JJA - Method 1

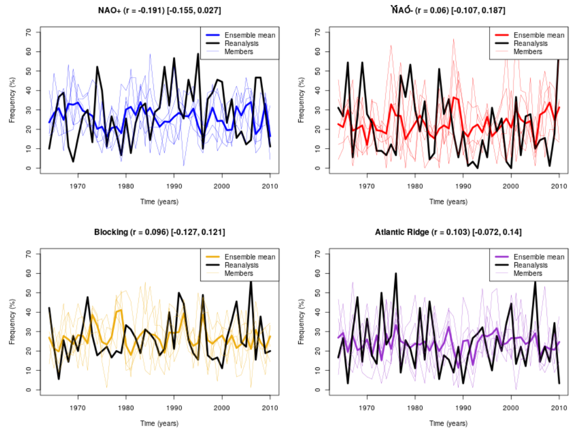

(c) DJF - Method 2

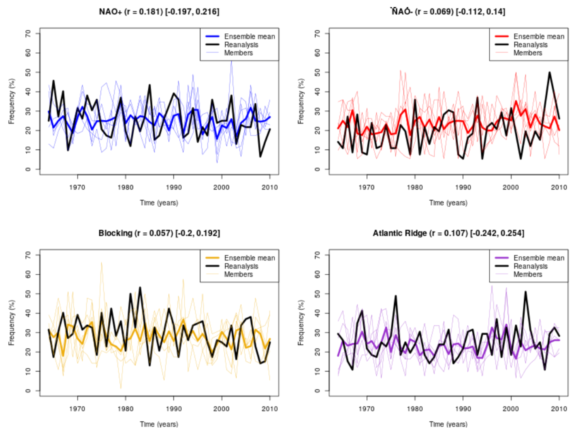

(d) JJA - Method 2

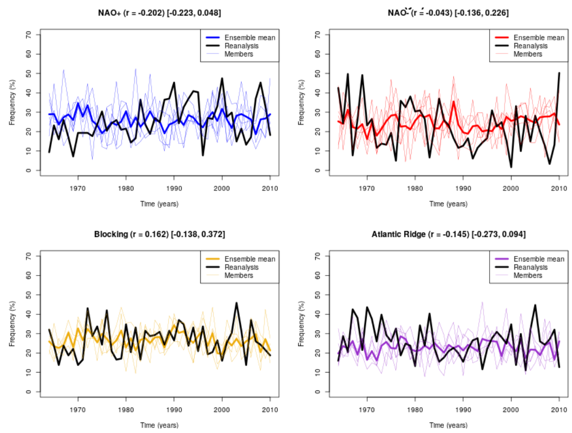

(e) NDJFMA - Method 1

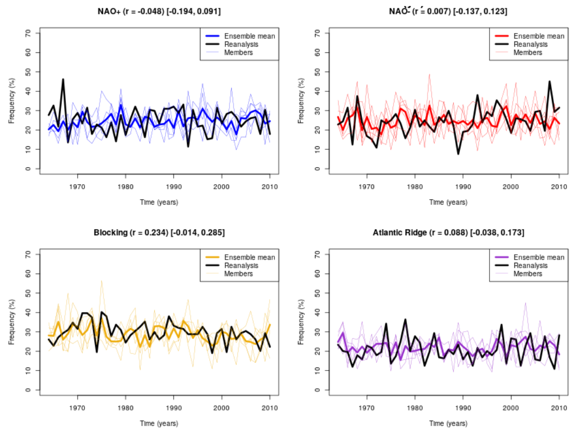

(f) MJJASO - Method 1

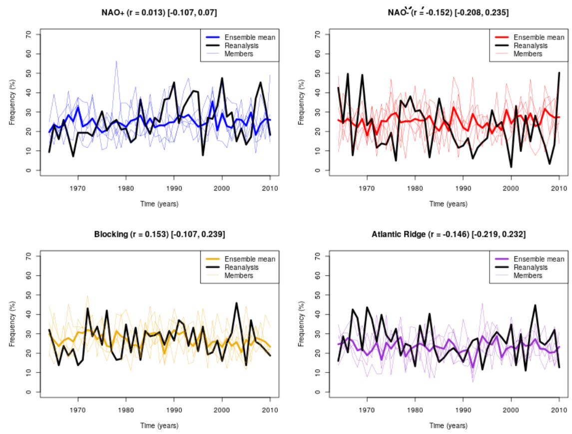

(g) NDJFMA - Method 2

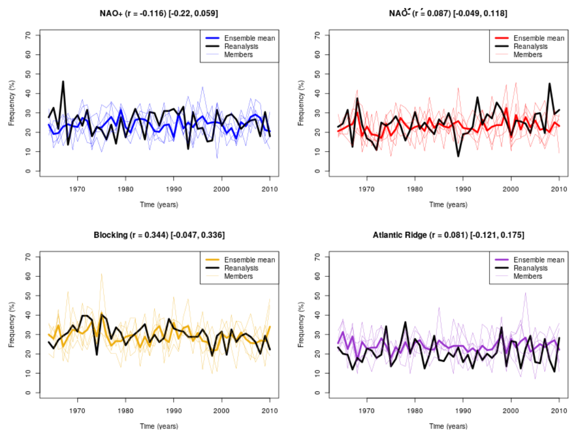

(h) MJJASO - Method 2

Figure B.8. Same as Figure 8, but for year 5. Extended seasons are also included.

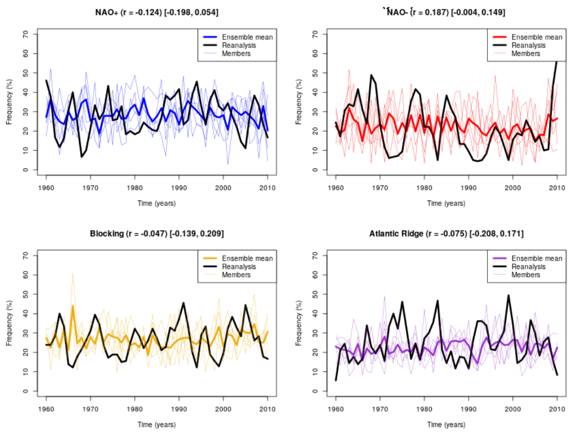

(a) DJF - Method 1

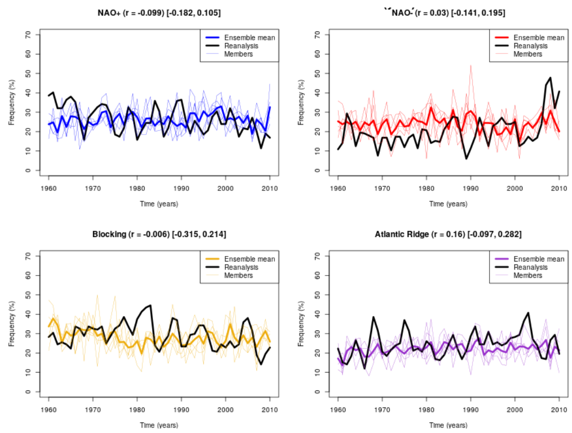

(b) JJA - Method 1

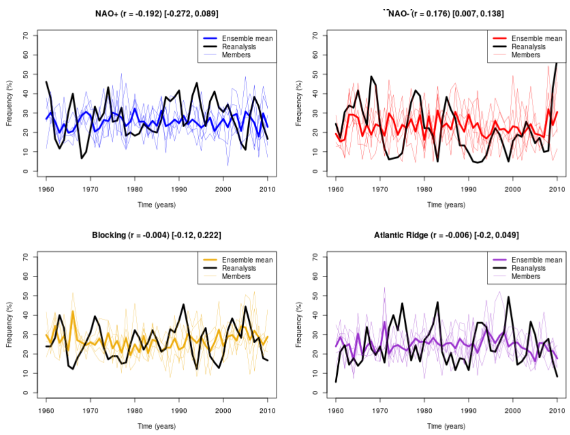

(c) DJF - Method 2

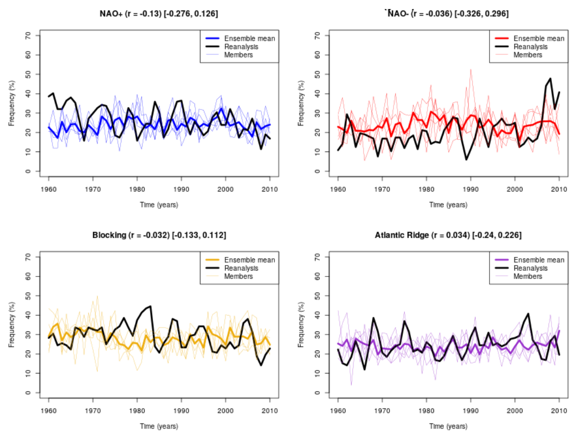

(d) JJA - Method 2

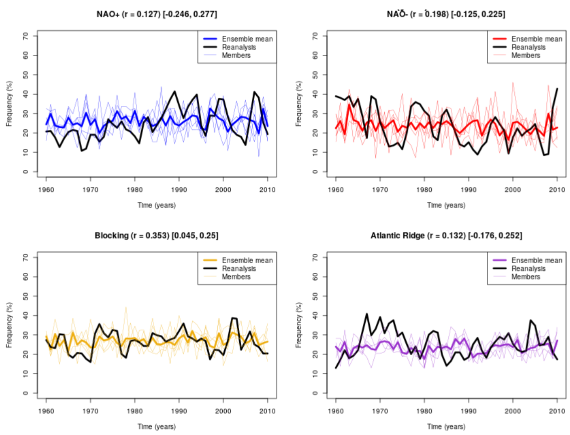

(e) NDJFMA - Method 1

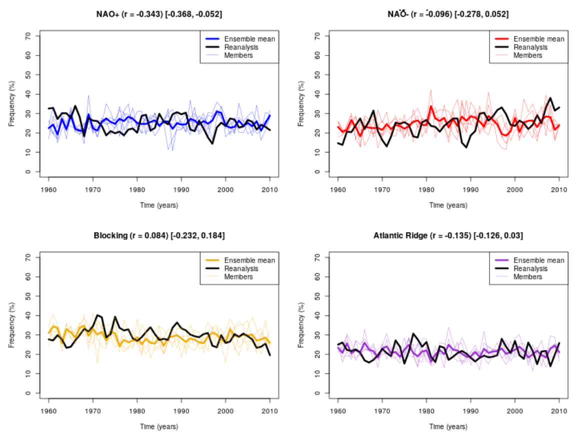

(f) MJJASO - Method 1

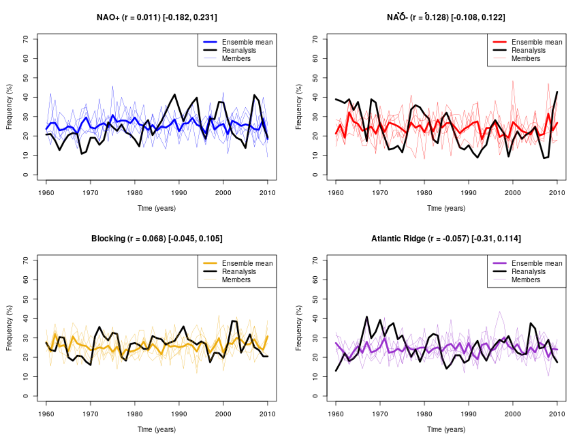

(g) NDJFMA - Method 2

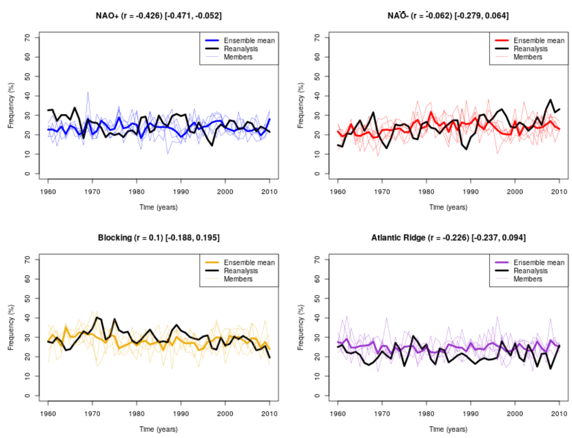

(h) MJJASO - Method 2

Figure B.9. Same as Figure 8, but averaging from year 1 to 2. Extended seasons are also included.

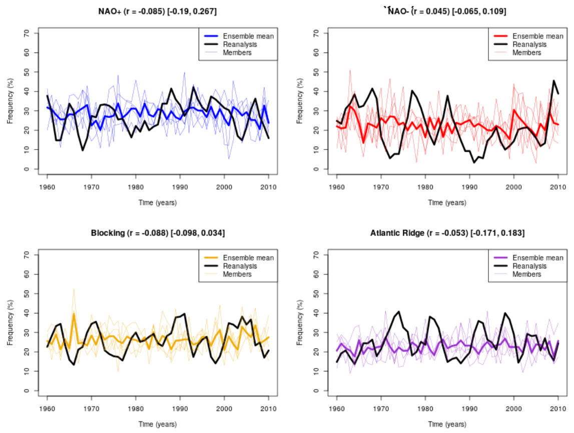

(a) DJF - Method 1

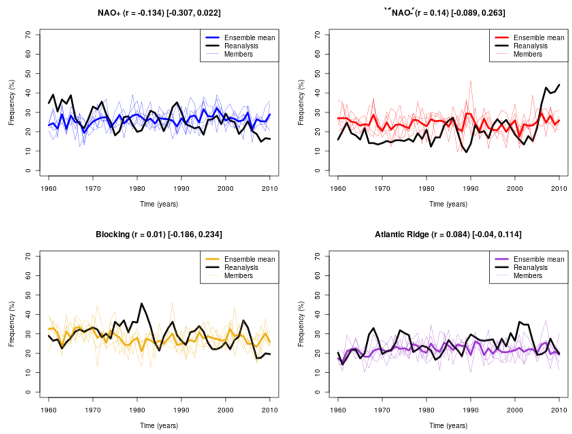

(b) JJA - Method 1

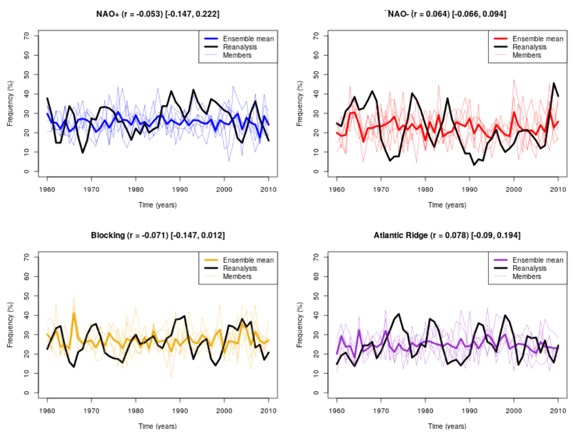

(c) DJF - Method 2

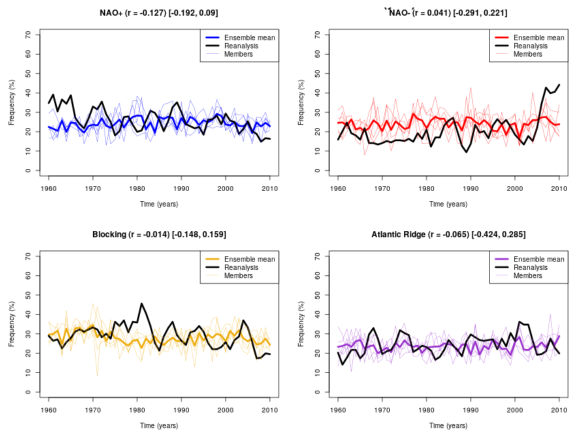

(d) JJA - Method 2

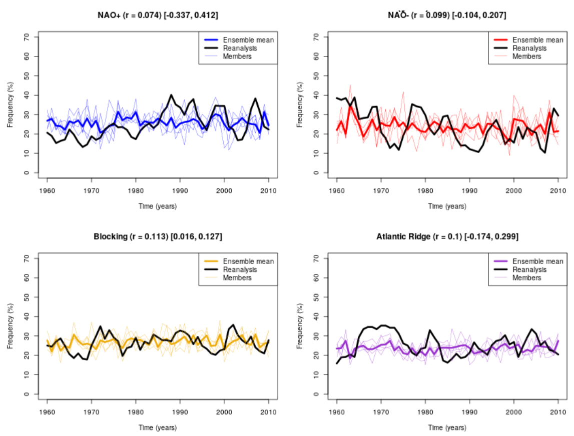

(e) NDJFMA - Method 1

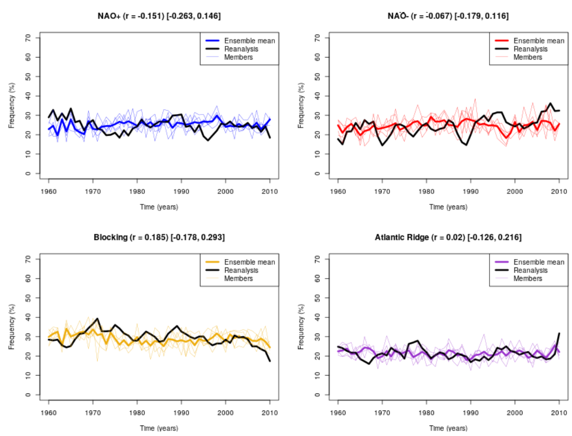

(f) MJJASO - Method 1

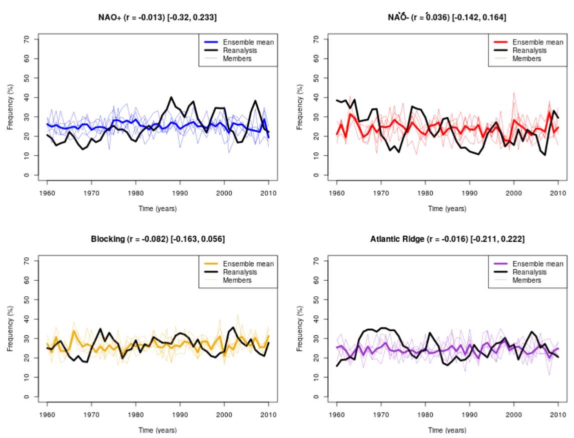

(g) NDJFMA - Method 2

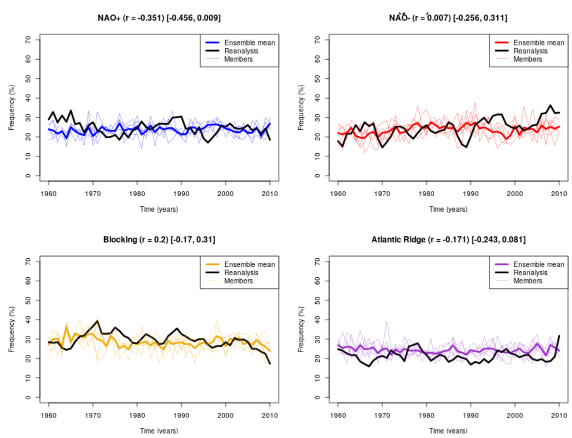

(h) MJJASO - Method 2

Figure B.10. Same as Figure 8, but averaging from year 1 to 3. Extended seasons are also included.

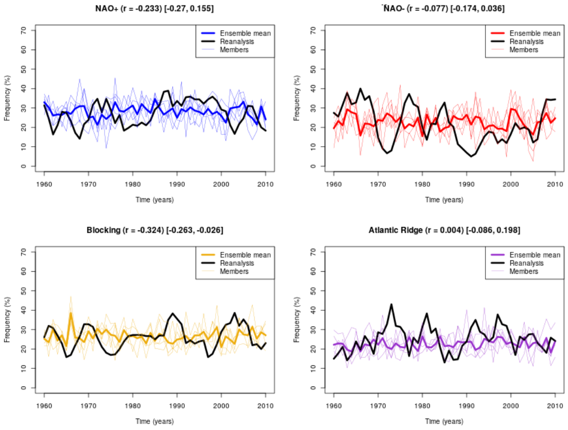

(a) DJF - Method 1

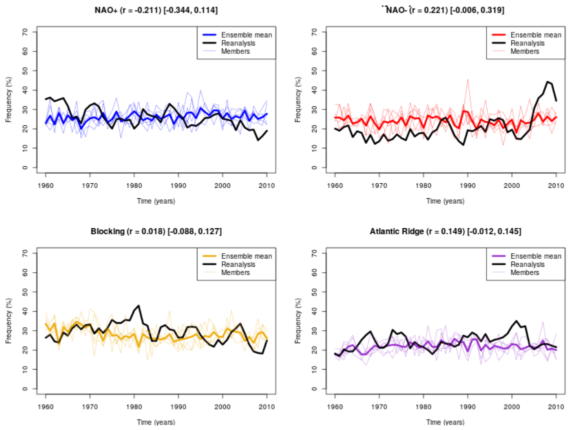

(b) JJA - Method 1

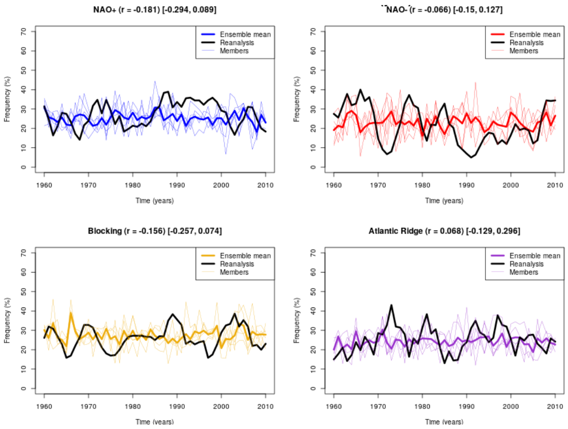

(c) DJF - Method 2

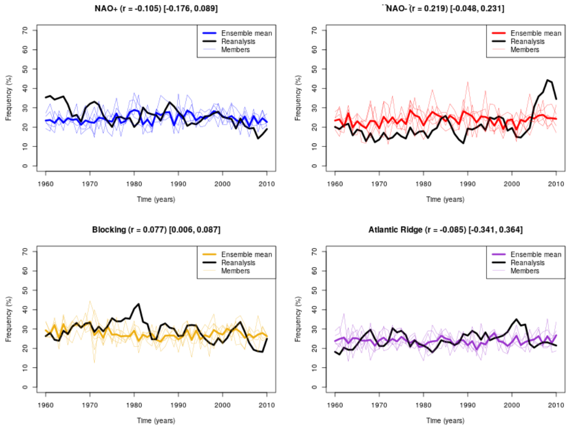

(d) JJA - Method 2

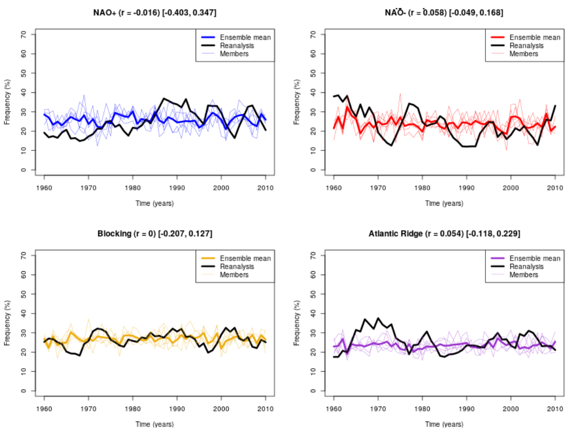

(e) NDJFMA - Method 1

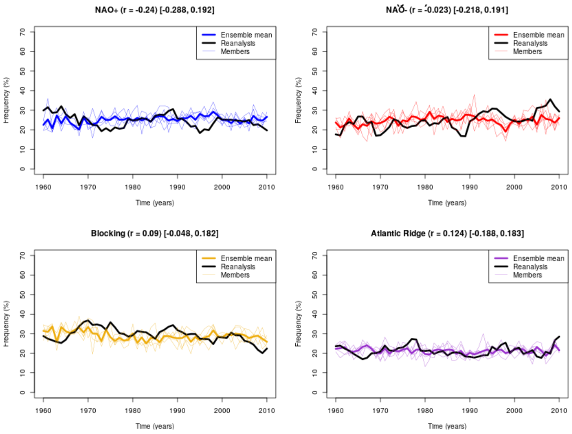

(f) MJJASO - Method 1

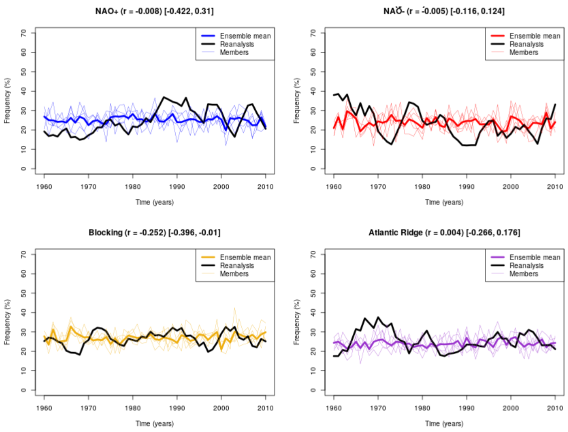

(g) NDJFMA - Method 2

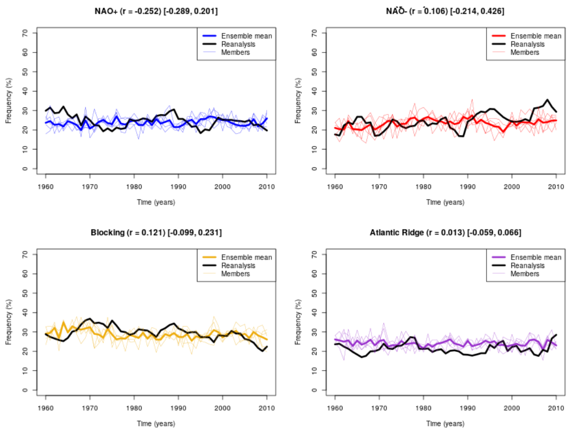

(h) MJJASO - Method 2

Figure B.11. Same as Figure 8, but averaging from year 1 to 4. Extended seasons are also included.

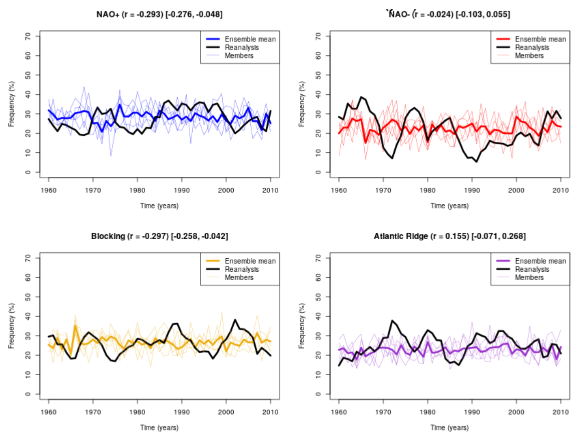

(a) DJF - Method 1

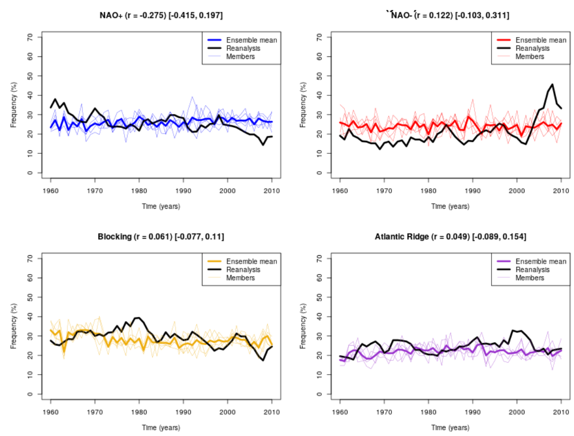

(b) JJA - Method 1

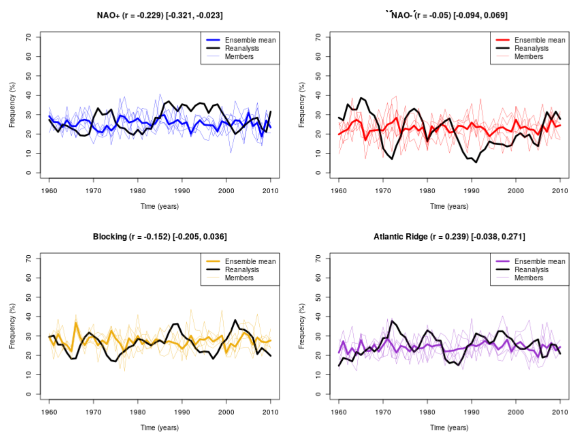

(c) DJF - Method 2

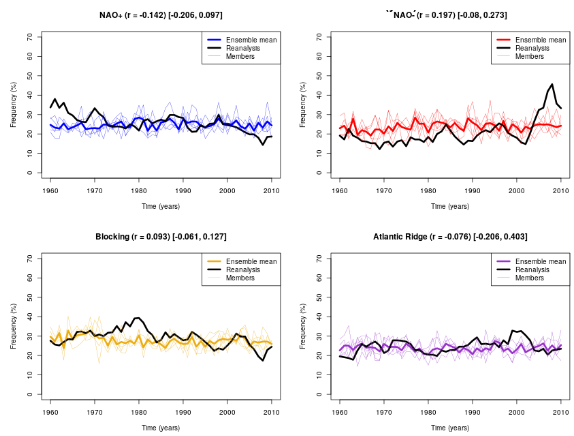

(d) JJA - Method 2

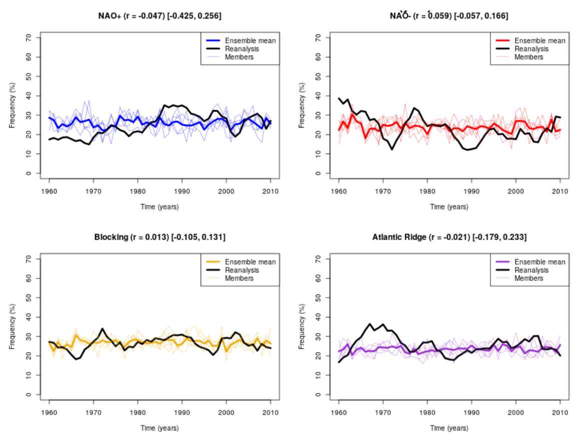

(e) NDJFMA - Method 1

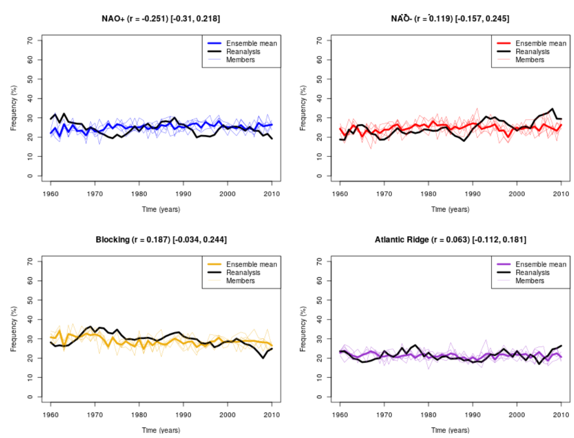

(f) MJJASO - Method 1

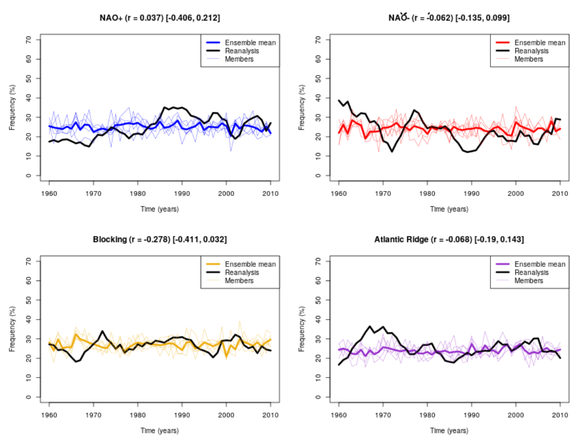

(g) NDJFMA - Method 2

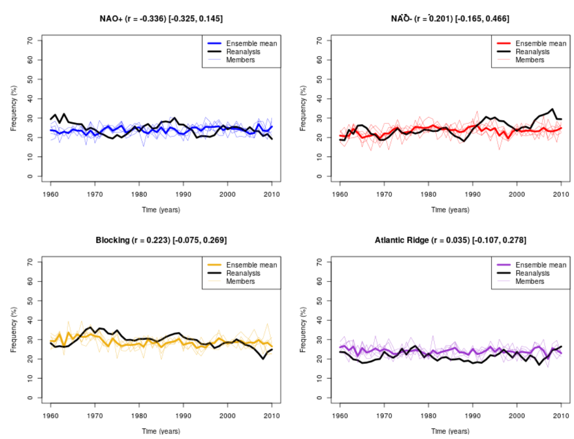

(h) MJJASO - Method 2

Figure B.12. Same as Figure 8, but averaging from year 1 to 5. Extended seasons are also included.

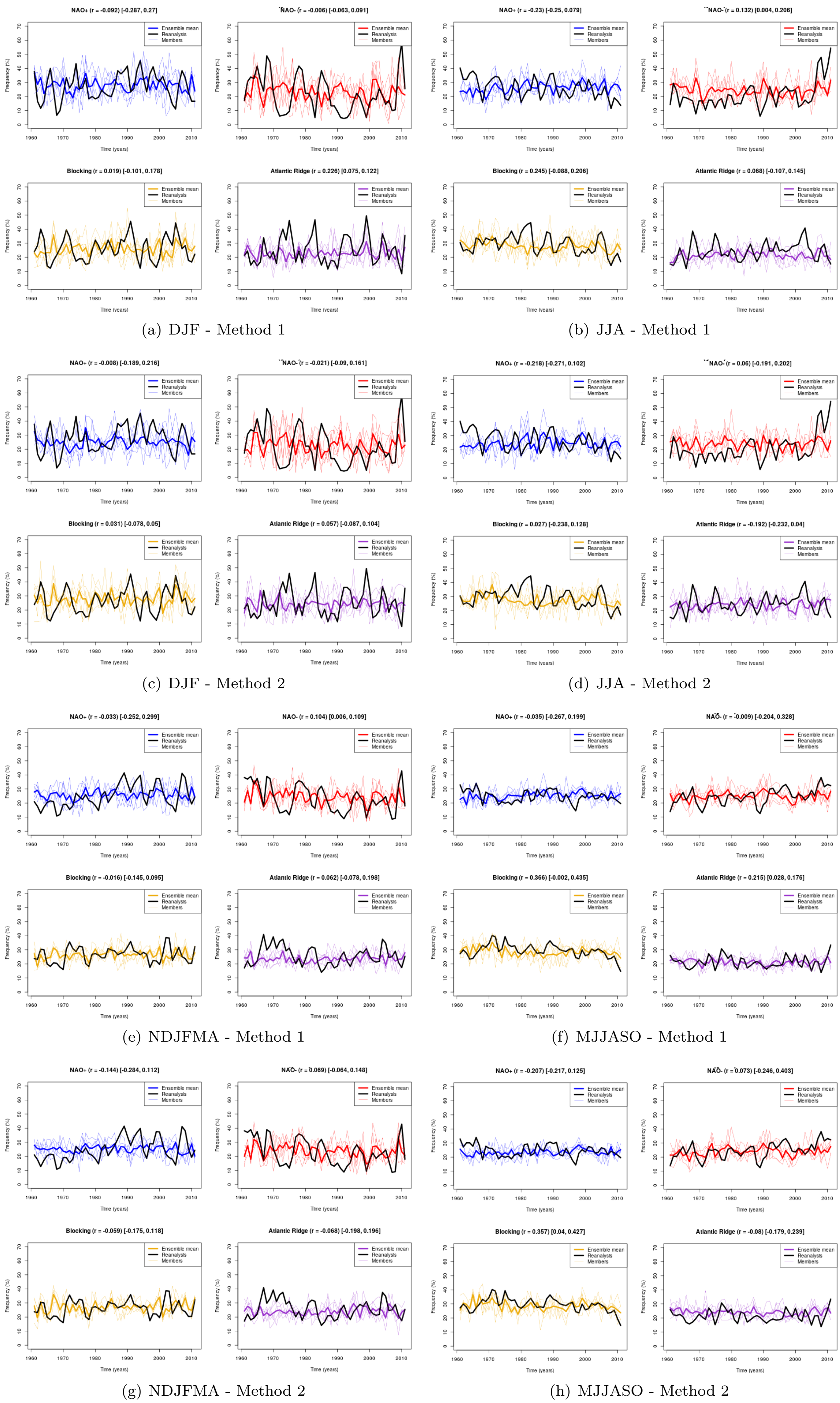

Figure B.13. Same as Figure 8, but averaging from year 2 to 3. Extended seasons are also included.

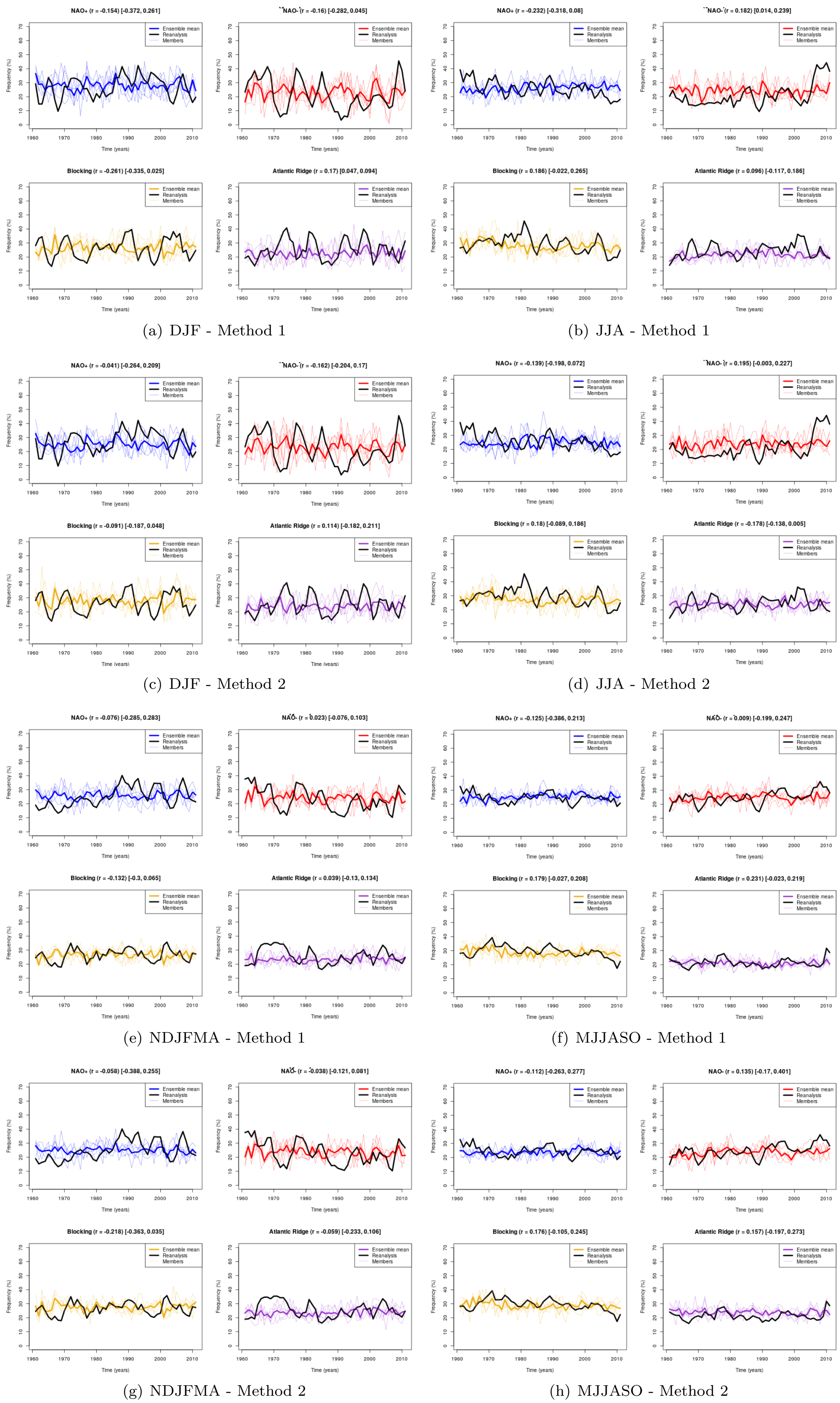

(a) DJF - Method 1

(b) JJA - Method 1

(c) DJF - Method 2

(d) JJA - Method 2

(e) NDJFMA - Method 1

(f) MJJASO - Method 1

(g) NDJFMA - Method 2

(h) MJJASO - Method 2

Figure B.14. Same as Figure 8, but averaging from year 2 to 4. Extended seasons are also included.

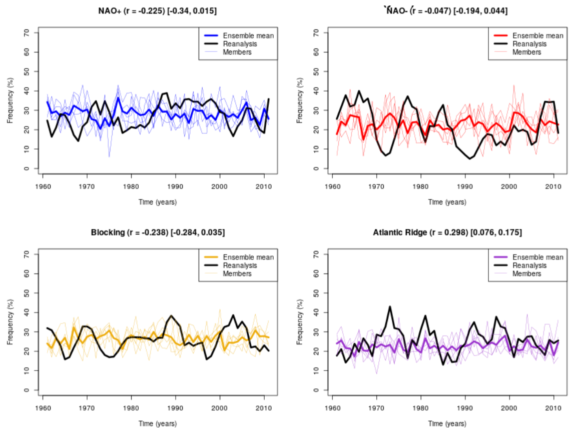

(a) DJF - Method 1

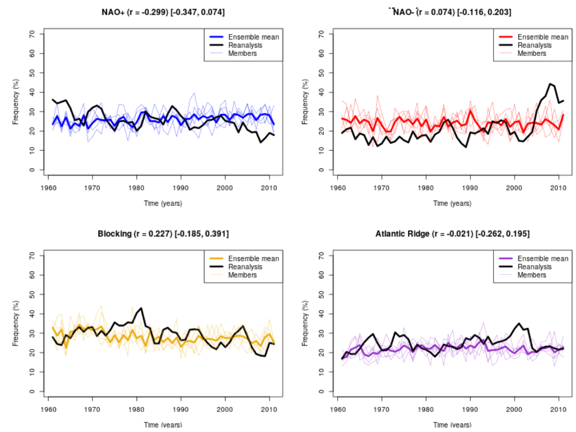

(b) JJA - Method 1

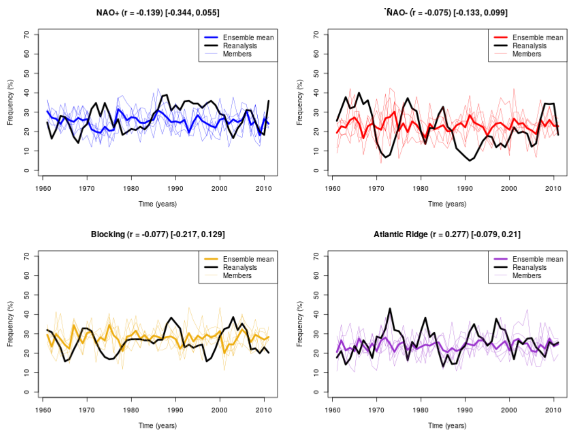

(c) DJF - Method 2

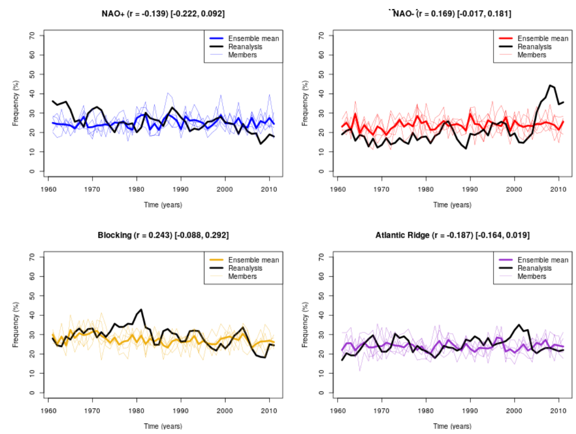

(d) JJA - Method 2

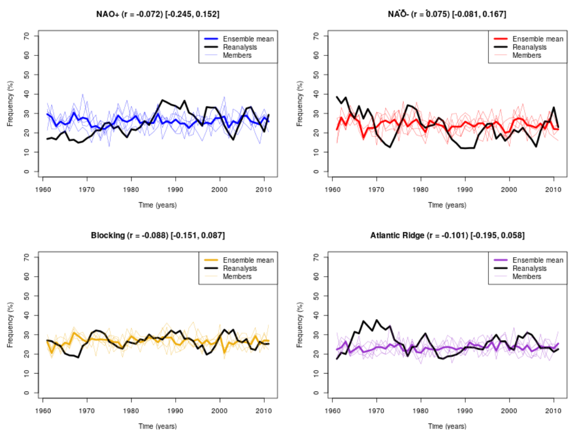

(e) NDJFMA - Method 1

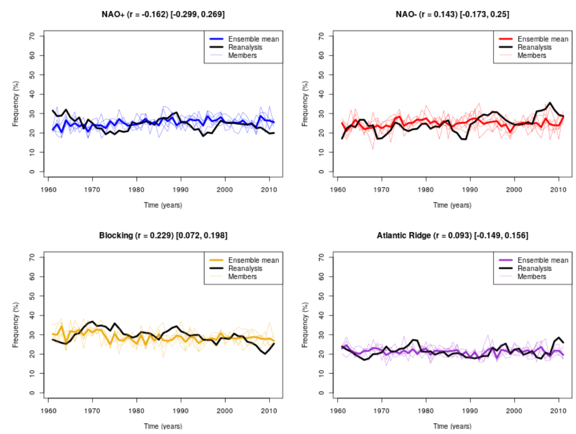

(f) MJJASO - Method 1

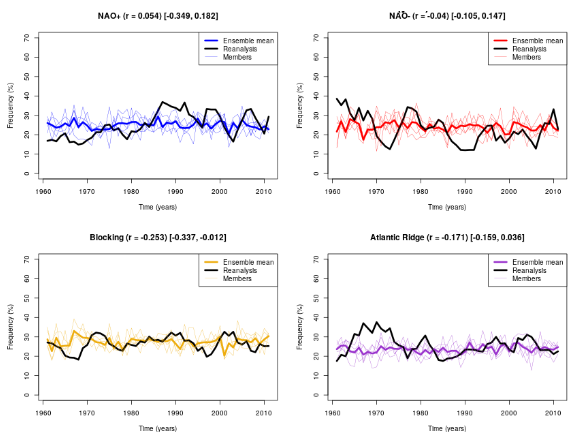

(g) NDJFMA - Method 2

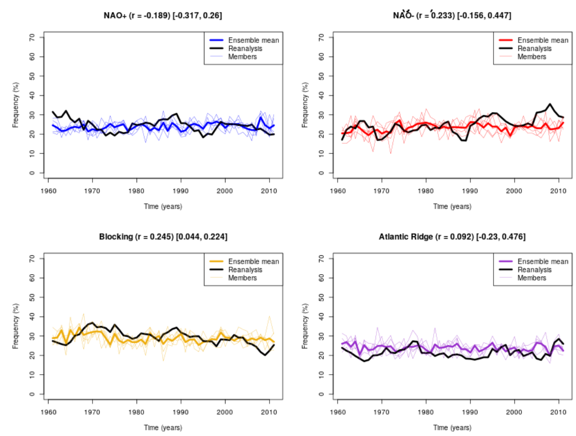

(h) MJJASO - Method 2

Figure B.15. Same as Figure 8, but averaging from year 2 to 5. Extended seasons are also included.

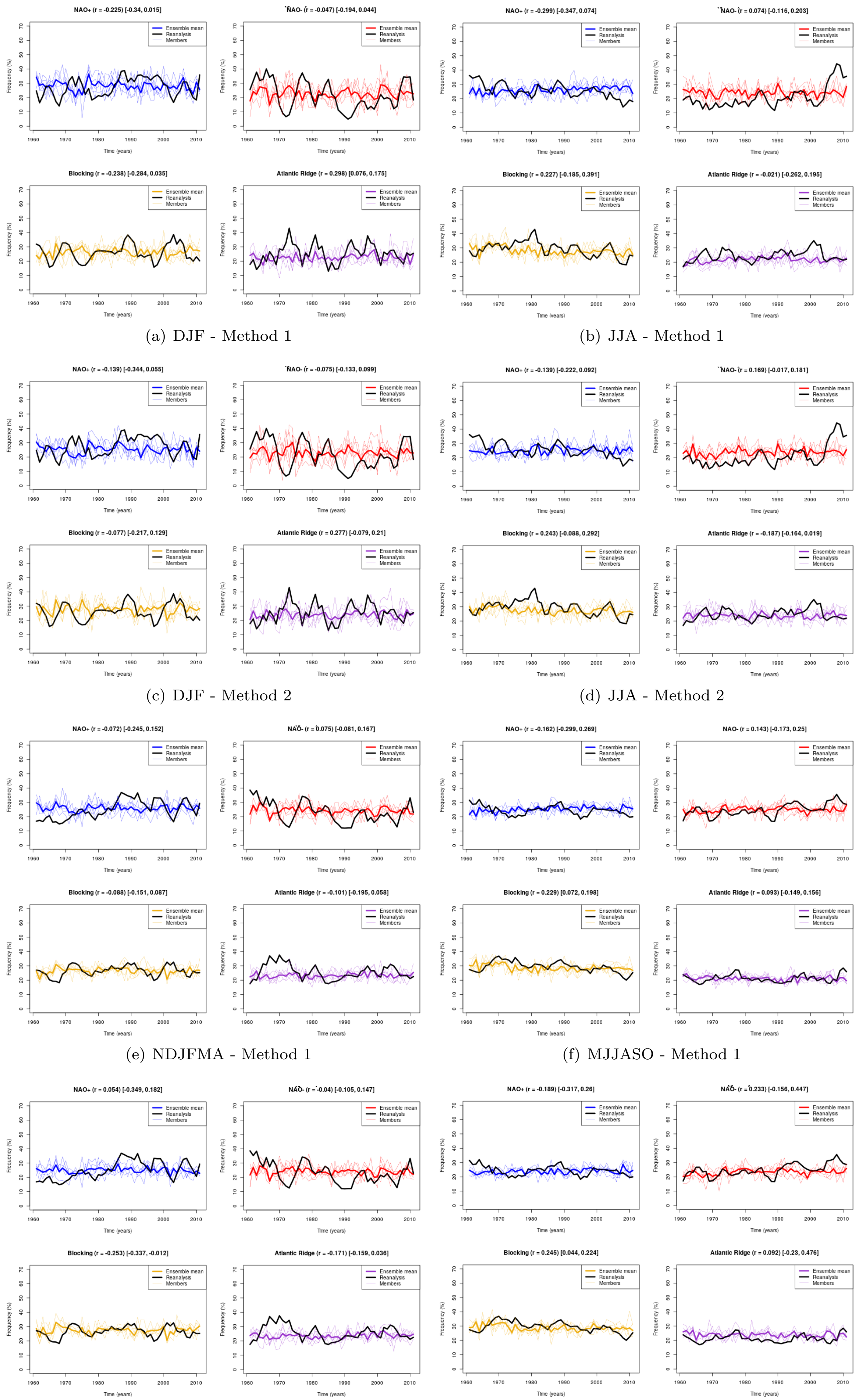

(a) DJF - Method 1
(b) JJA - Method 1
(c) DJF - Method 2
(d) JJA - Method 2
(e) NDJFMA - Method 1
(f) MJJASO - Method 1
(g) NDJFMA - Method 2
(h) MJJASO - Method 2

Figure B.16. Same as Figure 8, but averaging from year 3 to 4. Extended seasons are also included.

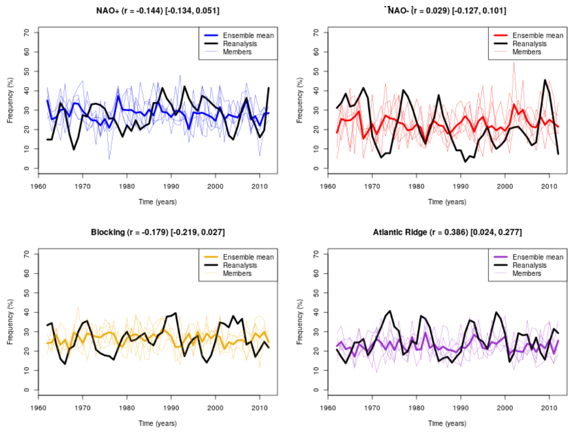

(a) DJF - Method 1

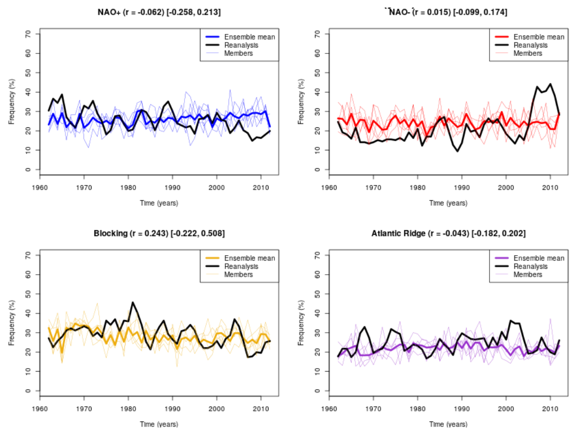

(b) JJA - Method 1

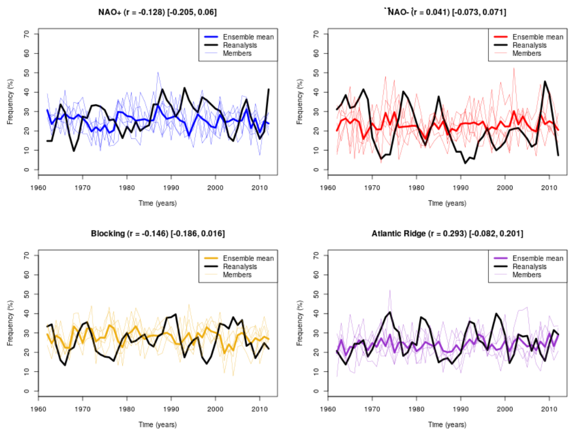

(c) DJF - Method 2

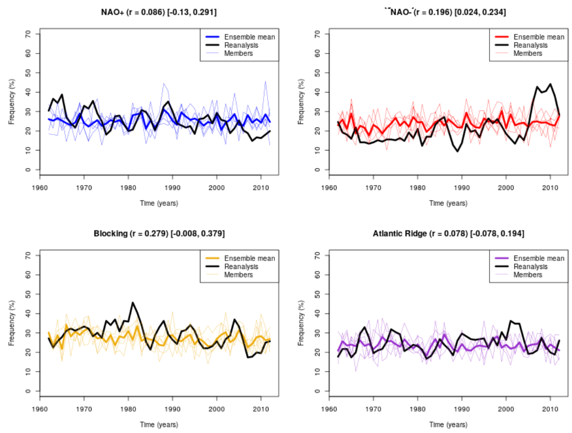

(d) JJA - Method 2

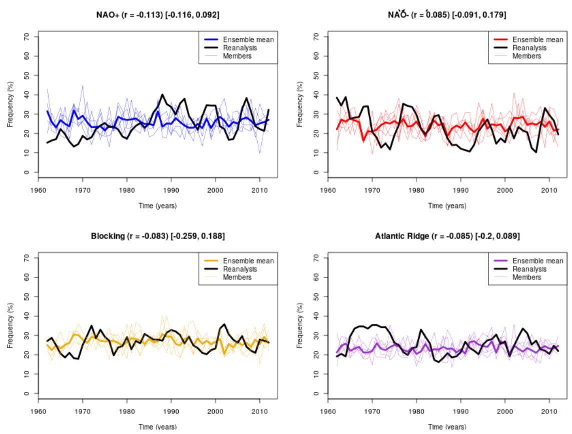

(e) NDJFMA - Method 1

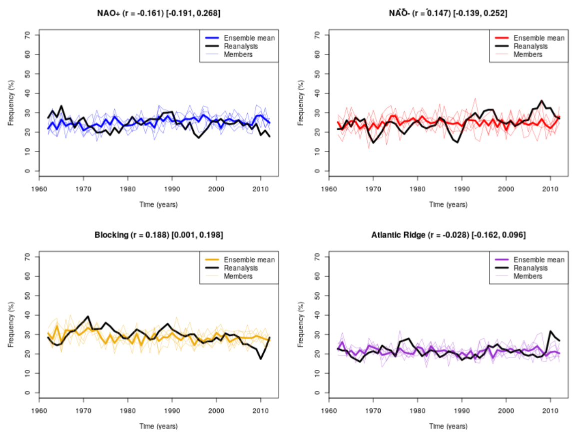

(f) MJJASO - Method 1

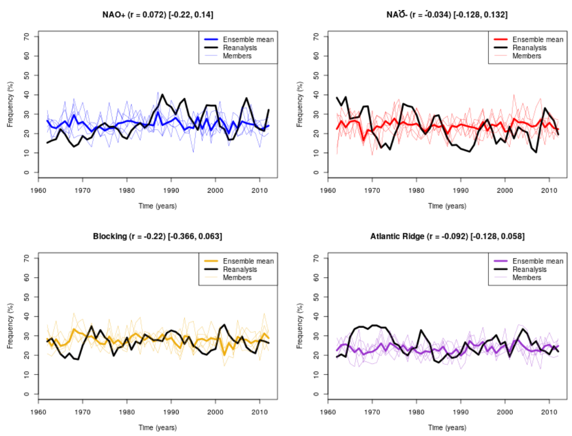

(g) NDJFMA - Method 2

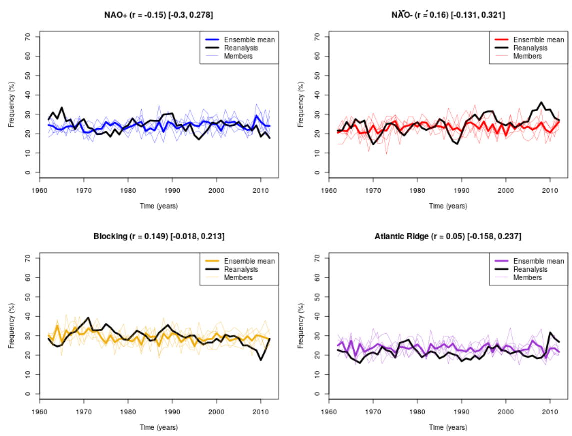

(h) MJJASO - Method 2

Figure B.17. Same as Figure 8, but averaging from year 3 to 5. Extended seasons are also included.

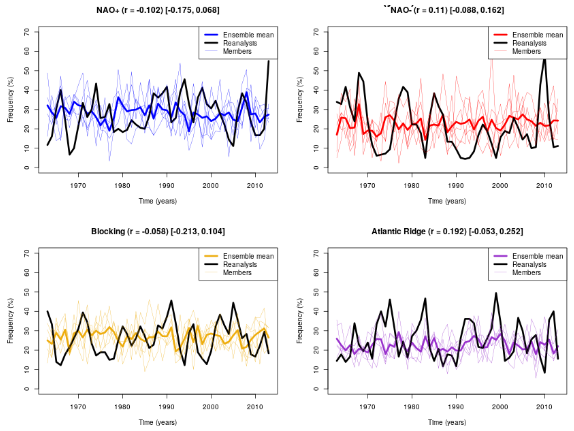

(a) DJF - Method 1

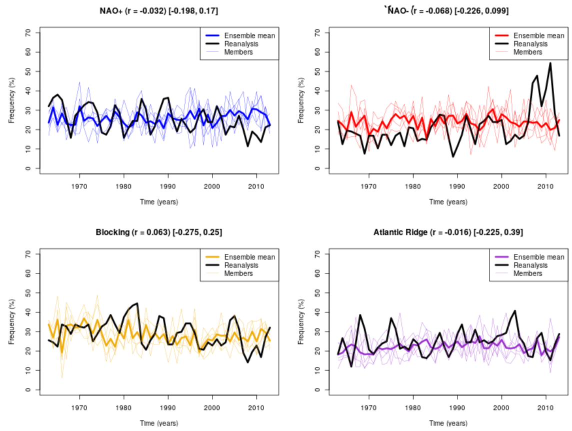

(b) JJA - Method 1

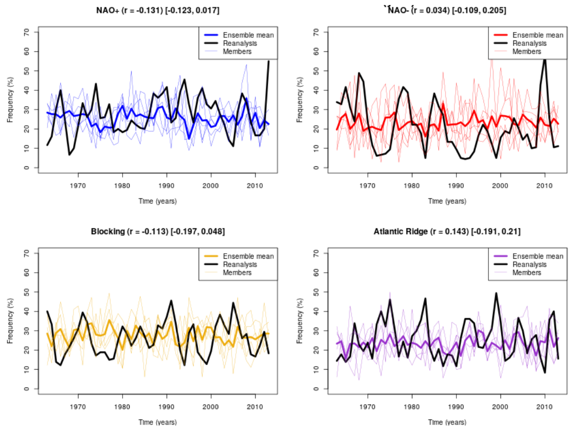

(c) DJF - Method 2

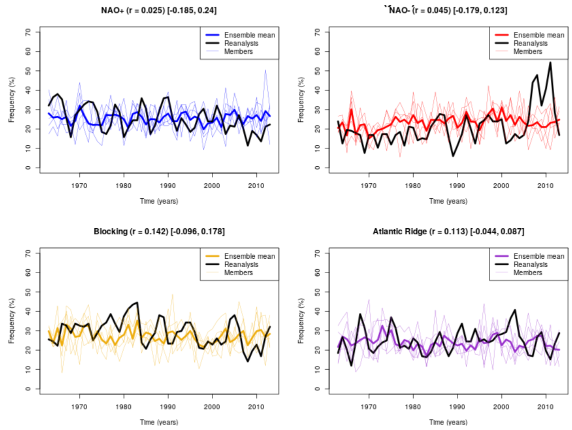

(d) JJA - Method 2

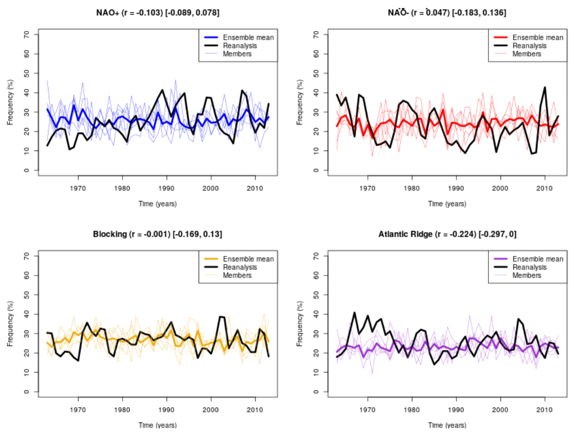

(e) NDJFMA - Method 1

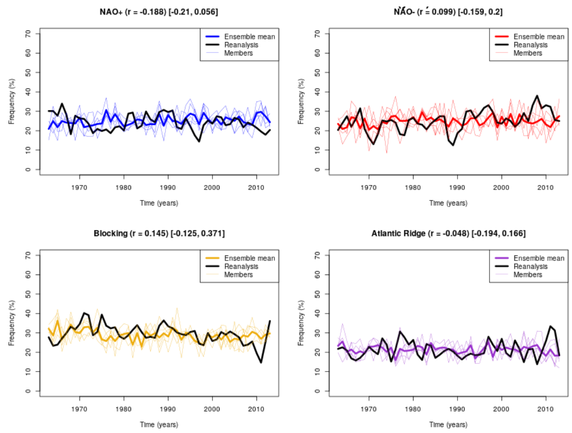

(f) MJJASO - Method 1

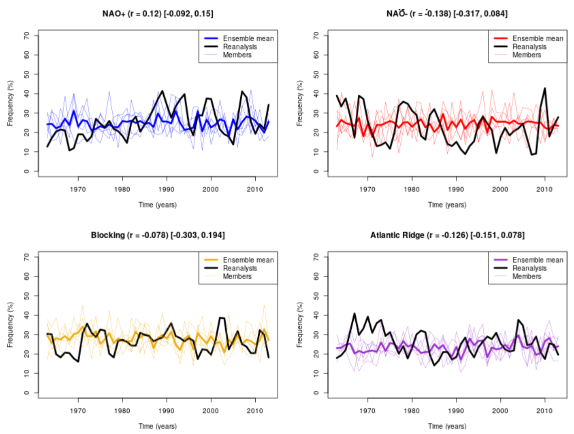

(g) NDJFMA - Method 2

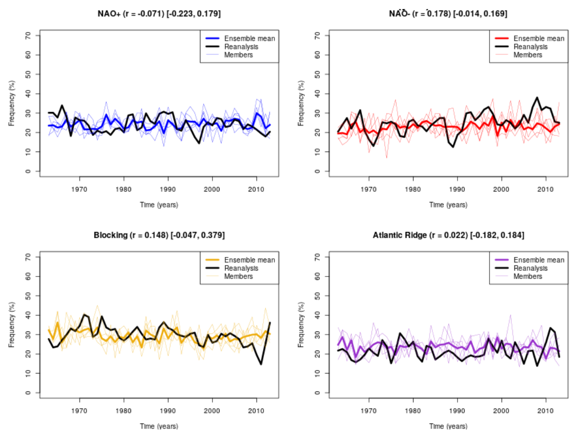

(h) MJJASO - Method 2

Figure B.18. Same as Figure 8, but averaging from year 4 to 5. Extended seasons are also included.

Annex C: List of figures

Annex D: List of acronyms

- ACC: Anomaly Correlation Coefficient
- AMO: Atlantic Multi-Decadal Oscillation
- AMOC: Atlantic Meridional Overturning Circulation
- AMV: Atlantic Multi-Decadal Variability
- AR: Atlantic Ridge
- BL: Blocking
- BSC: Barcelona Supercomputing Center
- CMIP: Coupled Model Intercomparison Project
- DJF: December, January and February
- DFS4.3: Drakkar Forcing Set, version 4.3
- EA: East Atlantic
- ECMWF: European Centre for Medium-Range Weather Forecasts
- EOF: Empirical Orthogonal Function
- ERSST.v4: Extended Reconstructed Sea Surface Temperature, version 4
- ESM: Earth System Model
- HTESSEL: Hydrology Tiled ECMWF Scheme of Surface Exchanges over Land
- ICOADS: International Comprehensive Ocean–Atmosphere Dataset
- IFS: Integrated Forecasting System
- JJA: June, July and August
- JRA-55: Japanese 55-year Reanalysis
- LIM2: Louvain-la-Neuve Sea Ice Model, version 2
- LOESS: Locally Estimated Scatterplot Smoothing
- MJJASO: May, June, July, August, September and October
- NAO: North Atlantic Oscillation
- NDJFMA: November, December, January, February, March and April
- NEMO: Nucleus for European Modelling of the Ocean
- NOAA: National Oceanic and Atmospheric Administration
- OASIS: Ocean Atmospheric Sea Ice Soil
- ORAS4: Ocean ReAnalysis System 4
- PI: Pre-Industrial
- SST: Sea Surface Temperature
- TM5: Tracer Model, version 5
- UCM: Universidad Complutense de Madrid